MEASUREMENT OF UNSATURATED HYDRAULIC CONDUCTIVITY IN THE FIELD

by

Akif Ali Hussen

A Dissertation Submitted to the Faculty of the

DEPARTMENT OF SOIL AND WATER SCIENCE

In Partial Fulfillment of the Requirements
For the Degree of

DOCTOR OF PHILOSOPHY

In the Graduate College

THE UNIVERSITY OF ARIZONA

1991

THE UNIVERSITY OF ARIZONA
GRADUATE COLLEGE

As members of the Final Examination Committee, we certify that we have read the dissertation prepared by Akif Ali Hussen

entitled Measurement of Unsaturated Hydraulic Conductivity in the Field

and recommend that it be accepted as fulfilling the dissertation requirement for the Degree of Doctor of Philosophy.

Allan D. Matthias Allan D. Matthias	15 Aug. 1991 Date
Alfredo R. Huete Alfredo R. Huete	15 Aug. 1991 Date
Arthur W. Warrick Arthur W. Warrick	14 Aug. 1991 Date
	Date
	Date

Final approval and acceptance of this dissertation is contingent upon the candidate's submission of the final copy of the dissertation to the Graduate College.

I hereby certify that I have read this dissertation prepared under my direction and recommend that it be accepted as fulfilling the dissertation requirement.

Arthur W. Warrick Dissertation Director	14 Aug. 1991 Date

STATEMENT BY AUTHOR

This dissertation has been submitted in partial fulfillment of requirements for an advanced degree at The University of Arizona and is deposited in the University Library to be made available to borrowers under rules of the Library.

Brief quotations from this dissertation are allowable without special permission, provided that accurate acknowledgement of source is made. Requests for permission for extended quotation from or reproduction of this manuscript in whole or in part may be granted by the head of the major department or the Dean of the Graduate College when in his or her judgment the proposed use of the material is in the interests of scholarship. In all other instances, however, permission must be obtained from the author.

SIGNED: 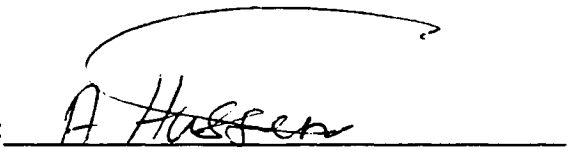

ACKNOWLEDGMENTS

I would like to express my deepest respect and appreciation to my major advisor Professor Dr. A. W. Warrick for his advice, constructive ideas, and guidance throughout this study.

I would like to thank the members of my committee. Special thanks goes to Ms. Sheri Musil for her valuable help through this study.

I wish to thank my father and mother for their support and encouragement.

Last, but not least, special gratitude is due to my wife, Anna, for her patience, support, and encouragement, and two sons, Allan and Arian, who brighten my life and made this accomplishment possible.

TABLE OF CONTENTS

TABLE OF CONTENTS--Continued

TABLE OF CONTENTS--Continued

TABLE OF CONTENTS--Continued

LIST OF TABLES

LIST OF TABLES--Continued

LIST OF TABLES--Continued

LIST OF FIGURES

LIST OF FIGURES--Continued

LIST OF FIGURES--Continued

ABSTRACT

Unsaturated hydraulic conductivity was measured using four different methods. Tension permeameters were used to measure unsaturated hydraulic conductivity in the field, using a single disc method, which depends on the measurements of sorptivity, steady state flow rate, initial and final water content (White and Perroux, 1987, 1989). Also, a double disc method was used which utilizes Wooding's (1968) equation for two different disc radii at the same tension for steady state flow rates. Undisturbed and disturbed soil cores were used to measure unsaturated hydraulic conductivity in the lab, using water retention curves with van Genuchten's equations. There were no significant differences in the mean of hydraulic conductivity between single and double disc methods in all the tensions used (0, 5, 10 and 15 cm). There were significant differences between the field methods and undisturbed soil cores in zero cm tension, and disturbed soil cores in 10 and 15 cm tension.

The effect of land preparation on the unsaturated hydraulic conductivity was studied using the double disc method. Tilling has significant effects on the unsaturated hydraulic conductivity at all tensions used.

The spatial variation of unsaturated hydraulic conductivity and steady state flow in different tensions using the double disc method was studied. We found exponential variogram models for unsaturated hydraulic conductivity at 5, 10 and 15 cm tensions and a random model for zero cm tension. Also, exponential models were best fitted for steady state flow corresponding to pores radii of 0.03 - 0.015 cm, 0.015

- 0.010 cm and steady state flow at 10 cm tension. A Michaelis-Menton model was used for steady state flow at 5 cm and 15 cm tension.

Disc permeameters were also used to add 5 cm depth of water, bromide and dye solution at 0, 5, 10 and 15 cm tensions with three replicates. A comparison was made between field data and simulated model under the same boundary and initial conditions as in the field. Results showed that the water and bromide move deeper than the prediction of the simulated model in all tensions used. The differences were larger between simulated model and field data for both water and bromide concentrations in the lower tension and smaller in the higher tension as a result of elimination of some preferential flow paths.

An equation was developed for cumulative infiltration valid for both small and large time. The parameters calculated using the developed equation closely matched the measured infiltration, and fit better than a three term series similar to the Philip equation for one-dimensional flow.

CHAPTER 1

INTRODUCTION

Knowledge of hydraulic conductivity and matric potential as functions of soil moisture content are the fundamental relationships for quantitative analysis of water flow in soils. Calculations of water and solute movement require hydraulic parameters as inputs. A common limitation is that parameters are measured under laboratory conditions ignoring the difference between these parameters in the field and laboratory. In addition, most analyses assume that the water and solute move through homogeneous soil even though transport in the soil often takes place along preferred pathways. Soils are variable over spatial dimensions and, in structured soils, preferred pathways consist of root pores, worm channels, and drying cracks. The importance of preferential flow in such macropores has been recently recognized in contaminant hydrology. The rapid transport of pesticides to groundwater can be explained by preferential flow.

Because the sensitivity of soil hydraulic properties to soil structure and difficulties in obtaining representative undisturbed samples, in situ methods are potentially more accurate. Unfortunately, they are also more time consuming and hard to perform. In recent years new methods and devices have been developed (White and Perroux, 1989; White and Sully, 1988; Smettem and Clothier, 1989) to measure soil hydraulic properties in situ.

The objectives of this study are to:

1. Compare and evaluate different in situ and laboratory methods to calculate and measure unsaturated hydraulic conductivity.

2. Study and compare the effects of land preparation on unsaturated hydraulic conductivity measured at the surface.

3. Study the spatial variation of unsaturated hydraulic conductivity and macropore flow at different tensions.

4. Study the effect of preferential flow of water and chemical movement in the soil profile and compare predicted model and field data.

CHAPTER 2

LOCATION, DESIGN AND METHODS

Experimental Location and Soil Series

The study has been conducted in Field No. F117 at the Maricopa Agricultural Center (Fig. 2.1) located three miles east of Maricopa and three miles north of the Casa Grande Maricopa Highway in Pinal County, Arizona. The farm is 770 hectares in size. The dominant soils at the farm are the Casa Grande, Trix and Shontik. The Casa Grande (fine-loamy, mixed, hyperthermic Natric Natrargids) is a deep, well drained slowly permeable soil formed in old alluvium and has a sandy loam or sandy clay loam surface horizon from the 0-30 cm depth. Trix (fine-loamy, mixed, calcareous, hyperthermic Type Torrifluvents) is a deep, well drained very slowly permeable soil whose upper horizons are formed in fine textured, recently deposited alluvium and has a clay loam or sandy clay loam surface horizon of 0-30 cm. Shontik (fine-loamy, mixed, hyperthermic Natric Camborthids) is a deep, well drained and moderately to moderately rapid permeable soil found in sand alluvium and has a sandy loam surface horizon 0-30 cm deep (Post et al., 1988).

Three plots and a long transect were chosen in Field 117 (see Figure 2.2). Two of the plots were 2 x 3 m and the third one was 1.75 x 2 m. The transect was 70 m long and 0.50 m wide. The field was plowed and rotatilled to make the soil surface soil smooth, except the third plot which was undisturbed.

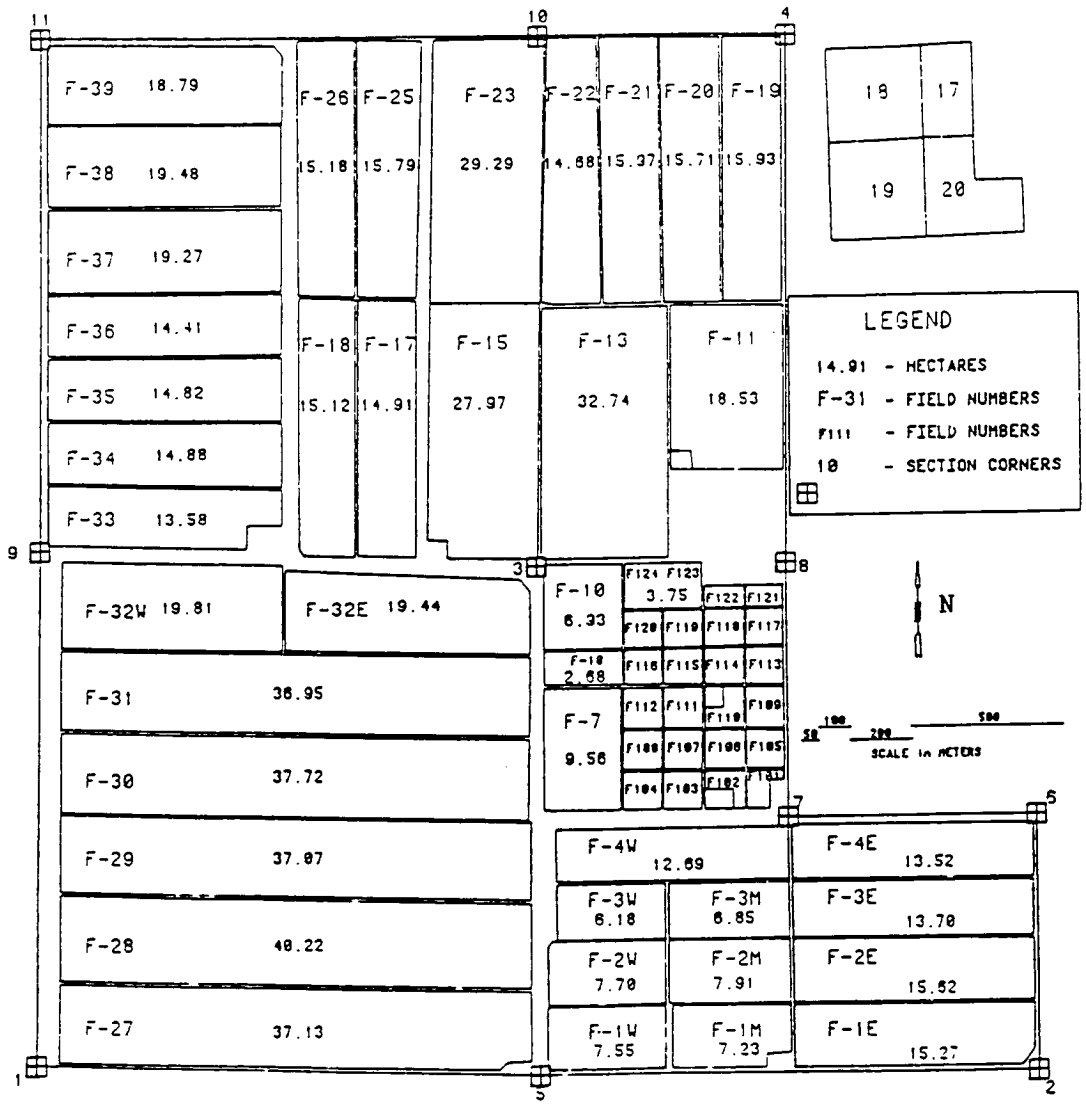

Figure 2.1. Location of field F-117 in Maricopa Farm.

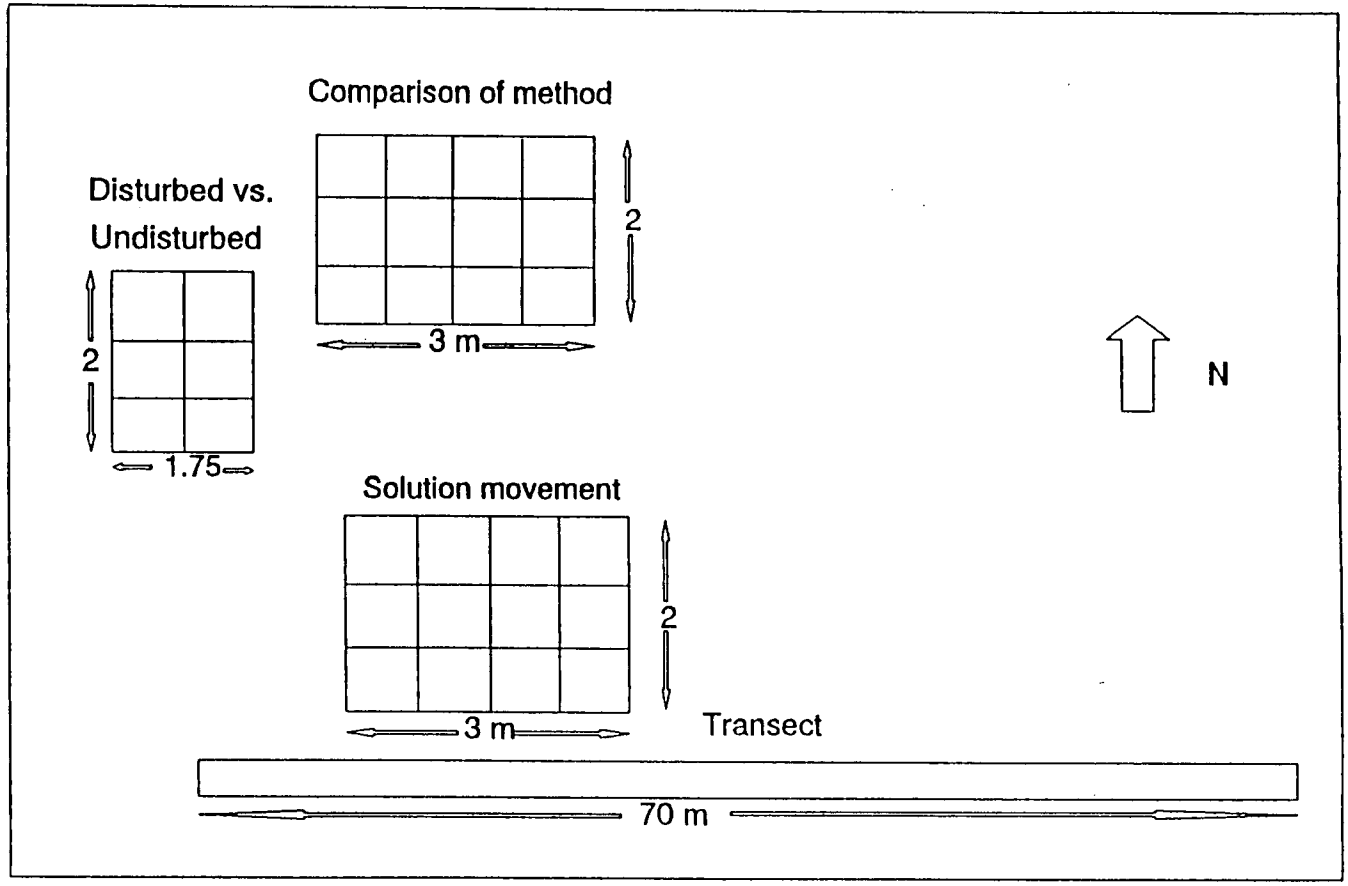

Figure 2.2. Location of plots and transect in the field F117 (not to scale)

Experimental Design

1. Experimental design for comparing different disc permeameter methods and for collecting soil core samples.

One of the two 3 x 2 m plots was divided into twelve equal 0.75 x 0.67 m subplots as shown in Figure 2.3. We used four tensions to measure unsaturated hydraulic conductivity (0, 5, 10, and 15 cm) with three replications. Within each subplot two disc radii were used, 23.6 and 10.4 cm which are referred to as "large" and "small" discs, respectively. Also, three surface core samples of 5.3 cm radius were taken from the plot at the indicated locations. The soil surface was smoothed carefully before the measurements.

2. Experimental design for comparing land preparation effect.

The small plot (1.75 x 2 m) was divided into two parts. One part was smoothed using a shovel the other part was left undisturbed (see Figure 2.4). Each part was further divided into three smaller plots. Within the smallest unit, hydraulic conductivity at four tensions (0, 5, 10, and 15 cm) was measured at the same spot using both small and large disc permeameters, with three replicates for every measurement. Altogether, there were two treatments (disturbed and undisturbed), four tensions (0, 5, 10 and 15 cm), three replicates, and two sizes of permeameters.

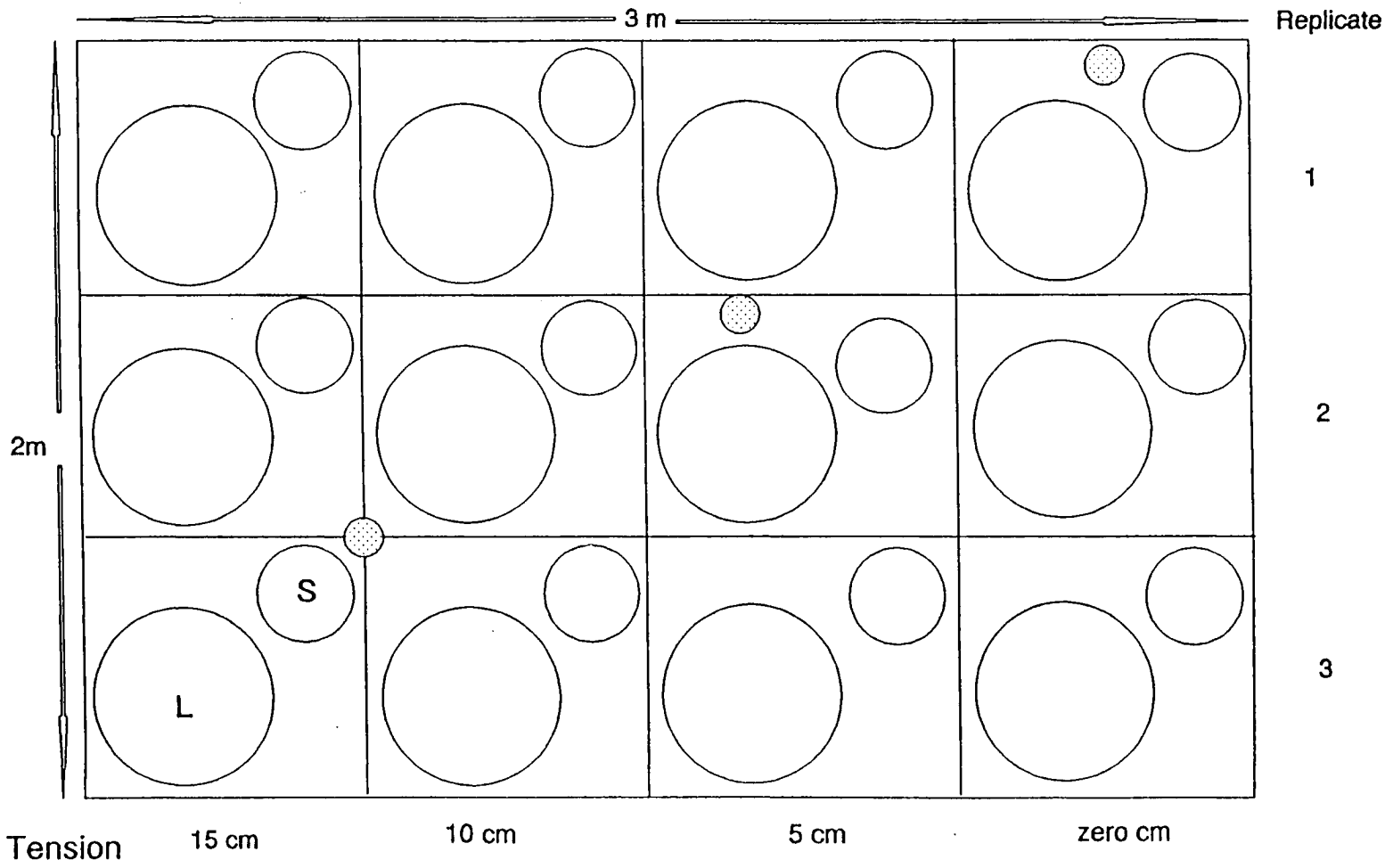

Figure 2.3. Field experimental design for measuring K unsaturated using different disc permeameter methods. L is large disc, S is small disc permeameter and the small shaded dash circle is the location of soil core samples.

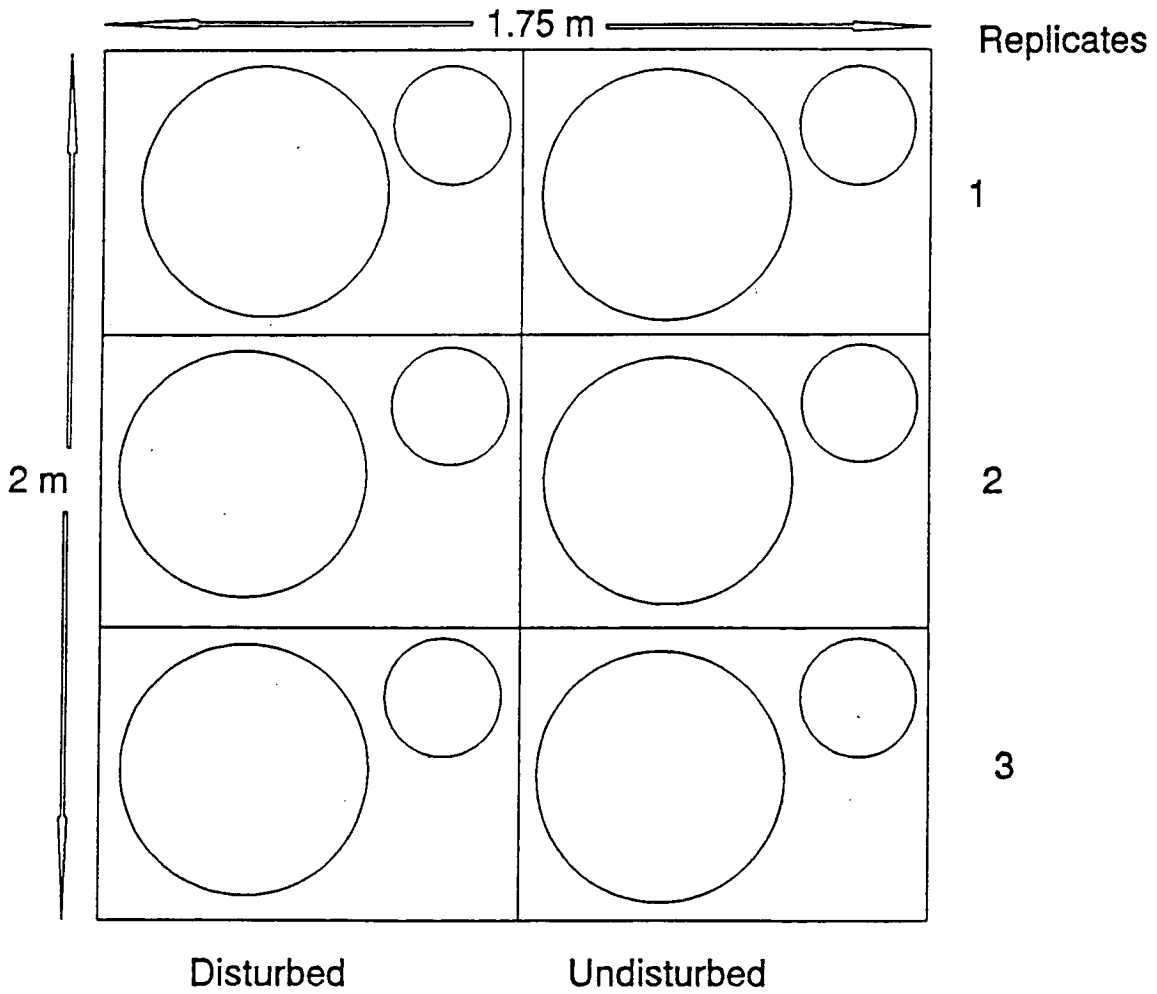

Figure 2.4. Field experimental design for measuring K unsaturated using multiple disc methods on disturbed soil vs. undisturbed soil.

3. Experimental design for spatial variation.

In this part we chose a transect 70 m long and 0.5 m wide, taking measurements every meter with both disc permeameters for the four tensions at the same spot for the large disc adjacent to small disc.

4. Experimental design for solute and water movement.

The remaining 3 x 2 m plot was divided into twelve 0.75 x 0.67 m subplots (Figure 2.5). A five centimeter depth of a dye solution (2186 cm^3 solution added for disc permeameter with diameter of 23.6 cm) including a bromide tracer was added to the center of each small plot using the large disc permeameter at 4 different tensions (0, 5, 10, and 15 cm) and with three replicates for each tension. The tension replicates were within the same column in the plot to reduce spatial variation of the soil. FD and C Blue #1 dye (Seltzer Chemicals, Inc., Carlsbad, CA 92008-3861) at a concentration of 0.3 g/l was used. After the 5 cm solution infiltrated, samples were taken below the center of the disc, using a small soil coring device (Oakfield probe). Soil samples were taken in 2.5 cm increments to measure water content and bromide concentration, eight to nine samples were taken depending on the wetting front.

Unsaturated Measurements with Disc Permeameters for Single Tension at One Spot

The construction of disc permeameters has been described in detail in Perroux and White (1988) and Lien (1989). Two sizes of disc permeameters were used. They are very similar except one has a diameter of 20 cm, and a steel

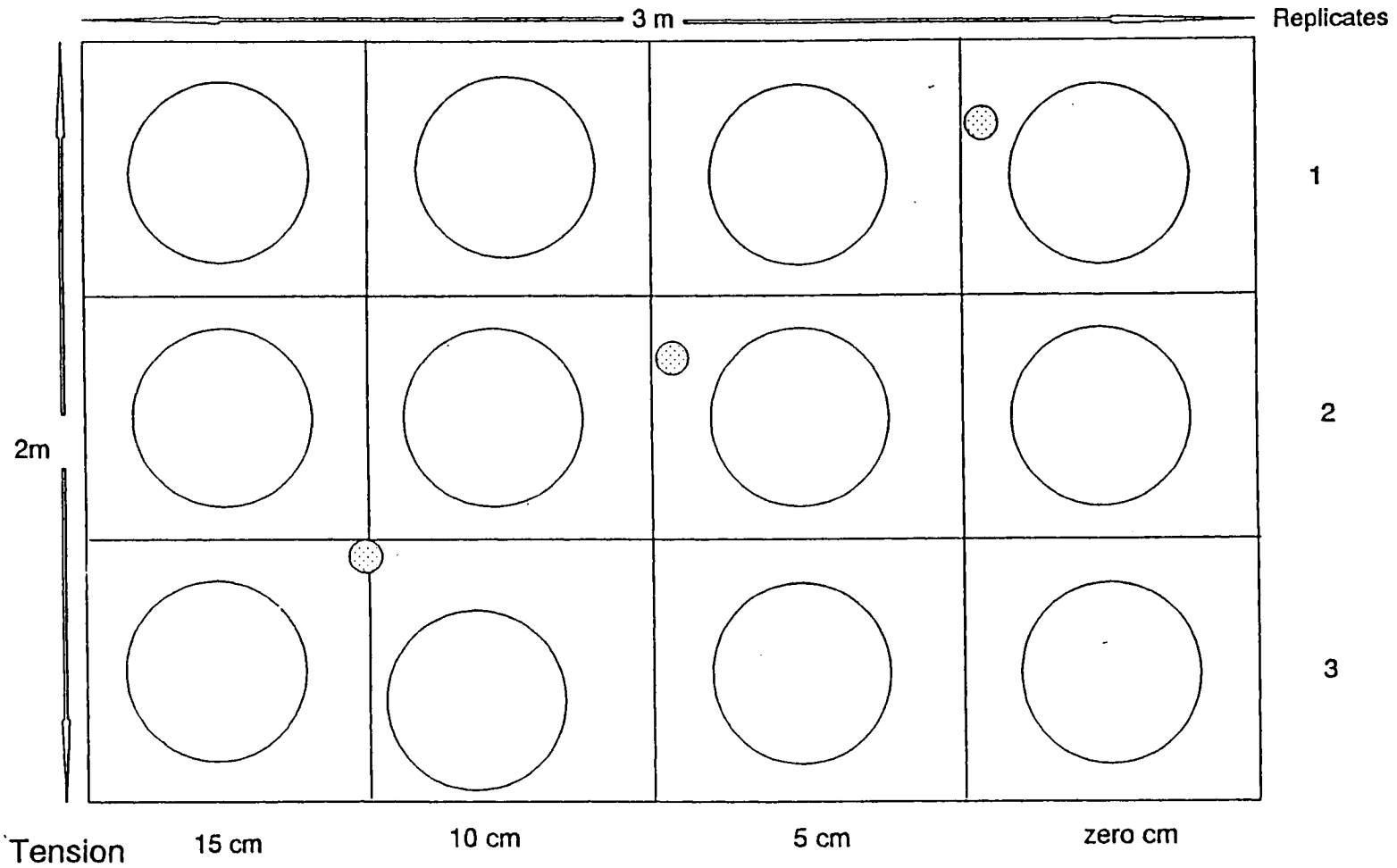

Figure 2.5. Field experimental design for measuring wetting front and bromide depth using constant water depth (5 cm) at different tensions for dry plowed soil, small shaded dash circle is the location of soil core samples.

retention ring of 23.6 cm, and the other a diameter of 9 cm and steel ring of 10.4 cm (Figs. 2.6 and 2.7).

Following is the field procedure to operate disc permeameter which is nearly identical to that of Lien (1989):

1. Prepare a smooth, level area about 30 x 30 cm wide for the large or 15 x 15 cm for the small disc permeameter.

2. Place a steel ring (0.2 cm thick, 23.6 cm I.D. for the large and 0.2 cm thick, 10.4 cm I.D. for the small disc) on the center of the prepared area by pressing it into the soil. The soil surface should be level so the steel ring touches the surface throughout.

3. Press soil sample cans for initial moisture content into the soil on opposite sides of the steel ring, with each can about 10 to 15 cm outside the ring.

4. Fill the inside area of the steel ring with moist sand contact material, and level it to the top edge of the ring using a ruler as a straight edge. Remove any excessive sand material.

5. Remove the disc permeameter from the water storage bucket. Gently blow air into the air inlet tube of the tension tower and clamp it shut while it is bubbling to eliminate water inside the air inlet tube. The provided tension is equal to the distance between the membrane and the air bubble entry points into the reservoir (which is 1.5 cm in the big disc and 6.0 cm in the small disc) minus the height of water above the bottom of each of the air inlet tubes (four inlet tubes).

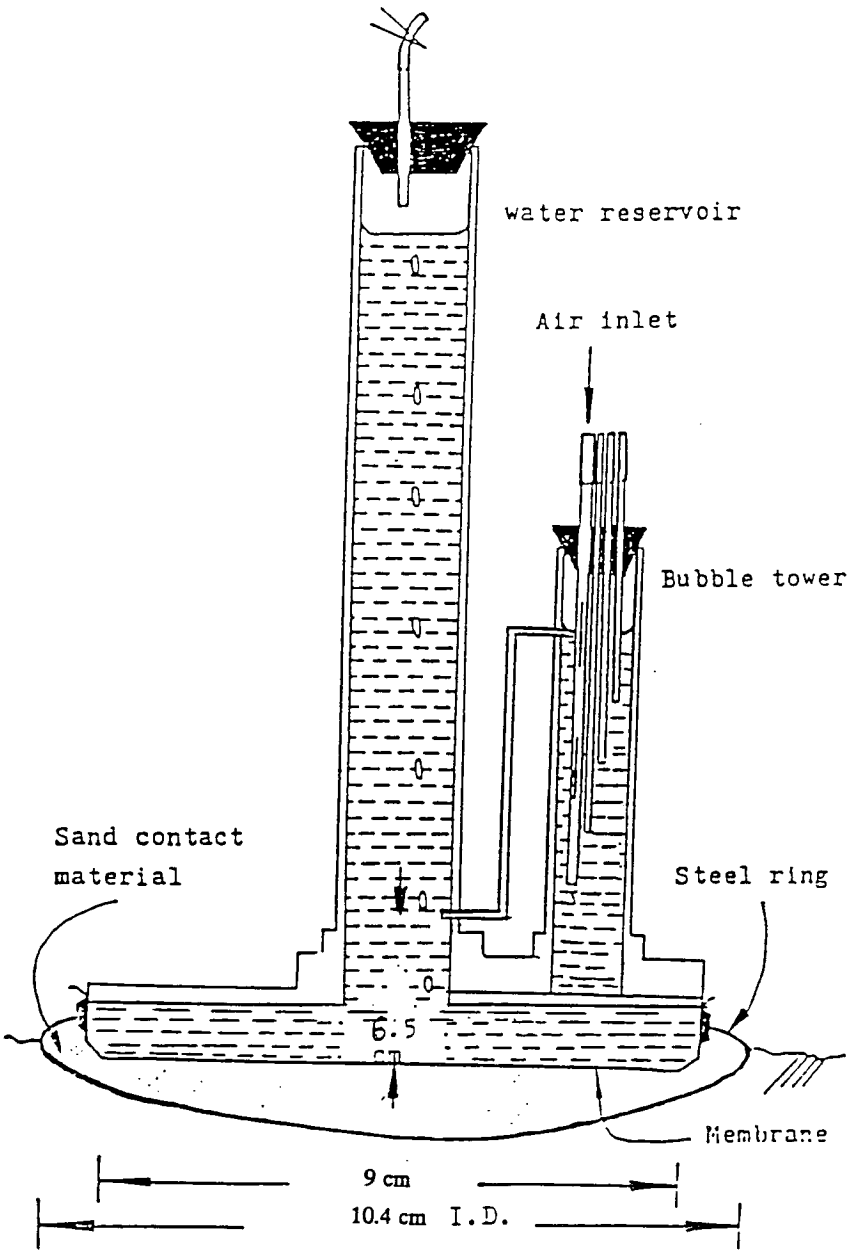

Figure 2.6. The small disc permeameter used for unsaturated water flow.

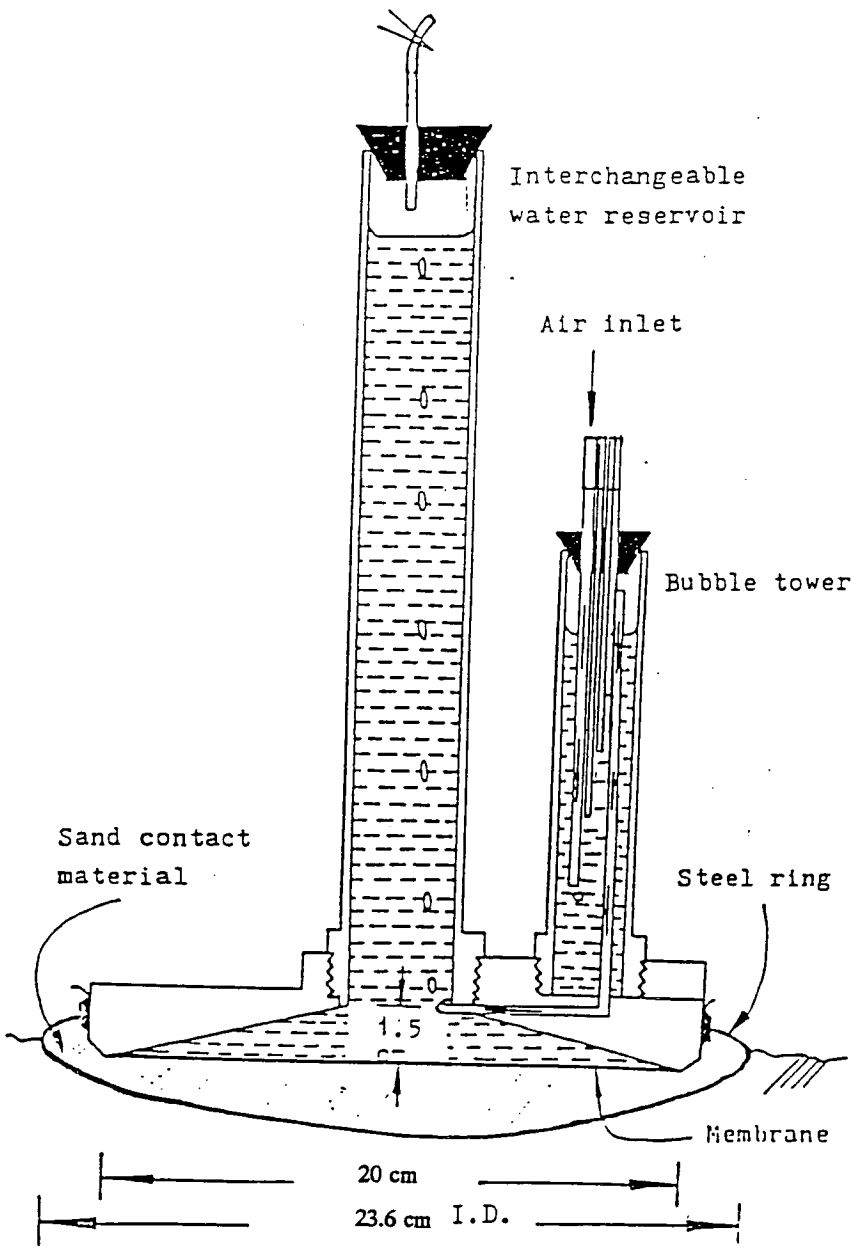

Figure 2.7. The large disc permeameter used for unsaturated water flow.

6. Place the disc permeameter back in the storage bucket and fill the reservoir tube with water, using a suction pump to remove air from the reservoir tube.

7. Read and record the initial water height in the water reservoir tube on a data sheet. Enter the predetermined depth marks to be read on data sheet.

8. Unclamp the air inlet tube of the bubble tower. Gently place the disc permeameter on the center of the sand covered ring.

9. Start the stopwatch as soon as the bubbles start to form in the bubble tower. Press the "split" button to record the time readings whenever the bottom of the meniscus reaches the subsequent predetermined depth mark. Press the "stop" button when the meniscus reaches the last depth mark or at least when one hour reading has been taken.

10. Wash away the sand material attached to the bottom of the membrane and return to water bucket.

11. Use a spatula to remove sand material from the ring and collect the top 0 - 0.4 cm depth soil sample for final moisture content determination.

12. Recall and record the time reading stored in the stopwatch on the data sheet. Use a shovel to remove the two soil sample cans from the soil for initial moisture content and bulk density determination.

Unsaturated Measurements with Disc Permeameters for Multiple Tensions at the Same Spot

Follow steps 1, 2, 4, 5, and 6 as before. Then,

1. Unclamp the air inlet tube for the biggest tension (which was 15 cm in our case) of the tension tower. Gently place the disc permeameter on the center of sand cap.

2. Start the stopwatch when the bubbles start to slow down. Press the "split" button to record the time readings whenever the meniscus reaches the subsequent predetermined depth mark until you reach a steady state flow, i.e. when the time interval between two subsequent predetermined depth marks become equal. Use another stopwatch to take 7 - 8 readings for steady state flow.

3. Unclamp the air inlet tube for the second highest tension (which was 10 cm in our case) of the tension tower. Start the stopwatch when the bubbles slow down (which happens very fast compared to the first time). Press the "split" button to record the time reading until you reach the steady state flow. Use the same watch as before and take 7 - 8 readings for steady state flow.

4. Follow the same step (3) for tension 5 and tension 0 and record the steady state flow with time.

5. Recall and record the time for steady state readings stored in the stopwatch on the data sheet for each tension separately.

Bulk Density (D_b)

The length (L), diameter (2r), and weight of oven dried undisturbed cores were measured and calculated from the ratio of mass (m) to volume of soil core as

$$D_b = m/(\pi r^2 L)$$

Soil Moisture Characteristics

Moisture retention values at saturation, 5, 10, 15, 30, 60, 100, 200, 300, 1000 and 15000 cm were determined for undisturbed and disturbed soil cores using a hanging water column for low tensions (5, 10, 15, and 30 cm), a Tempe cell for 60, 100, 200 and 300 cm and pressure plate for the two highest pressures. For the pressure plates, soil cores were placed on the plate and soaked overnight in a pan containing a 0.05 M $CaCl_2$ solution prior to applying each pressure. Gravimetric moisture content was determined after each pressure applied using subsamples of the soil core.

Bromide Analysis

A 10 g air-dried sample was mixed with 20 ml distilled water to produce a 1:2 soil to water ratio. The sample was placed in 50 ml centrifuge tube and shaken for 30 minutes in a reciprocating shaker, then centrifuged at 3000 rpm for 20 min and filtered through filter paper, the extract collected, and the bromide determined on an Alpkem continuous flow spectrophotometer.

Measurement of Saturated and Unsaturated Hydraulic Conductivity for Disturbed and Undisturbed Soil Cores

Saturated hydraulic conductivity was measured using a constant head (Klute and Dirksen, 1986) for six undisturbed samples and three disturbed samples. The same soil cores were used to measure unsaturated hydraulic conductivity (using water retention curve). A hanging water column was used for low tensions of 5, 10, 15 and 30 cm; a Tempe cell for tensions of 60, 100, 200 and 300 cm; and a pressure chamber for higher tensions of 1, 15 bar. The hydraulic parameters of α and n with θ at different tensions have been calculated and fitted using van Genuchten's equations (1980).

CHAPTER 3

CALCULATION OF UNSATURATED HYDRAULIC CONDUCTIVITY AND DISCUSSION

Previous Studies

Measurements of saturated and unsaturated hydraulic conductivity in situ are very important for modeling solute movement, in addition to optimization of agricultural practices such as irrigation, drainage and runoff control. Many researchers have compared the field and laboratory determinations of hydraulic conductivity.

Dane (1980) compared four different procedures. The first procedure consisted of in situ measurements of water content and pressure head profiles following irrigation. The second procedure consisted of a model that used water retention curves and saturated K values determined on undisturbed core samples. The third method was a variation of the second in that water retention data were used as measured in situ. The fourth method used in situ measured water content data only. The four methods resulted in $K(\theta)$ relations that were in fairly good agreement.

Field et al. (1984) compared field and laboratory-measured and predicted hydraulic properties for a soil with macropores. The model of van Genuchten (1980) was successful in predicting unsaturated conductivities within the scatter of in situ values when field-measured moisture retention data were used and the mean in situ

saturated conductivity was employed as a matching point. Correspondence between predicted and in situ conductivities was poorer when using laboratory retention data, reflecting difficulties in obtaining representative undisturbed core samples.

Recently a new method was developed (White and Perroux, 1988; White et al., 1989; Smettem and Clothier, 1989) to measured soil hydraulic properties in situ. Perroux and White (1988) described the use of disc permeameters. They modified the sorptivity instrument of Clothier and White (1981), for the measurement of hydraulic properties of field soils containing macropores and preferential flow paths. White et al. (1989) described a method for determination of hydraulic properties based on Wooding's (1968) three-dimensional flow from a shallow circular pond or disc surface. Data obtained from each infiltration measurement at any supply water potential can be analyzed in terms of the sorptivity for short time and in the term of steady-state flow, for large times. With knowledge of soil moisture content, and bulk density, the hydraulic conductivity and macroscopic capillary length can be calculated.

Smettem and Clothier (1989) introduced a new way for measuring unsaturated sorptivity and hydraulic conductivity using multiple disc permeameters. The proportions of flow contributed by hydraulic conductivity and sorptivity change with radius. These parameters may be obtained by measuring steady state flow for large times using disc of different radii. The advantage of this method is that only long-time, quasi-steady discharges are needed to obtain K_o and S_o. The advantage of the disc permeameter method is that it is simple, efficient, accurate, fast, and requires a small amount of water.

Lien (1989) measured steady state flow at two tensions for the same disc permeameter radius, and he calculated macroscopic capillary length and hydraulic conductivity. His results were consistent to that measured using sorptivity and steady state flow. The approach is somewhat similar to that of Yitayew and Watson (1986) who measured wetting surfaces for multiple flow rates of point sources.

Calculation of Hydraulic Properties Using Disc Permeameters

Sorptivity (S)

Sorptivity is a measure of water uptake by the soil without gravitational effects (Philip, 1969). It is calculated from the cumulative infiltration for short times by

$$I = St^{1/2} \tag{3.1}$$

where I is cumulative infiltration (cm) at time t (sec). S is sorptivity (cm $sec^{-1/2}$) and equal to the slope of the cumulative infiltration versus the square root of time for small times.

Philip (1969) mentioned that during the early stage of infiltration a multiple-dimensional flow system behaves as though one-dimensional and is dominated by capillarity. To estimate the time range of convergence of infiltration rate series solutions for one-dimensional flow, Philip (1969) introduced a gravitational characteristic time

$$t_{grav} = \left(\frac{S}{K_o - K_n} \right)^2 \tag{3.2}$$

where K_o is the hydraulic conductivity at supply potential, K_n is the hydraulic conductivity at initial soil water potential, and t_{grav} represents the order of magnitude of time at which the effect of the gravity on flow equals that of capillarity.

In two-and three-dimensional infiltration flows, the geometry of the system soon overrides the initial one-dimensional character of the capillarity-driven flow. Philip designated a geometrical characteristic time t_{geom} which gives the order of magnitude of this time, where

$$t_{geom} = \left(\frac{r(\theta_o - \theta_n)}{S} \right)^2 \tag{3.3}$$

where θ_o is the moisture content at supply potential, and θ_n is the initial moisture content. The r is a characteristic length of the source of water.

Philip (1986) mentioned that in such time-dependent flows, λ_c (which is the macropore capillary length) is associated with a capillary or sorptive-time scale t_c, which emerges from the scaled flow equation

$$t_c = \frac{\Delta\theta\lambda_c}{\Delta K} \tag{3.4}$$

To infer whether the geometry, capillarity, or gravity dominates time-dependent, multidimensional flows, we need to consider the ratio t_{geom}/t_c. When this ratio is greater than 1, $t_c < t_{geom}$, and capillarity will influence flow before the geometry of the

system is apparent. For $t_{geom} < t_c$ and $t_c < t_{grav}$, flow will move from being capillarity driven to being influenced by the dimensionality of the system before gravity becomes apparent.

Talsma (1969) found the effect of gravity negligible for time less than 0.02 t_{grav}. Smettem and Clothier (1989) mentioned that there is small change in flow rate between 5 min and 2 h for disc permeameter measurements. In our case, the time from 0 to 150 sec was used to calculate sorptivity for each stage by plotting cumulative infiltration versus the square root of time. All the data from time zero has been used for the calculations.

Hydraulic Conductivity (K)

At large times, the steady state flow rate q_∞ (cm^3/s) is determined by both gravity and capillarity as seen in Wooding's (1968) equation

$$q_\infty = \pi r^2 K_o + 4 r K_o \lambda_c \qquad (3.5)$$

where r is the radius of disc permeameter or sand cap. The K_o is the hydraulic conductivity corresponding to the supply potential and the λ_c is the macropore capillary length. The first term on the right of equation 3.5 represents the contribution of gravity to the total flow from the surface disc and the second term represents the contribution of capillarity to the flow.

White and Sully (1987) showed that λ_c is a function of the sorptivity and the hydraulic conductivity.

$$\lambda_c = bS_o^2/[(\theta_o - \theta_n)K_o] \quad (3.6)$$

where θ_o is the moisture content at supply potential, θ_n is the initial moisture content, S_o is the sorptivity at the supply potential and b is a dimensionless constant with values between 1/2 and $\pi/4$. The b depends only on initial and supply potential (λ_n, λ_o) and the shape of the soil-water diffusivity ($D = K\, d\psi/d\theta$). They suggested that $b = 0.55$ is a reasonable approximation for most situations, a value confirmed by Warrick and Broadbridge (1991) for several hydraulic functions. The larger the λ_c, the higher the contribution of capillarity to the flow transport process.

Equations 3.5 and 3.6 can be considered together to give:

$$q_\infty = \pi r^2 K_o + 4rbS_o^2/(\theta_o - \theta_n) \quad (3.7)$$

The corresponding steady state flow rate per unit area is:

$$q_\infty/\pi r^2 = K_o + 4bS_o^2/[\pi r(\theta_o - \theta_n)] \quad (3.8)$$

or by considering $b = 0.55$ is

$$\frac{q_\infty}{\pi r^2} = K_o + 2.2S_o^2/[\pi r(\theta_o - \theta_n)] \quad (3.9)$$

The value of $q_\infty/\pi r^2$ for large time can be found by plotting the cumulative infiltration versus time. S is calculated as a slope of cumulative infiltration versus the square root of time (Figure 3.1) and the slope of the linear plot at large times is the steady state flow rate $q_\infty/\pi r^2$ (Figs. 3.2, 3.3, 3.4, and 3.5). Therefore, for each field

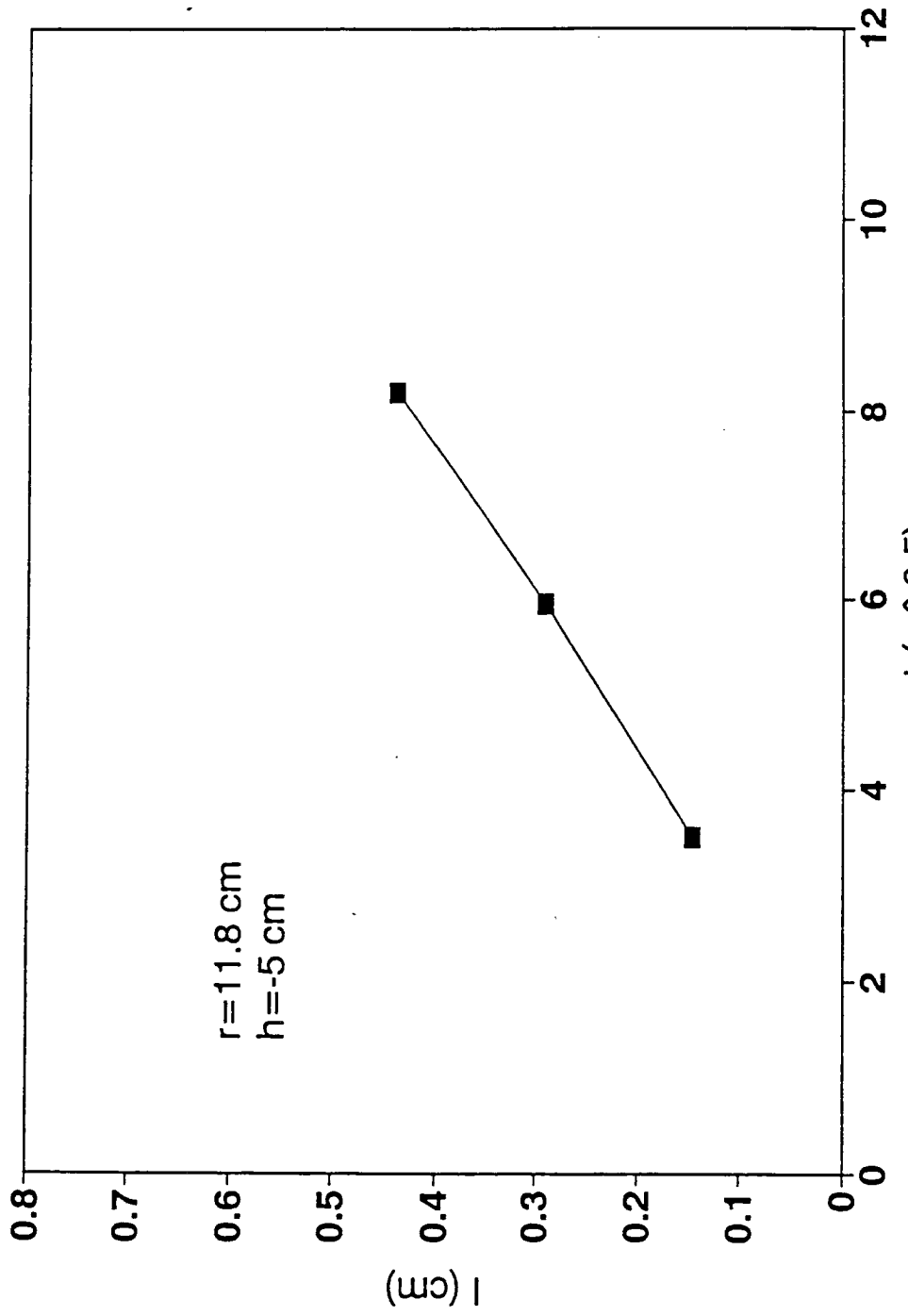

Figure 3.1. Infiltration vs. square root of short time at -15 cm tension. Second replicate.

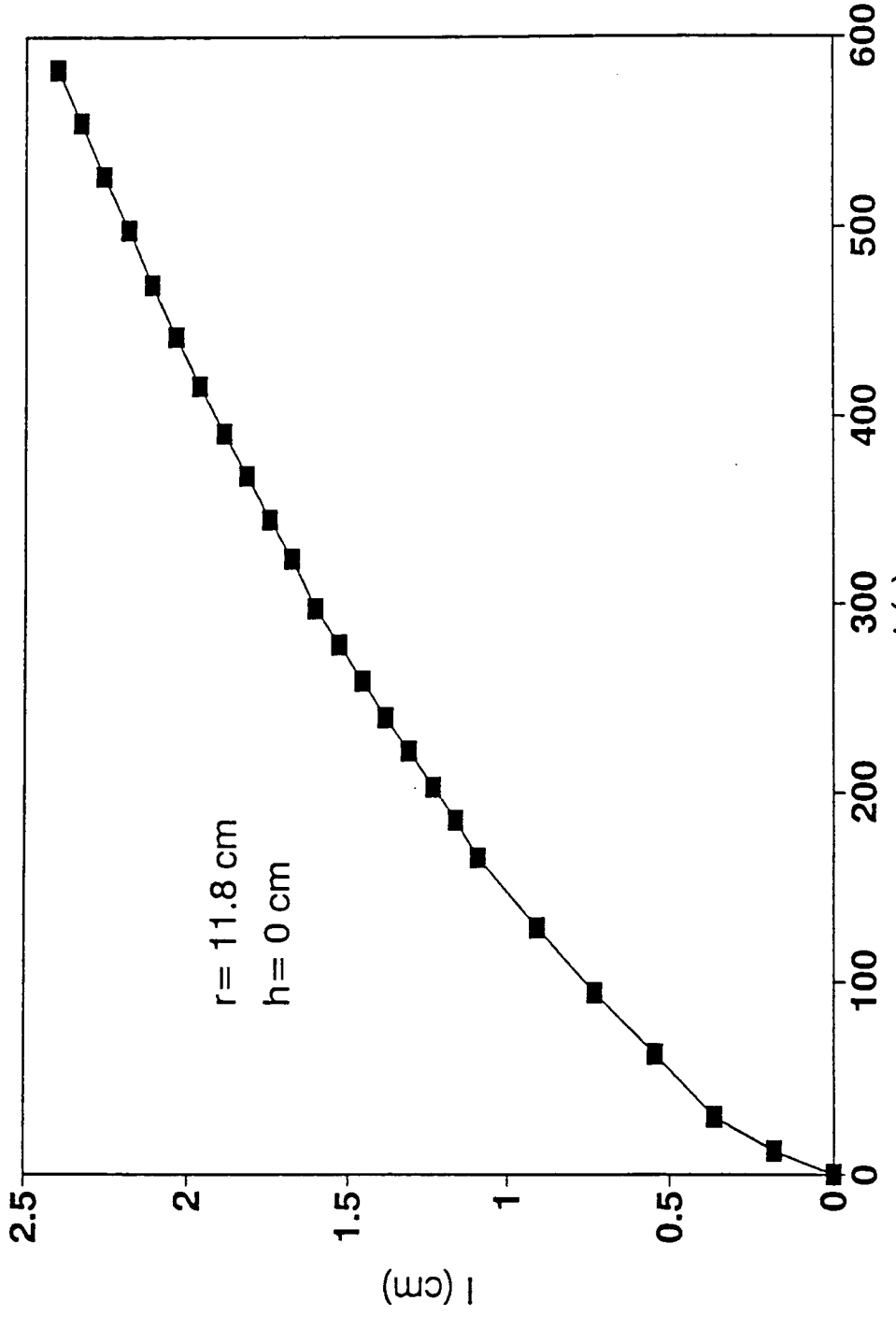

Figure 3.2. Infiltration vs. large time to measured steady state flow (zero cm tension).

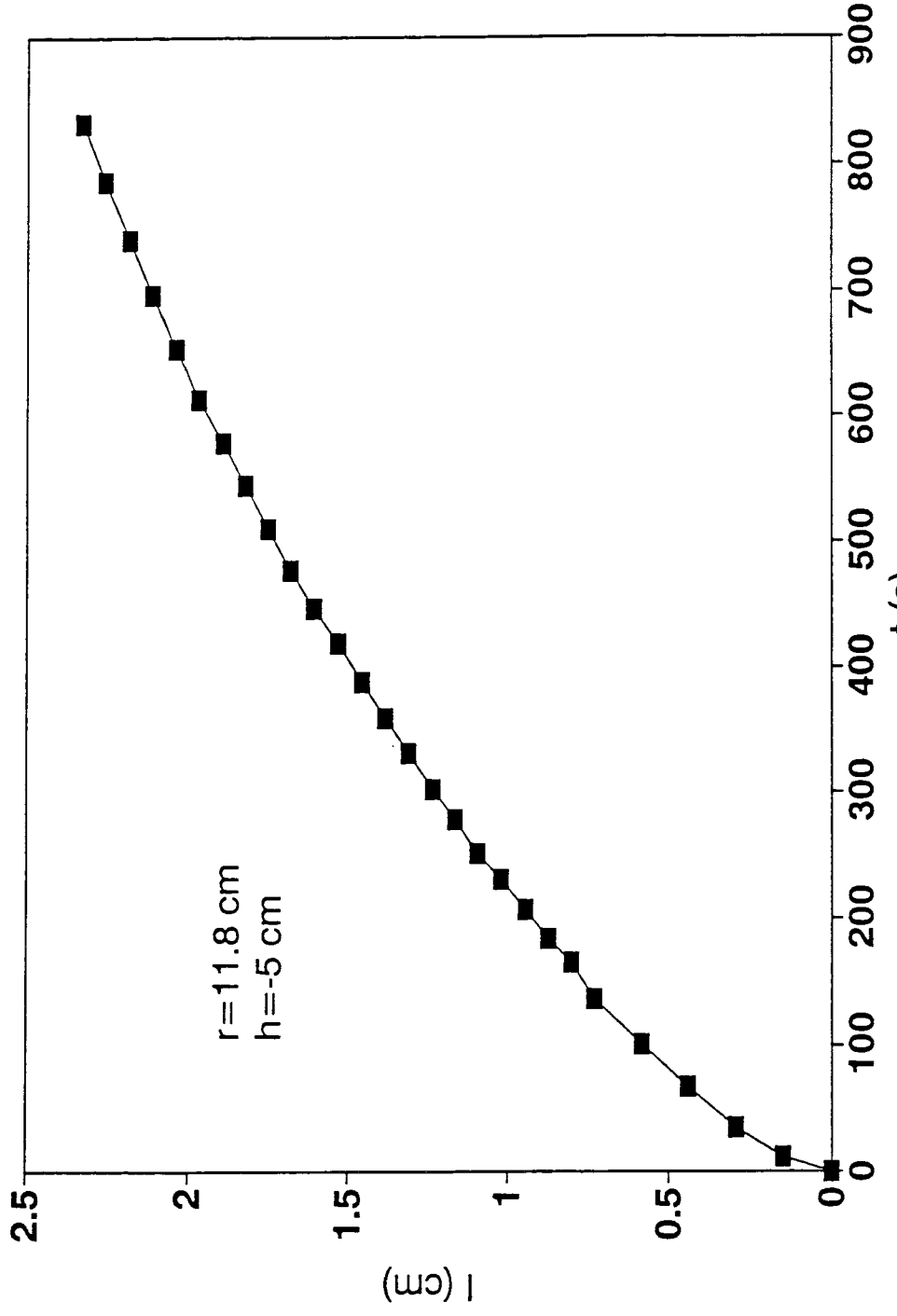

Figure 3.3. Infiltration vs. time to measured steady state flow (five cm tension).

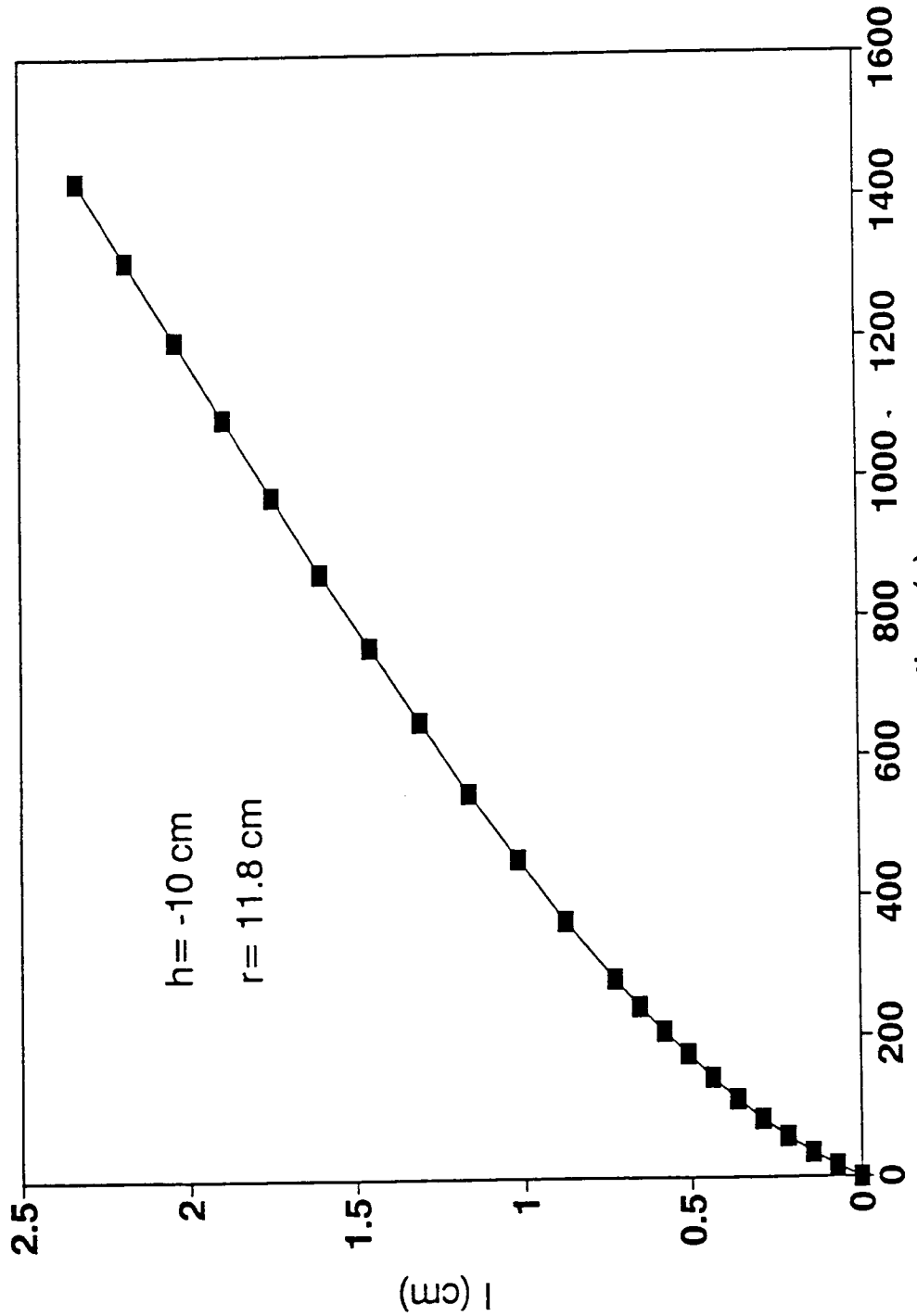

Figure 3.4. Infiltration vs. large time to measured steady state flow (ten cm tension).

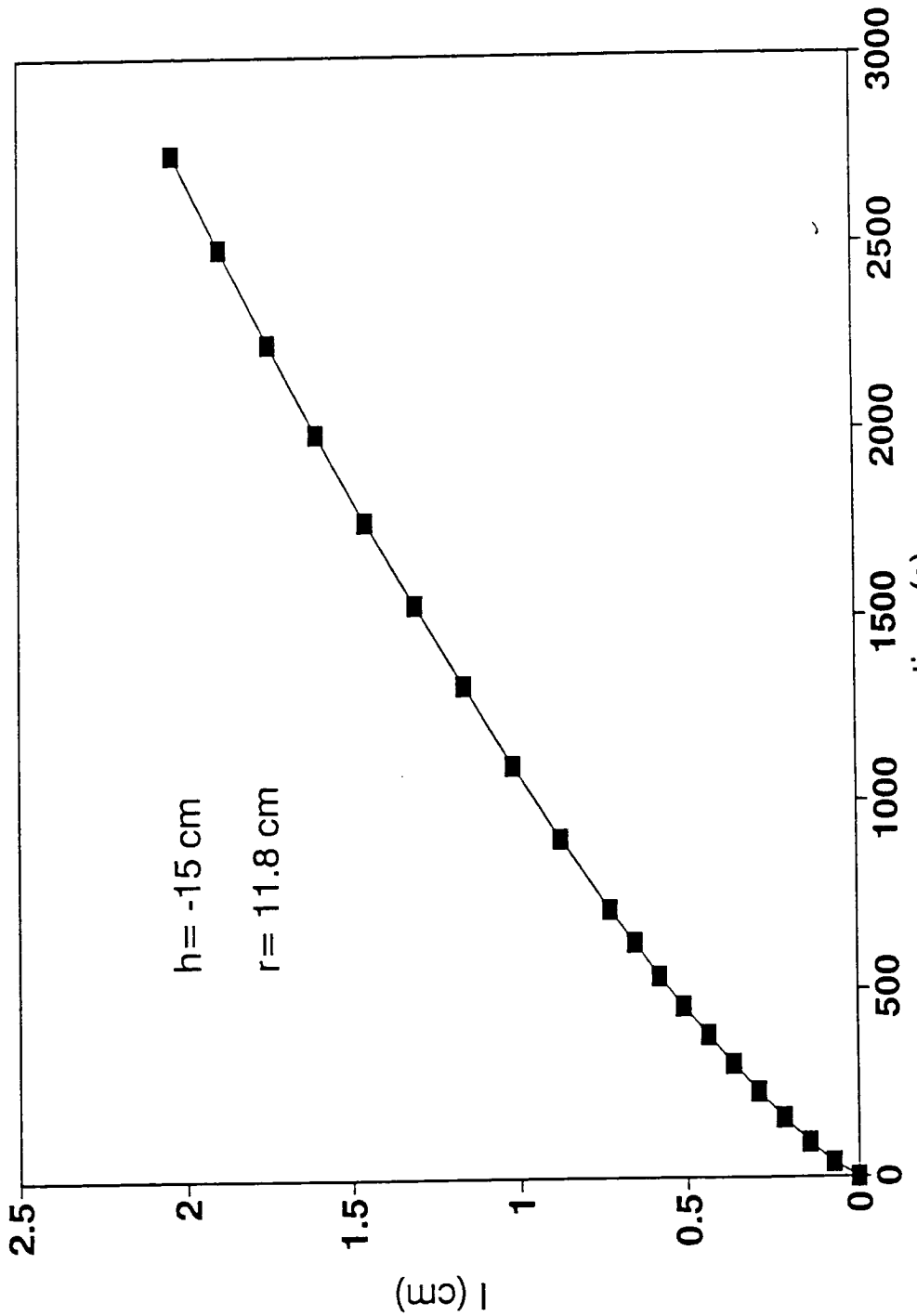

Figure 3.5. Infiltration vs. large time to measured steady state flow (fifteen cm tension).

measurement, once the steady state flow rate, sorptivity, initial and final soil moisture content and the area of source were determined, the hydraulic conductivity can be found by

$$K_o = q_\infty/\pi r^2 - 2.2S_o^2/[\pi r(\theta_o - \theta_n)] \qquad (3.10)$$

Equation 3.7 has been used for calculating the hydraulic conductivity using the single disc method and to calculate unsaturated hydraulic conductivity at different tensions (0, 5, 10 and 15 cm).

The second method to measure hydraulic conductivity is the multiple disc method which depends on solving Wooding's (1968) equation 3.5 for two different disc radii at the same tension and solving for the two unknowns λ_c and K_o. Rewriting Wooding's equation gives

$$Q_\infty = K_o\left(1 + \frac{4\lambda_c}{\pi r}\right) \qquad (3.11)$$

where $Q_\infty = \frac{q_\infty}{\pi r^2}$ is the steady state flow rate (cm/s). The only measurement we need is the steady state flow for the same tension for different disc radius, in order to solve for λ_c

$$\lambda_c = \frac{\pi}{4}\left[\frac{(Q_\infty^1 - Q_\infty^2)}{\frac{Q_\infty^2}{r_1} - \frac{Q_\infty^1}{r_2}}\right] \qquad (3.12)$$

where Q_∞^1 and Q_∞^2 are the steady state flow rate for large and small discs, respectively, r_1 and r_2 are the radius of large and small disc, respectively. Then substitute λ_c in equation 3.8 and solve for K_o

Steady state flow for large time was measured using different radii (small disc sand cap radius 5.2 cm and large disc sand cap radius 11.6 cm) side by side for four tensions (0, 5, 10 and 15 cm) with three replicates (Fig. 2.3).

Calculation of Hydraulic Properties Using Disturbed and Undisturbed Soil Cores

The soil water retention curve was used to calculate unsaturated hydraulic conductivity at 5, 10 and 15 cm. The closed forms of van Genuchten's equations (1980) used for that purpose are:

$$S = \frac{\theta - \theta_r}{\theta_s - \theta_r} = [1 + (1 + (\alpha h)^{1/(1-m)}]^{-m} \qquad (3.13)$$

$$K = K_s S^{1/2}[1 - (1 - S^{1/m})^m]^2 \qquad (3.14)$$

Where θ_s and θ_r are saturated and residual water content, K_s is saturated hydraulic conductivity, K is unsaturated hydraulic conductivity, h is absolute value of pressure

head, α and m are empirical parameters describing the shape of the soil water retention curve.

A program written by DaSilva (1990) was used to find the best fitting hydraulic permeameters α and m. The fitted parameters used for each tension and replicate to calculate unsaturated hydraulic conductivity using equations 3.13 and 3.14, as well as the output of these parameters and the fitted data, are shown in Appendix A.

Results and Discussion

Table 3.1 shows the sorptivity volumetric water content, steady state flow, and unsaturated hydraulic conductivity using both the single disc (Eq. 3.7) and the double disc (Eqs. 3.11 and 3.12) methods with four tensions used (0, 5, 10 and 15 cm). Table 3.2 shows the hydraulic conductivity at different tensions using four methods, single and double disc permeameters (in situ measurement), disturbed soil cores, and undisturbed soil cores (laboratory measurement). The value of hydraulic conductivity increases with decreasing tension for all four methods. The lowest value (0.93 cm/h) is at the 15 cm tension in disturbed cores and the highest value of 5.63 cm/h at zero tension for an undisturbed soil core.

An analysis of variance (ANOVA) was applied to compare unsaturated hydraulic conductivity measured using different methods at four different water tensions (0, 5, 10 and 15 cm). The hypothesis for the analysis is no significant

Table 3.1. Showing the sorptivity (cm $s^{-0.5}$), steady state flow (cm s^{-1}) and hydraulic conductivity (cm s^{-1}) using both single disc method and double disc method and the % of error.

Code*	θ_{dry}	θ_{wet}	S	St. Flow	λ_c	K.Mult	K.Single	% Err**
B151	1.80	27.38	.0230	.0006	1.003	.0005	.0005	-14.0
B152	1.67	27.83	.0230	.0006	1.392	.0005	.0005	- 9.6
B153	1.73	27.05	.0230	.0006	1.089	.0005	.0004	-14.1
B101	1.86	28.31	.0514	.0013	7.440	.0007	.0007	- 1.1
B102	1.76	28.94	.0434	.0012	7.443	.0006	.0007	13.8
B103	2.18	28.97	.0474	.0013	7.203	.0007	.0008	8.7
B51	2.18	30.43	.0618	.0016	9.236	.0008	.0008	- 3.4
B52	2.06	29.84	.0619	.0016	9.388	.0008	.0008	- 2.0
B53	2.38	30.43	.0645	.0016	10.629	.0008	.0007	- 1.9
B01	2.06	32.37	.0920	.0024	15.558	.0009	.0011	16.9
B02	2.18	32.82	.0826	.0024	15.863	.0009	.0011	19.1
B03	2.12	32.60	.0831	.0026	14.001	.0010	.0012	16.1
S151	1.80	27.13	.0242	.0007			.0003	
S152	1.67	26.30	.0270	.0007			.0003	
S153	1.73	26.87	.0262	.0006			.0003	
S101	1.86	28.58	.0511	.0021			.0007	
S102	1.76	29.69	.0469	.0018			.0007	
S103	2.18	29.18	.0505	.0020			.0007	
S51	2.18	30.61	.0594	.0025			.0009	
S52	2.06	30.18	.0648	.0026			.0008	
S53	2.38	30.15	.0612	.0027			.0009	
S01	2.06	32.22	.0842	.0043			.0011	
S02	2.18	31.87	.0849	.0044			.0011	
S03	2.12	32.50	.0862	.0045			.0012	

*B is the big disc permeameter followed by tension used (0, 5, 10 or 15 cm), and the last number is the replicate (1, 2, or 3).

** % of error in K measured using single disc method and double disc method.

Table 3.2. Results for different methods for measuring K (cm/h), single and double disc, disturbed and undisturbed soil cores.

	K(cm/h)			
CODE*	Single	Multiple	Disturbed	Undisturbed
B151	1.65	1.88	0.93	1.70
B152	1.65	1.81	1.45	1.71
B153	1.61	1.83	1.27	1.61
B101	2.60	2.63	1.32	2.41
B102	2.67	2.30	2.01	2.58
B103	2.87	2.62	1.76	2.16
B51	2.71	2.80	2.31	3.43
B52	2.80	2.85	2.76	4.12
B53	2.66	2.71	2.45	3.01
B01	3.87	3.21	3.23	5.39
B02	3.99	3.23	3.88	5.63
B03	4.38	3.67	3.66	5.15

*B is the big disc permeameter followed by tension used (0, 5, 10 or 15 cm), and the last number is the replicate (1, 2, or 3).

Table 3.3a. One way ANOVA of unsaturated hydraulic conductivity (cm/h) for four methods at zero cm tension.

Source	SS	df	MS	F
Methods	7.39	3	2.46	31.86***
Error	0.62	8	0.077	
Total	8.01	11		

*** highly significant difference at 99.9% confidence level.

Table 3.3b. Student-Newman-Keults Test of unsaturated hydraulic conductivity (cm/h) for four methods at zero cm tension.

Factor: Methods
Error mean square = 0.077
Degrees of freedom = 8
Significance level = .01
LSD .01 = 0.76

Rank	Trt #	Mean	n	Non-significant ranges†
1	2	3.37	3	a
2	3	3.59	3	a
3	1	4.08	3	a
4	4	5.39	3	b

1-single disc method, 2-double disc method, 3-disturbed soil core method and 4-undisturbed soil core.

† Treatments followed by the same letter are not significantly different at $P < 0.01$.

difference of unsaturated hydraulic conductivity among the four methods. If the methods variation is significantly larger than the experimental error, then the differences between the methods is said to be real and significant based on a complete randomized design (Gomez and Gomez, 1984, esp. p. 7-20).

Results from the analysis of variance (Table 3.3a) for hydraulic conductivity at zero tension show significant differences between the methods used at the 99.9% confidence level. Meanwhile, in Table 3.3b, the Student-Newman-Keults Test shows that there are no significant differences between the mean of unsaturated hydraulic conductivity measured using single disc, double disc and disturbed soil core methods at the 99% confidence level, and there is significant differences between the undisturbed soil core method for measuring unsaturated hydraulic conductivity and other methods at 99% confidence level.

Table 3.4a show the results of analysis of variance for 5 cm tension hydraulic conductivity using four different methods. There are significant differences between the methods used to measure unsaturated hydraulic conductivity at the 95% confidence level. A comparison of the mean of unsaturated hydraulic conductivity by the different methods using a Student-Neuman-Keults Test (Table 3.4b) shows that there are no significant differences at the 99% confidence level between methods used.

The analysis of variance using different methods for measuring unsaturated hydraulic conductivity at 10 cm tension (Table 3.5a) shows that there are significant

Table 3.4a. One way ANOVA of unsaturated hydraulic conductivity (cm/h) for four methods at 5 cm tension.

Source	SS	df	MS	F
Methods	1.81	3	0.06	6.77*
Error	0.71	8	0.09	
Total	2.53	11		

* highly significant difference at 95% confidence level.

Table 3.4b. Student-Newman-Keults Test of unsaturated hydraulic conductivity (cm/h) for four methods at 5 cm tension.

Factor: Methods
Error mean square = 0.09
Degrees of freedom = 8
Significance level = .01
LSD .01 = 0.82

Rank	Trt #	Mean	n	Non-significant ranges†
1	3	2.48	3	a
2	1	2.72	3	a
3	2	2.79	3	a
4	4	3.52	3	a

1-single disc method, 2-double disc method, 3-disturbed soil core method and 4-undisturbed soil core.

† Treatments followed by the same letter are not significantly different at $P < 0.01$.

Table 3.5a. One way ANOVA of unsaturated hydraulic conductivity (cm/h) for four methods at 10 cm tension.

Source	SS	df	MS	F
Methods	1.78	3	0.59	10.52**
Error	0.45	8	0.056	
Total	2.23	11		

** highly significant difference at 99% confidence level.

Table 3.5b. Student-Newman-Keults Test of unsaturated hydraulic conductivity (cm/h) for four methods at 10 cm tension.

Factor: Methods
Error mean square = 0.056
Degrees of freedom = 8
Significance level = .01
LSD .01 = 0.65

Rank	Trt #	Mean	n	Non-significant ranges†
1	3	1.69	3	a
2	4	2.38	3	b
3	2	2.51	3	b
4	1	2.71	3	b

1-single disc method, 2-double disc method, 3-disturbed soil core method and 4-undisturbed soil core.

† Treatments followed by the same letter are not significantly different at $P < 0.01$.

Analysis of variance for unsaturated hydraulic conductivity for 15 cm tension

differences between the methods used at the 99% confidence level. On the other hand, the Student-Newman-Keults Test (Table 3.5b) shows that there are significant differences at the 99% confidence level only between the disturbed core results and the other three methods.

Analysis of variance for unsaturated hydraulic conductivity for 15 cm tension (Table 3.6a) shows that there are significant differences between methods used at the 99% confidence level. The Student-Newman-Keults Test (Table 3.6b) shows that there are no significant differences at the 99% confidence level between the methods except for the disturbed soil core method.

We concluded that there is no significant difference between the means of measured hydraulic conductivity in all the tensions using single and double disc methods. Apparently, the undisturbed soil core more closely represents soil conditions in situ than the disturbed soil core for measuring unsaturated hydraulic conductivity under laboratory conditions as evidenced by Table 3.2.

Operationally, the double disc method is much faster and easier to measure hydraulic conductivity in situ than the single disc method. This is because we do not need small time measurements for finding the sorptivity which is a function of water content in soil and critical in measuring wet or moist soil. Also, we do not need to take soil water content in the beginning and at the end of the measurement for steady-state methods.

Table 3.6a. One way ANOVA of unsaturated hydraulic conductivity (cm/h) for four methods at 15 cm tension.

Source	SS	df	MS	F
Methods	0.63	3	0.211	11.31***
Error	0.15	8	0.018	
Total	8.01	11		

*** highly significant difference at 99.9% confidence level.

Table 3.6b. Student-Newman-Keults Test of unsaturated hydraulic conductivity (cm/h) for four methods at 15 cm tension.

Factor: Methods
Error mean square = 0.019
Degrees of freedom = 8
Significance level = .01
LSD .01 = 0.37

Rank	Trt #	Mean	n	Non-significant ranges†
1	3	1.22	3	a
2	1	1.64	3	b
3	4	1.67	3	b
4	2	1.84	3	b

1-single disc method, 2-double disc method, 3-disturbed soil core method and 4-undisturbed soil core.

† Treatments followed by the same letter are not significantly different at $P < 0.01$.

CHAPTER 4

LAND PREPARATION EFFECT ON HYDRAULIC CONDUCTIVITY

Pivetz and Steenhuis (1989) found that the dye solution in no-till plots moved preferentially through the earthworm burrows of the upper layer which was not disturbed by plowing. Roth et al. (1990) refers to preferential flow as the rapid transport of water and solutes through some small portion of soil volume. Mechanisms which contribute to flow could include movement through structure voids and instable flow of the invading fluid.

I studied the effect of land preparation on the hydraulic conductivity at different tensions using the double disc method to measure the hydraulic conductivity. Table 4.1 shows the steady state flow and unsaturated hydraulic conductivity in two different plots -- one was disturbed and the other undisturbed (Fig. 2.3). We found that the hydraulic conductivity in disturbed soil was higher than the undisturbed soil for all the tensions (0, 5, 10, and 15 cm), thus disturbance increases the hydraulic conductivity on the soil surface. Comparing the average decrease in hydraulic conductivity for the three replicates at the four tensions, we find that the greatest decrease was for the 15 cm tension, followed by the 10, 5 and finally 0 cm tensions. That means that disturbing the soil had a larger effect on the hydraulic conductivity at the highest tension then that at the lower tension. In other words, disturbance increased the macropores generally but its increase is much higher in smaller macropores than in bigger macropores.

Table 4.1. Comparing K between disturbed and undisturbed soil.

	Undisturbed		Disturbed			
Code*	Steady Flow (cm/s)	K (cm/h)	Steady Flow (cm/s)	K (cm/h)	Dec. K%	Av. Dec.K
B151	.0004	1.433	.0009	3.024	52.613	43.731
B152	.0005	1.622	.0008	2.602	37.235	
B153	.0005	1.789	.0009	3.049	41.347	
B101	.0005	1.808	.0011	3.755	51.848	41.940
B102	.0006	2.093	.0010	3.672	43.004	
B103	.0007	2.467	.0107	3.574	30.967	
B51	.0009	3.028	.0015	4.807	37.006	31.345
B52	.0010	3.108	.0014	4.474	30.540	
B53	.0010	3.094	.0014	4.209	26.488	
B01	.0014	4.151	.0020	5.845	28.985	25.657
B02	.0015	4.058	.0019	5.393	24.760	
B03	.0015	4.038	.0018	5.260	23.226	
S151	.0005		.0010			
S152	.0005		.0008			
S153	.0005		.0010			
S101	.0006		.0011			
S102	.0007		.0011			
S103	.0008		.0012			
S51	.0009		.0017			
S52	.0011		.0015			
S53	.0011		.0016			
S01	.0016		.0024			
S02	.0019		.0024			
S03	.0019		.0023			

*B is the big disc permeameter and S is the small disc permeameter followed by the tension used (0, 5, 10 or 15), and the last number is the replicate (1, 2 or 3).

An analysis of variance was applied to compare the effects of land preparation on the hydraulic conductivity at different tensions. Complete randomized design has been used to compare hydraulic conductivity at each tension on disturbed and undisturbed soil. The hypothesis for the analysis is no significant difference in hydraulic conductivity between disturbed and undisturbed soil.

Results from the analysis of variance (Tables 4.2, 4.3, 4.4 and 4.5) showed significant differences between hydraulic conductivity at different tensions in disturbed and undisturbed soil at the 99% confidence level. We concluded that disturbing the soil increased the hydraulic conductivity at all the tensions.

Table 4.2a. One way ANOVA of unsaturated hydraulic conductivity (cm/h) for disturbed and undisturbed soil at zero tension.

Source	SS	df	MS	F
Main Effects				
K	3.00	1	3.00	62.38**
Error	0.19	4	0.05	
Total	3.19	5		

**highly significant difference at 99% confidence level.

Table 4.2b. Student-Newman-Keults Test of unsaturated hydraulic conductivity (cm/h) for disturbed and undisturbed soil at zero tension.

Factor: K
Error Mean square = 0.05
Degrees of freedom = 4
Significance level = .01
LSD .01 = 0.82

Rank	Treatment #	Mean	n	Non-significant ranges †
1	1	4.08	3	a
2	2	5.50	3	b

1 - undisturbed soil, 2 - disturbed soil.

† Treatments followed by the same letter are not different at $p < 0.01$.

Table 4.3a. One way ANOVA of unsaturated hydraulic conductivity (cm/h) for disturbed and undisturbed soil at five cm tension.

Source	SS	df	MS	F
Main Effects				
K	3.02	1	3.02	65.56**
Error	0.18	4	0.05	
Total	3.21	5		

**highly significant difference at 99% confidence level.

Table 4.3b. Student-Newman-Keults Test of unsaturated hydraulic conductivity (cm/h) for disturbed and undisturbed soil at five cm tension.

Factor: K
Error mean square = 0.05
Degrees of freedom = 4
Significance level = .01
LSD .01 = 0.81

Rank	Treatment #	Mean	n	Non-significant ranges †
1	1	3.08	3	a
2	2	4.50	3	b

1 - undisturbed soil, 2 - disturbed soil.

† Treatments followed by the same letter are not different at $p < 0.01$.

Table 4.4a. One way ANOVA of unsaturated hydraulic conductivity (cm/h) for disturbed and undisturbed soil at ten cm tension.

Source	SS	df	MS	F
Main Effects				
K	3.56	1	3.56	60.36**
Error	0.24	4	0.06	
Total	3.79	5		

**highly significant difference at 99% confidence level.

Table 4.4b. Student-Newman-Keults Test of unsaturated hydraulic conductivity (cm/h) for disturbed and undisturbed soil at ten cm tension.

Factor: K
Error mean square = 0.059
Degrees of freedom = 4
Significance level = .01
LSD .01 = 0.91

Rank	Treatment #	Mean	n	Non-significant ranges †
1	1	2.12	3	a
2	2	3.66	3	b

1 - undisturbed soil, 2 - disturbed soil.

† Treatments followed by the same letter are not different at $p < 0.01$.

Table 4.5a. One way ANOVA of unsaturated hydraulic conductivity (cm/h) for disturbed and undisturbed soil at fifteen cm tension.

Source	SS	df	MS	F
Main Effects				
K	2.43	1	2.43	50.76**
Error	0.19	4	0.05	
Total	2.63	5		

**highly significant difference at 99% confidence level.

Table 4.5b. Student-Newman-Keults Test of unsaturated hydraulic conductivity (cm/h) for disturbed and undisturbed soil at fifteen cm tension.

Factor: K
Error mean square = 0.048
Degrees of freedom = 4
Significance level = .01
LSD .01 = 0.82

Rank	Treatment #	Mean	n	Non-significant ranges †
1	1	1.62	3	a
2	2	2.89	3	b

1 - undisturbed soil, 2 - disturbed soil.

† Treatments followed by the same letter are not different at $p < 0.01$.

CHAPTER 5

SPATIAL VARIATION AND VARIOGRAM MODELING FOR HYDRAULIC PROPERTIES

The most basic tool of geostatistics is the variogram function which expresses the spatial correlation of adjoining samples. This spatial correlation is the structured aspect of regionalized variables and, hence, also of the underlying random process. Also, variograms provide other useful information such as the range of influence of the sample.

Let us consider a random function which has realization $Z(x_1)$, $Z(x_2)$, ..., $Z(x_n)$ at locations x_1, x_2, ..., x_n defined as points in two dimensional space. The variogram is defined (Journel and Huijbregts, 1978) as

$$\gamma(h) = \left(\frac{1}{2}\right) \text{Var } [Z(x + h) - Z(x)] \tag{5.1}$$

Where Var is the variance, $Z(x)$ is the random function at x, and $Z(x + h)$ is the random function at $x + h$, with h the distance apart. The graph of $\gamma(h)$ against h distance is called variogram, with an unbiased estimator $\gamma^*(h)$ of

$$\gamma*(h) = \frac{1}{2N(h)} \sum_{i=1}^{N} [Z(x + h) - Z(x)]^2 \tag{5.2}$$

where $\gamma^*(h)$ is the sample variogram. The variogram has no general formula to describe its shape, but there are several acceptable mathematical models. Common models are linear, spherical, exponential, gaussian, and Michaelis-Menton.

The spherical model is defined by

$$\gamma(h) = C_o + C\left[\left(\frac{3}{2}\right)\left(\frac{h}{a}\right) - \left(\frac{1}{2}\right)\left(\frac{h}{a}\right)^3\right], \qquad 0 \le h \le a$$
$$\gamma(h) = C_o + C, \qquad h > a \tag{5.3}$$

The exponential model is

$$\gamma(h) = C_o + C\,(1 - e^{-h/a}), \qquad h > 0 \tag{5.4}$$

The linear model without a sill is

$$\gamma(h) = C_o + rh, \qquad h > 0 \tag{5.5}$$

The linear model with a sill is

$$\gamma(h) = C_o + C\left(\frac{h}{a}\right), \qquad 0 \le h \le a$$
$$= C_o + C, \qquad h > a \tag{5.6}$$

The gaussian model is

$$\gamma(h) = C_o + C\,[1 - e^{(-h/a)^2}] \qquad \text{for } h > 0 \tag{5.7}$$

The Michaelis-Menton model is

$$\gamma(h) = C_o + C\left[\left(\frac{h}{a}\right) \Big/ \left(1 + \frac{h}{a}\right)\right] \tag{5.8}$$

In the above equations "a" is the range and is related to the limit of spatial dependence of the property. "C_o" is the nugget, and corresponds to the random variability and the value of $\gamma(h)$ as h approaches zero. The "$C_o + C$" is the sill which

represents the total variability and maximum attained by the variogram. In 5.5, "r" is the slope and the linear model has no maximum.

Fitting a theoretical variogram model is often quite simple, as long as the experimental data is well behaved. Usually, visual fits are satisfactory under these conditions. Unfortunately, some experimental data do not closely resemble any of the theoretical models.

Cross-validation is a technique used to evaluate the adequacy of the variogram model for experimental data. A model that minimizes the estimation errors of Z is desirable. For the most usual approach, the method consists of deleting the measured value Z_i and finding an estimate Z_i^* by kriging using the rest of the measured values. Desirable results for cross-validation of actual and estimated values include (Samper-Calvete, 1986; Russo and Jury, 1987):

(1) The mean error (ME) should be close to zero where

$$ME = \left(\frac{1}{n}\right) \sum_{i=1}^{N} (Z_i^* - Z_i) \tag{5.9}$$

where n is the number of measured locations.

(2) The mean square error (MSE) should be a minimum

$$MSE = \left(\frac{1}{n}\right) \sum_{i=1}^{n} (Z_i^* - Z_i)^2 \tag{5.10}$$

(3) The average kriging variance (AKV) should be a minimum and equal to the expected MSE.

$$AKV = \left(\frac{1}{n}\right) \sum_{i=1}^{n} \sigma_K^2 \tag{5.11}$$

(4) The reduced mean error (RME) should be close to zero

$$RME = \left(\frac{1}{n}\right) \sum_{i=1}^{n} \frac{(Z_i^* - Z_i)}{\sigma_{Ki}} \tag{5.12}$$

(5) The variance of errors (VE) should approximately equal to average kriging variance (AKV).

$$VE = \left(\frac{1}{n}\right) \sum_{i=1}^{n} [(Z_i^* - Z_i) - \overline{(Z_i^* - Z_i)}]^2 \tag{5.13}$$

where $\overline{(Z_i^* - Z_i)}$ is the average error between measured value and estimate value.

(6) The correlation coefficient between kriged and measured values should be close to one.

(7) The negative log likelihood (NLL) should be a minimum (Samper and Newman, 1989a).

$$NLL = M \ln(2\pi) + \sum_{i=1}^{M} \ln(\sigma_i^2) + \sum_{i=1}^{M} \left(\frac{l_i}{\sigma_i}\right)^2 \tag{5.14}$$

where M is the number of observations, l_i the difference between the observed and kriged $(Z_i^* - Z_i)$ values at the point i, and σ_i the kriging standard deviation at point i.

The seven criteria above are all desirable, but can be contradictory. An over reliance on a single criteria can be misleading. As an example, if Z_i^* is taken as the mean value, the ME will be 0. This would be excellent with respect to (5.9) but would not be optimal for the remaining criteria.

Spatial Variation for Hydraulic Conductivity

Unsaturated hydraulic conductivity at 0, 5 cm, 10 cm, and 15 cm tensions were determined along the transect using the double disc method. The result of hydraulic conductivity at different tensions (70 points) is shown in Appendix B. The average semi-variance $\gamma^*(h)$ by interval was calculated according to Eq. 5.2 based on 70 data points using a program GAM2D.BAS (personal communication, A. W. Warrick). The sample variograms are plots of $\gamma^*(h)$ vs. h. The variogram model was fitted using a program VARCAL1.BAS (personal communication, R. Zhang) based on minimizing the sum of square error (SS) with pair weighting, that is,

$$SS = \Sigma w_i [\gamma(h_i) - \gamma^*(h_i)]^2 \qquad (5.15)$$

where the weight w_i depends on pairs with a class of sample variogram, $\gamma^*(h_i)$ is the sample variogram and $\gamma(h_i)$ value of variogram model at distance h_i. The variogram model was from the output of the program and based on combining (5.15) with the above criteria. Specifically, consideration was made that

(1) Sum of square error (SS) should be minimized.

(2) Slope of linear regression between sample and modeled variograms should be close to one.

(3) Intercept should be close to zero.

The exponential models were the best fitting models for hydraulic conductivity at 5 cm, 10 cm, and 15 cm tension. Zero tension hydraulic conductivity appeared random.

Cross-validation was used to adjust parameters of the models. Maximum likelihood method was used to estimate values at each sampled location by kriging with the chosen model and the neighboring sample values. The estimates were compared to the original values in order to test if the hypothetical variogram model will accurately reproduce the spatial variability of sample observations.

A program CR.BAS (personal communication, Dr. A.W. Warrick) was used for cross-validation to adjust parameters of the variogram models. The results of the original variogram model parameters and adjusted parameters are shown in Table 5.1 and Figures 5.1, 5.2, and 5.3 for unsaturated K at tension 15 cm, 5 cm and 10 cm, respectively. The fitted and adjusted models have been plotted beyond half of transect in the figures.

Spatial Variation for Steady State Flow at Different Tensions

Steady state flow for large disc permeameters at different tensions (0, 5, 10 and 15 cm) has been calculated and is shown in Appendix B. These eliminated pore radii (cm) larger than

Table 5.1. Fitted models and adjusted exponential models parameters using cross validation for 70 points. (Unsaturated hydraulic conductivity at 5, 10, and 15 cm tension).

Fitted Models Parameters								
Tension	C_o	C	Range	Mean	VAR	ME	MSE	NLL
15	0.357	0.365	30.98	1.93	0.51	0.007	0.42	136.48
10	0.458	0.861	6.60	3.29	1.13	0.006	0.78	179.28
5	0.482	0.910	6.14	3.91	1.21	0.005	0.87	186.93

Adjusted Models Parameters								
Tension	C_o	C	Range	Mean	VAR	ME	MSE	NLL
15	0.27	0.47	26	1.93	0.51	0.006	0.42	136.54
10	0.25	1.10	7	3.29	1.13	0.002	0.79	180.31
5	0.25	1.10	4.2	3.91	1.21	0.000	0.86	185.76

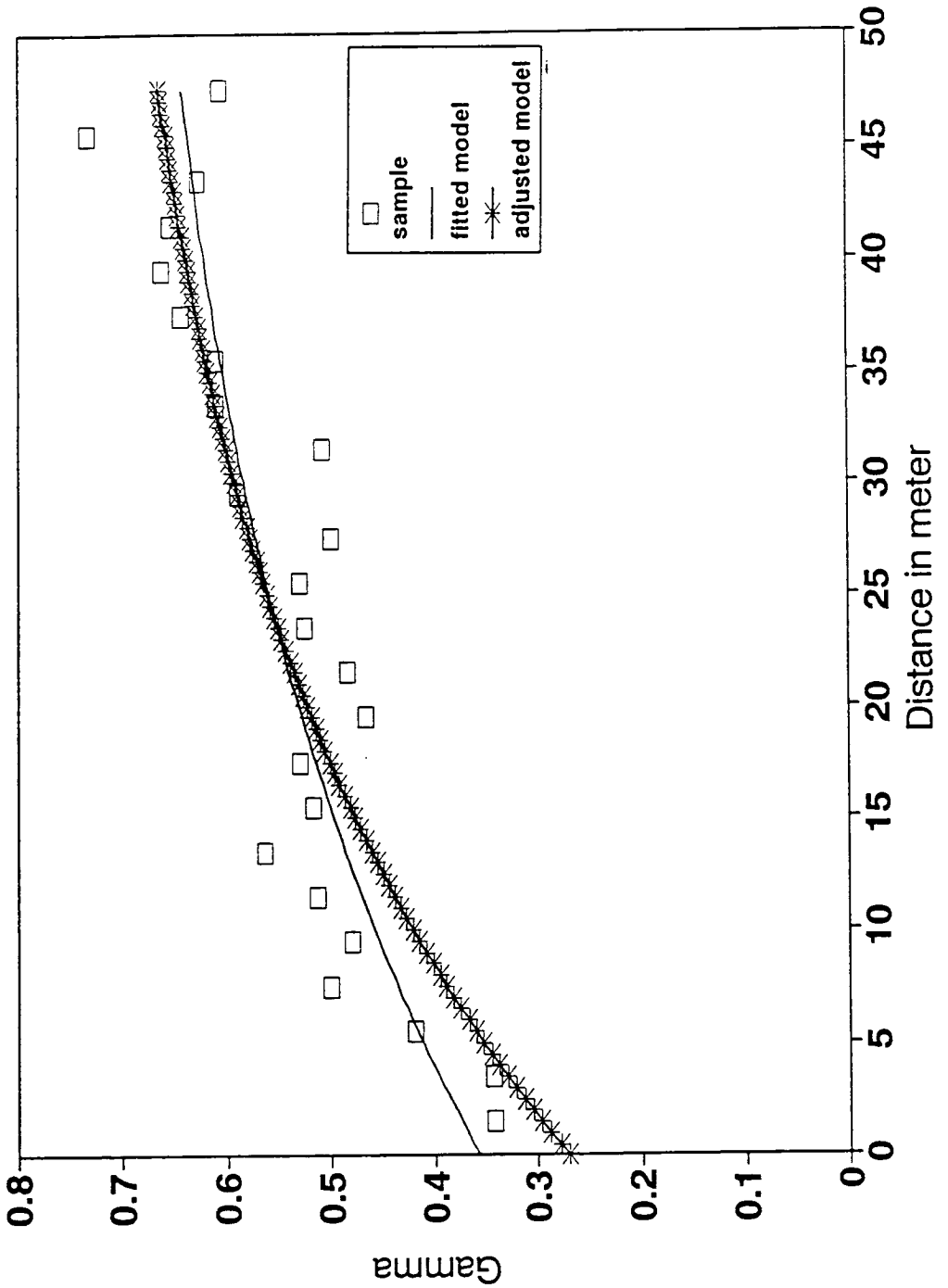

Figure 5.1. Variogram for unsaturated K at 15 cm tension.

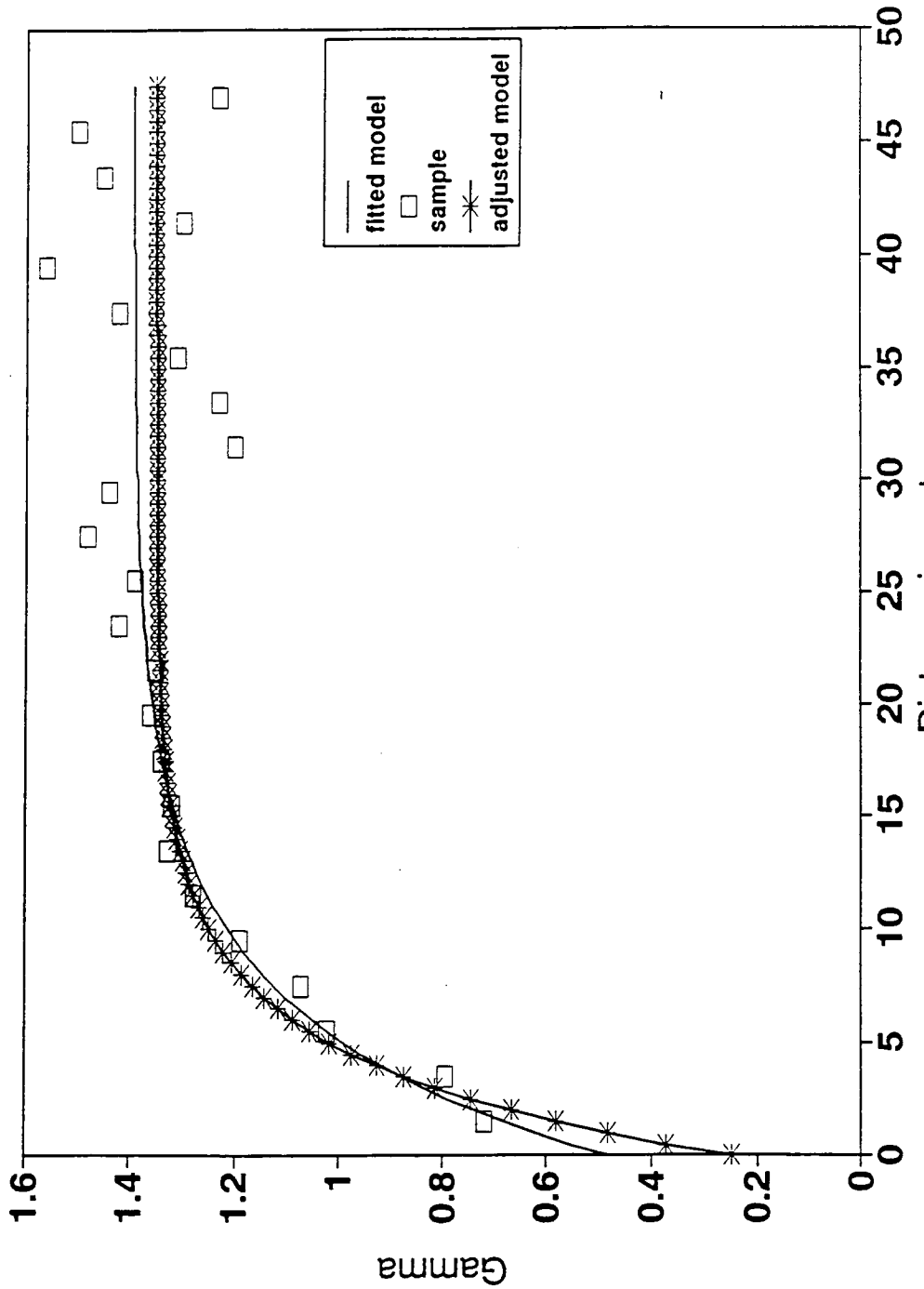

Figure 5.2. Variogram for unsaturated K at 5 cm tension.

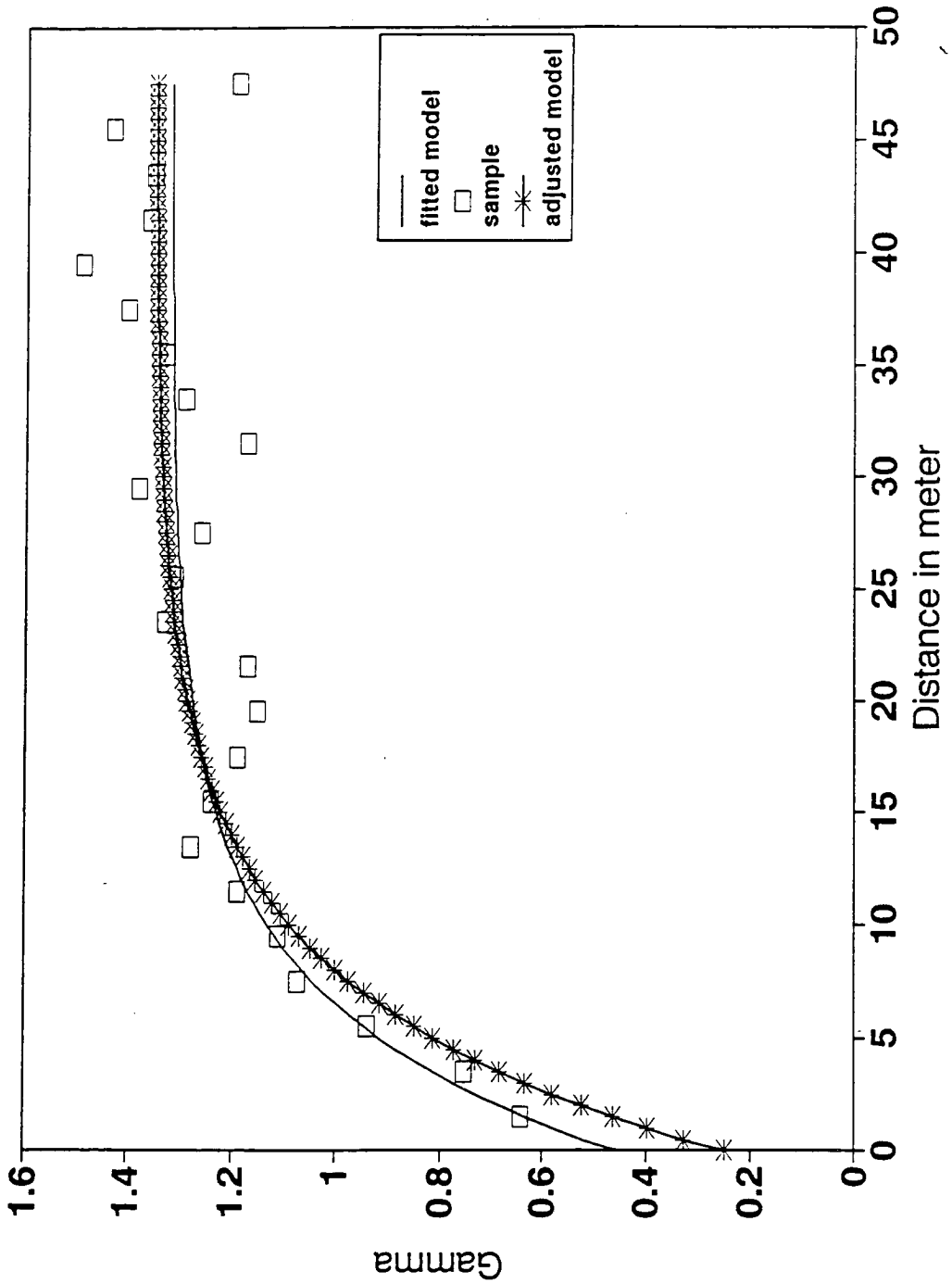

Figure 5.3. Variogram for unsaturated K at 10 cm tension.

$$r = -2\sigma \cos(\alpha)/\rho g h \approx -0.15/h \qquad (5.16)$$

where σ is the surface tension of water (g/sec^2), α is the contact angle between the water and the pore wall (assumed zero), ρ is the density of water (g/cm^3), g is acceleration due to gravity (cm/sec^2) and h (cm) is the water supply potential provided by the disc permeameter. When we use 5 cm tension for steady state flow, we eliminated any pore radius bigger than 0.03 cm and the water flow will be in pores of radius equal or smaller than 0.03 cm. For 10 cm and 15 cm tension the water flow in pore radius is equal or smaller than 0.015 cm and 0.010 cm, respectively.

The same method was used for measuring and fitting variogram models for hydraulic conductivity. Table 5.2 and Figures 5.4, 5.5 and 5.6 show the variogram model with original adjusted parameter. Michaelis-Menton models were the best fitting models for 10 cm and 15 cm tension ($\leq$ 0.015 and $\leq$ 0.010 cm pore radius) steady state flow. An exponential model was the best fitting model for 5 cm tension ($\leq$ 0.030 cm pore radius) steady state flow.

Spatial Variation for Steady State Flow at Different Pore Radii

Steady state flow calculated for different pore radius (0.010 - 0.015, 0.015 - 0.030, and > 0.030) by subtracting the steady state flow of smaller tensions from the bigger one (0, 5 cm, 10 cm, and 15 cm tension). Subtracting the steady state flow

Table 5.2. Fitted models and adjusted models parameters using cross validation for 70 point values of hydraulic conductivity. (Steady state flow at pores radius > 0.010, > 0.015, and > 0.030 cm.)

Fitted Models Parameters									
Pore radii	Model	C_o	C	Range	Mean	VAR	ME	MSE	NLL
>0.010	M-M	0.264	0.358	20.86	2.28	0.41	0.006	0.345	122.46
>0.015	M-M	0.244	0.807	4.3	3.59	0.82	0.004	0.570	157.43
>0.030	exp	0.575	1.537	4.3	6.23	1.89	0.004	1.290	213.93

Adjusted Models Parameters									
Pore radii	Model	C_o	C	Range	Mean	VAR	ME	MSE	NLL
≥0.010	M-M	0.24	0.358	22.5	2.28	0.41	0.005	0.345	122.47
≥0.015	M-M	0.20	0.807	5.5	3.59	0.82	0.004	0.571	157.52
≥0.030	exp	0.25	1.950	5.5	6.23	1.89	0.000	1.280	213.54

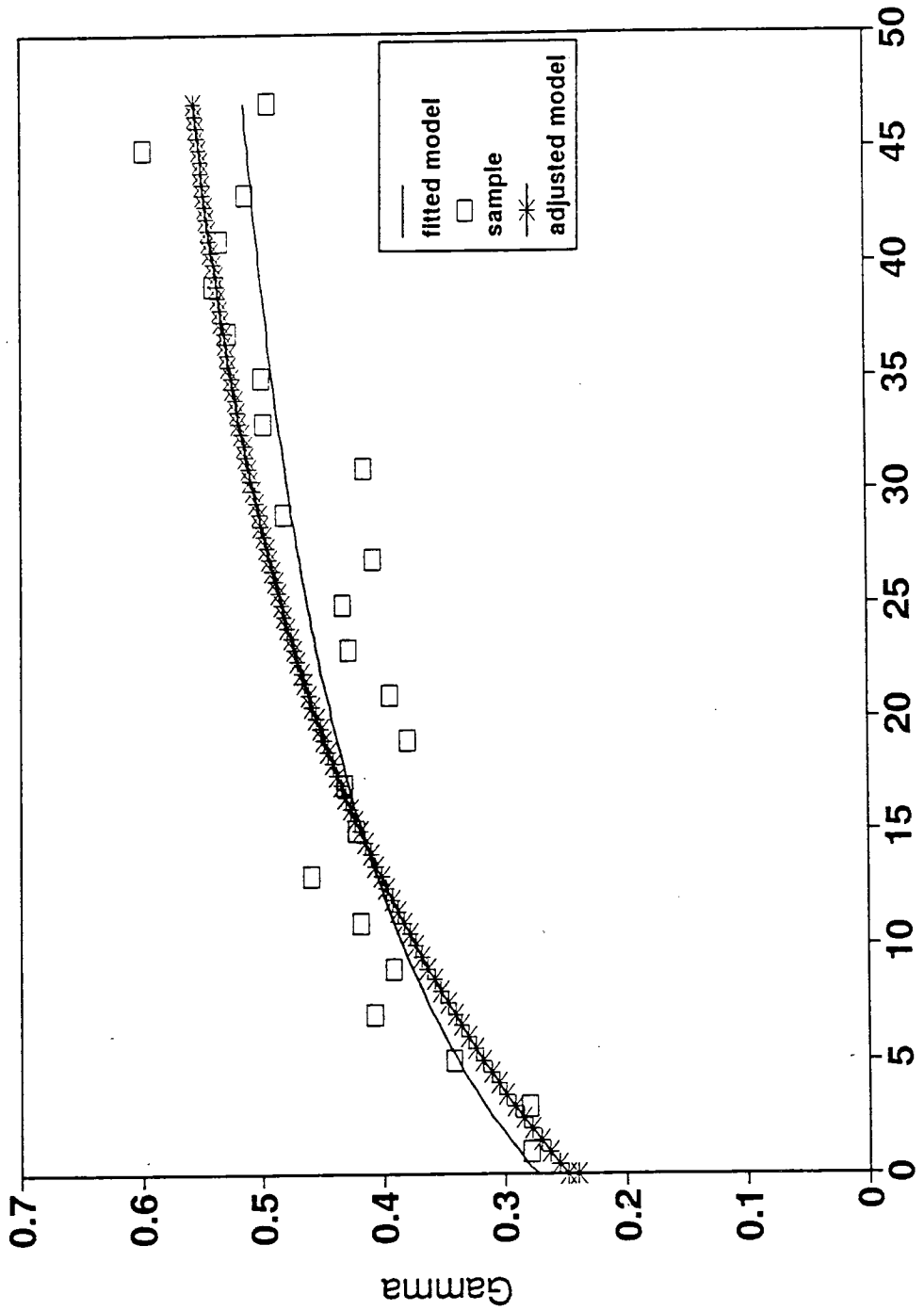

Figure 5.4. Variogram (M-M model) for steady state flow when pore radii is larger than $\geq$ 0.010 cm are eliminated.

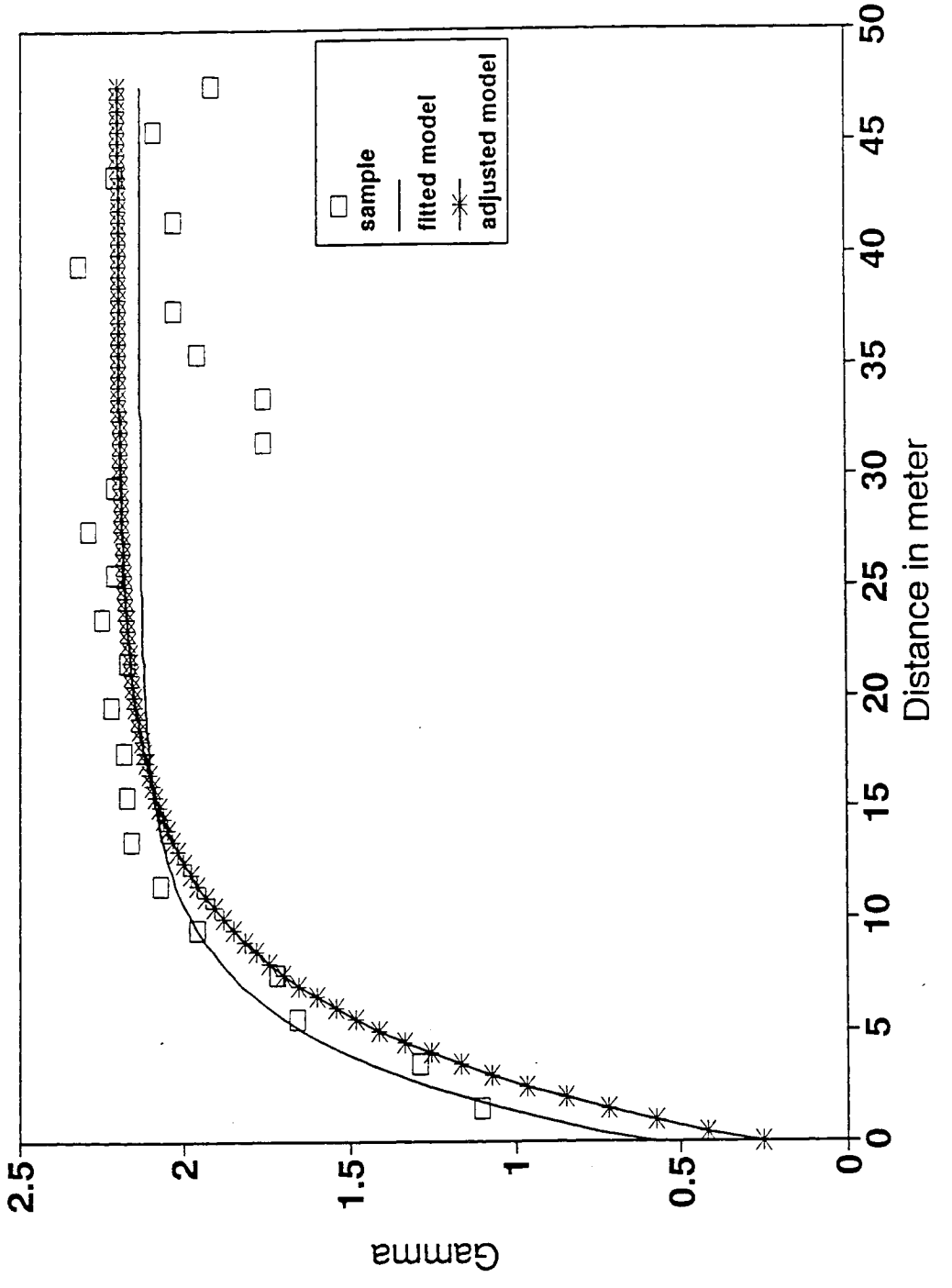

Figure 5.5. Variogram (M-M model) for steady state flow when pore radii is larger then $\geq$ 0.030 cm are eliminated.

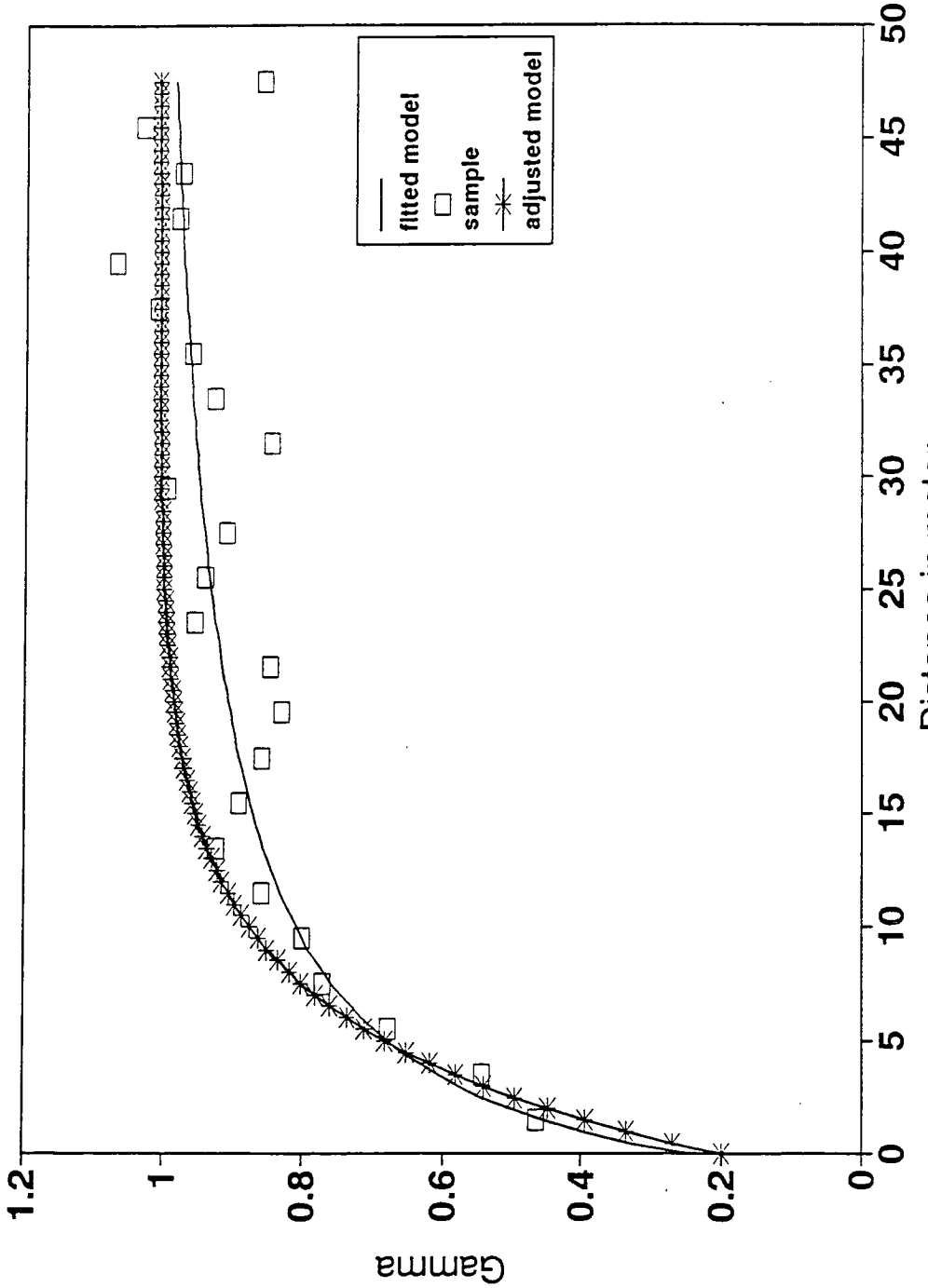

Figure 5.6. Variogram (M-M model) model fitted using Michaelis Menton model for pore flow $\geq$ 0.015 cm are eliminated.

rate at 10 cm tension from 15 cm tension gives us the steady state flow rate at pore radius 0.010 - 0.015 cm (Appendix B).

The same method is used to calculate variogram models. Exponential models were the best fitting models for both steady state flow rate at pore radius 0.015 - 0.030 cm and 0.010 - 0.015 cm, respectively. Table 5.3 and Figures 5.7 and 5.8 show the variogram models with original parameters and adjusted parameter. The steady state flow rate at the other pore radius (> 0.030 cm) was random.

Table 5.3. Fitted and adjusted exponential models parameters using cross validation for point values of hydraulic conductivity. (Steady state flow at pores radius 0.010-0.015 and 0.015-0.030 cm.)

Fitted Model Parameters								
Pore radii	C_o	C	Range	Mean	VAR	ME	MSE	NLL
0.010-0.015	0.077	0.084	4.3	1.31	0.15	0.001	0.12	49.76
0.015-0.030	0.343	0.161	4.3	2.65	0.49	0.004	0.52	150.90

Adjusted Model Parameters								
Pore radii	C_o	C	Range	Mean	VAR	ME	MSE	NLL
0.010-0.015	0.051	0.116	4	1.31	0.15	0.001	0.118	49.18
0.15-0.030	0.143	0.360	3.5	2.65	0.49	0.001	0.510	149.92

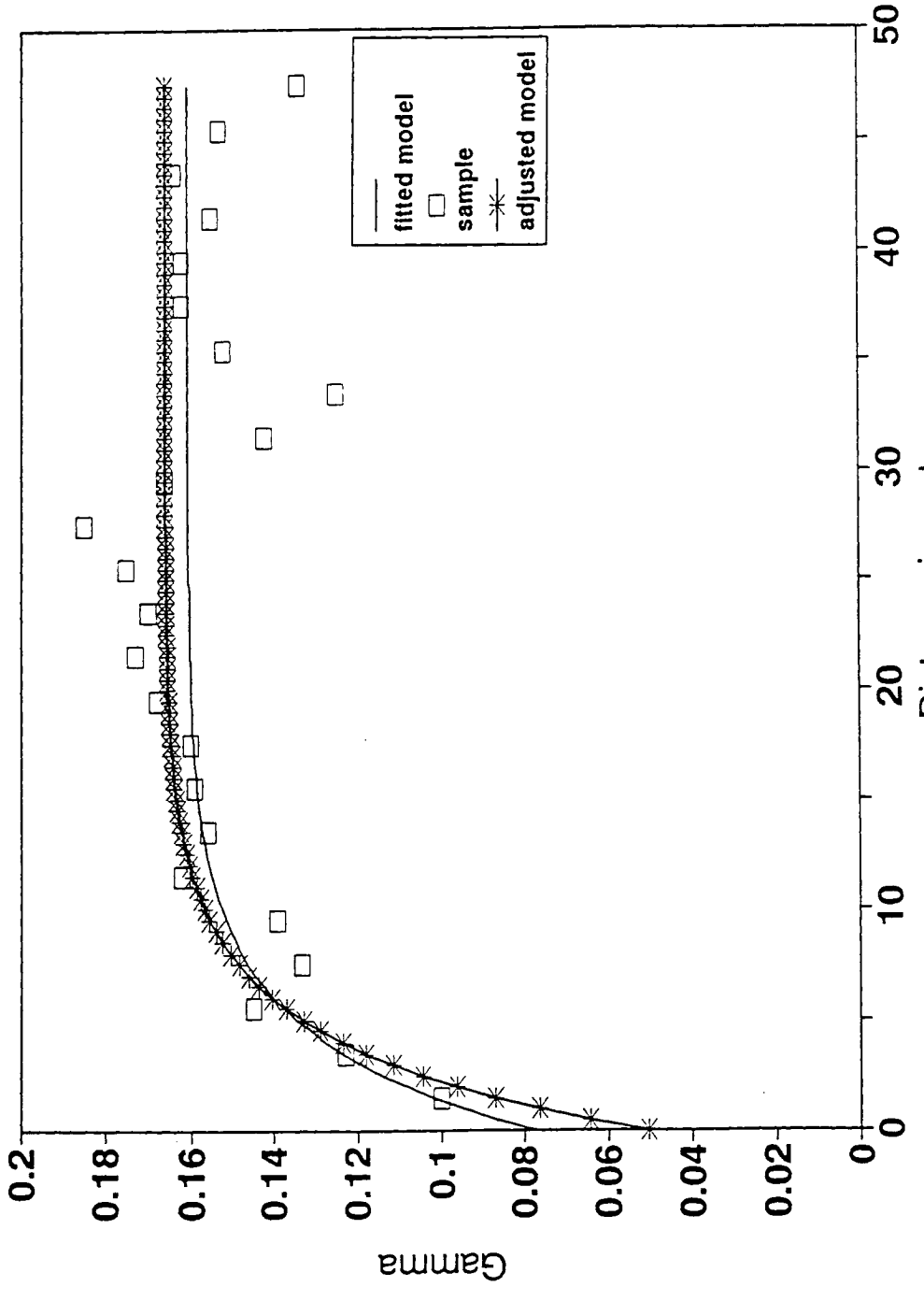

Figure 5.7. Variogram of steady state flow in pores radius 0.015 - 0.010 cm exponential model.

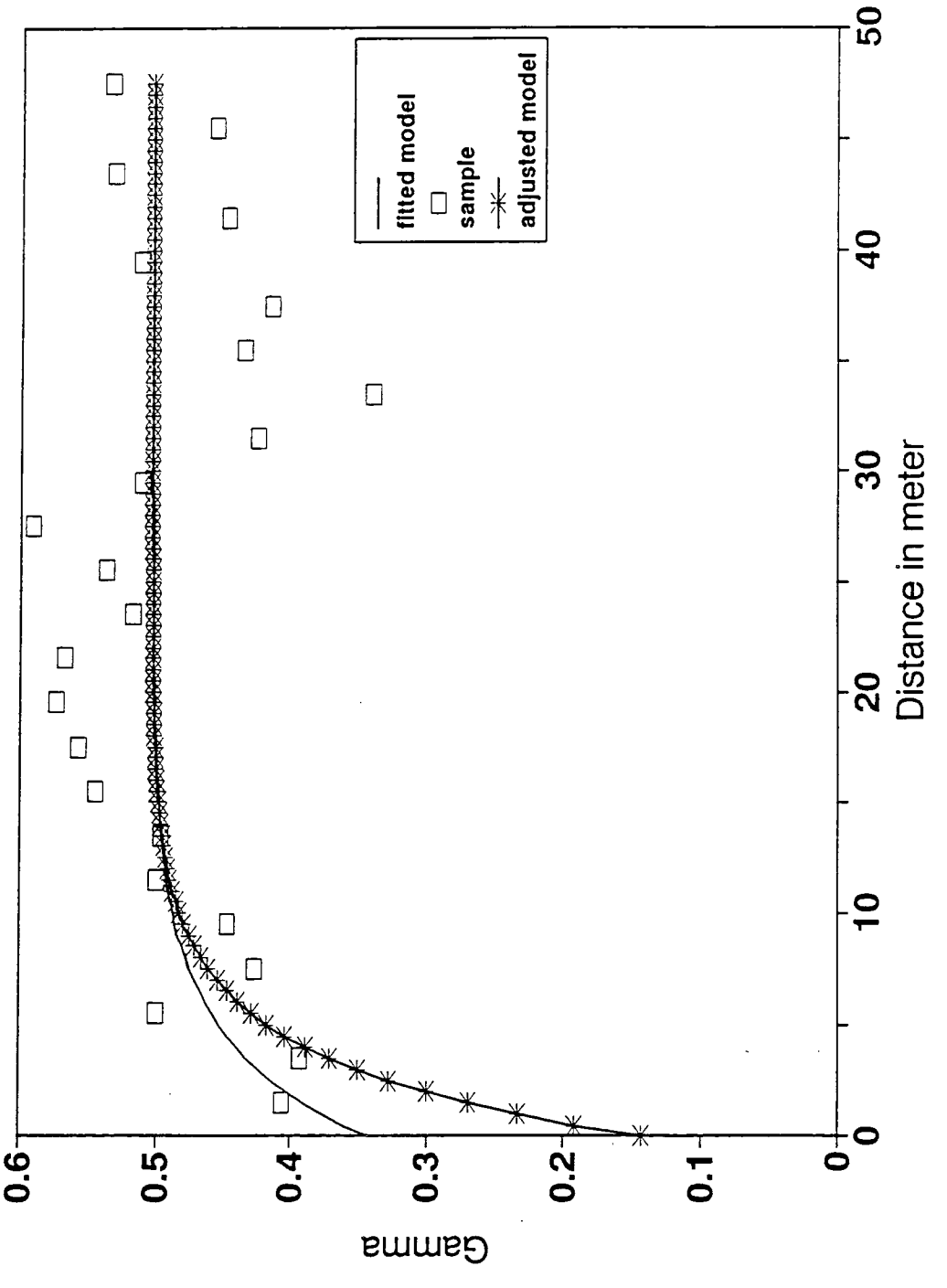

Figure 5.8. Variogram of steady state flow in pores radius 0.03 - 0.015 cm exponential model.

CHAPTER 6

WATER AND BROMIDE MOVEMENT

Solute and water movement in porous media is of crucial importance in a variety of fields relevant to groundwater contamination. Increasing food demand, in particular, has resulted in greater use of fertilizer and pesticides which become potential environmental hazards. Although soil water flow is usually described by the Richards' equation and solute transport described by a convection dispersion equation, these models and equations are unable to predict all spatial and temporal variations of water and solute concentration in the soil and groundwater. For example, these models do not explicitly consider flow through cracks and wormholes. A number of studies have demonstrated that water and solute may flow in large pores. Ehlers (1975) studied water flow in single worm holes, Bouma et al. (1977, 1978, and 1979) described the geometry and spatial distribution of large pores and also estimated the hydraulic conductivity from this information.

Beven and Germann (1982) showed the importance of large openings (macropores) on water flow in soils. The presence of macropores may lead to spatial concentrations of water flow through unsaturated soil that will not be described well by a Darcy approach to flow through porous media. Germann and Beven (1981) investigated the macropore system of two large, undisturbed soil samples. The volumes of macropores were 0.01 and 0.045 of the sample volumes, respectively. When the samples were drained from fully saturated to the point where it may be

assumed that there was no more water in the macropore system, the hydraulic conductivity decreased by factors of 18 and 4.3, respectively. Included was a one-dimensional model of bulk flow in combined micropore and macropore system on the infiltration.

Recently, a new expression has become popular (cf., Roth et al., 1990) called preferential flow. It refers to the rapid transport of water and solutes through some small portion of the soil volume which is receiving input over its entire inlet boundary. The mechanisms which contribute to preferential flow could include movement through structural voids, unstable flow of the invading fluid, or lateral convergence of water into channels by partial surface clogging or subsurface lateral flow. Bowman and Rice (1986) indicated that significant preferential flow can occur even in a soil which exhibits little structure. Also, they found that the rate of downward water movement, as measured by the tracers, was more than 60% greater than predicted in the absence of preferential flow. They mentioned that simple water balance models may overestimate arrival times of surface-applied water and chemicals to groundwater.

Steenhuis and Parlange (1988) presented a model for preferential flow on hillslopes. The conceptual framework of their model depended on dividing the flow paths into groups of pores with about equal sizes but with different pore velocities in each pore group. The pore size groupings were established by introducing a piecewise linear conductivity function (which was introduced by Steenhuis et al., 1988).

Andreini and Steenhuis (1990) studied the effect of preferential flows on solute movement and the effects of tillage practices on these preferential flows. Spatial variations in the solute flow were observed. In both tilled and untilled soils, preferential flows were established with much of the soil well below saturation. Steenhuis et al. (1990) presented a numerical model for preferential solute movement in structured soils using the same idea of pore grouping and a piecewise linear approximation of the hydraulic conductivity as a function of water content as he used in 1988.

Mathematical Models

Two partial differential equations were used to describe water movement and bromide transport in the soil surface. These are following the conventional approach without consideration of preferential flow.

Governing Equation for Water Movement

The partial differential equation used to describe one-dimensional water movement is Richards' equation

$$C(h)\frac{\partial h}{\partial t} = \frac{\partial}{\partial z}[K(h)(\frac{\partial h}{\partial z} \quad -1)] \tag{6-1}$$

where h is the matric potential, z is the distance downward, t is the time, K(h) is the hydraulic conductivity as a function of the matric potential, and C(h) is the specific water capacity ($C(h) = d\theta/dh$ where θ is the volumetric water content).

The initial condition for water used to simulate and predict water movement with depth for a finite soil length (L) 15 cm is

$$h(z,t) = h(z) \text{ for } t = 0 \text{ and } 0 < z < L \tag{6-2}$$

A constant potential is used for the upper boundary condition for water with choice of h_o = 0, -5, -10, and -15 cm representing the actual tension of the disc permeameter at the upper boundary:

$$h(0,t) = h_O \tag{6-3}$$

The boundary condition which is imposed at the lower boundary (at L = z = 15 cm) was also a constant potential:

$$\begin{aligned} h(L,t) &= h_L \\ h(15,t) &= -50000cm. \end{aligned} \tag{6-4}$$

Governing Equation for Bromide Transport

Movement of bromide in this model is described by the convection-dispersion equation.

$$\frac{\partial}{\partial t}(\theta C + \rho S) = \frac{\partial}{\partial z}[\theta D(\frac{\partial C}{\partial z} - qC)] - \alpha\theta C - \beta\rho S + \gamma\theta \quad (6\text{-}5)$$

where C is the concentration of the bromide in the liquid phase, S is the concentration of the bromide in the solid phase, D is the dispersion coefficient, θ is the volumetric water content, q is the flux of water, ρ is the soil bulk density, α is the first-order degradation rate constant in the liquid phase, β is the first-order degradation rate constant in the solid phase, and γ is the zero-order rate constant in the liquid phase.

If the concentration of the chemical adsorbed on the solid phase is assumed to be directly proportional to the concentration in the liquid phase, then

$$S = kC \quad (6\text{-}6)$$

where k is the partition coefficient. Incorporating this relationship into equation (6.5) yields

$$\frac{\partial}{\partial t}(\theta RC) = \frac{\partial}{\partial z}[\theta D(\frac{\partial C}{\partial z} - qC)] - (\alpha\theta + \beta\rho k)C + \gamma\theta \quad (6\text{-}7)$$

where $R = 1 + \rho k/\theta$ is the retardation factor for the chemical in the soil. The concentration of a chemical in the liquid phase at any location and time is determined by solving equation (6-7) coupled with equation (6-1) for water movement. Initial condition for the bromide used is

$$C(z,t) = C(z,0) \text{ for } t = 0 \text{ and } 0 < z < L \qquad (6\text{-}8)$$

where L = 15 cm. The upper boundary condition was a constant for chemical imposed at the soil surfaces:

$$-\theta D\frac{\partial C}{\partial Z} + q(0,t)C = q(0,t)Cs \qquad q(0,t) > 0 \qquad (6\text{-}9)$$

with the concentration of inflowing solution Cs. The lower boundary condition at z = L = 15 cm is taken at zero concentration:

$$C(L,t) = C_L = 0 \qquad (6\text{-}10)$$

Numerical Solution for Mathematical Models

Governing partial differential equations for water and bromide are solved for one-dimension numerically using finite difference techniques. The program developed by Nofziger et al. (1989) is described below.

Solution of Richards' Equation

An implicit finite difference scheme with explicit linearization described by Haverkamp et al. (1977) was used. In this scheme, the partial differential equation takes the form

$$C(i,j)\frac{h(i,j+1)-h(i,j)}{\Delta t} = \frac{1}{\Delta z}\left[K(i+1/2,j)\left\{\frac{h(i+1,j+1)-h(i,j+1)}{\Delta z} - 1\right\}\right. \\ \left. - K(i-1/2,j)\left\{\frac{h(i,j+1)-h(i-1,j+1)}{\Delta z} - 1\right\}\right] \tag{6-11}$$

where $h(i,j) = h(i\Delta z, j\Delta t)$,

$C(i,j) = C(h(i,j))$,

$K(i+1/2,j) = [K(h(i,j)) + K(h(i+1,j))]/2$,

$K(i-1/2,j) = [K(h(i-1,j)) + K(h(i,j))]/2$,

Δt and Δz are the mesh sizes in time and depth, respectively. The indices i and j take on values of 0, 1, 2, ... The finite difference equation (6-11) is used for all interior mesh points in depth (i = 1, 2, 3, ...) for the soil system. Special forms of this equation are used to represent mesh points on the boundaries of the soil.

The upper boundary condition with constant potential h_o at Z = 0 equation (6-3) will translate to the $h(0,j) = h_o$ for all j. Therefore, h(0,j) is known for each time step. Equation (6-11) point i = 1 then becomes

$$C(1,j)\frac{h(1,j+1)-h(1,j)}{\Delta t} = \frac{1}{\Delta z}\left[K(3/2,j)\left\{\frac{h(2,j+1)-h(1,j+1)}{\Delta z} - 1\right\}\right. \\ \left. - K(1/2,j)\left\{\frac{h(1,j+1)-h_o}{\Delta z} - 1\right\}\right] \tag{6-12}$$

The lower boundary condition with constant potential h_L at z = L, equation (6-4) becomes $h(I,j) = h_L$ for all j(IΔZ = L). Therefore, h(I,j) is known for each time step. Equation (6-11) at mesh point i = I - 1 then becomes

$$C(I-1,j)\frac{h(I-1,j+1)-h(I-1,j)}{\Delta t} = \frac{1}{\Delta z}\left[K(I-1/2,j)\left\{\frac{h_L-h(I-1,j+1)}{\Delta z} - 1\right\}\right. \quad (6\text{-}13)$$
$$\left. - K(I-3/2,j)\left\{\frac{h(I-1,j+1)-h(I-2,j)}{\Delta z} - 1\right\}\right]$$

Solution of Convection-Dispersion Equation

The numerical solution to equation (6-7) is based on that of van Genuchten (1978) who derived a correction for numerical dispersion. The finite difference equation was (Nofziger et al., 1989)

$$\frac{\{\theta RC\}(i,j+1)-\{\theta RC\}(i,j)}{\Delta t} =$$

$$+ \frac{1}{2}\left\{\frac{\partial}{\partial z}\left[\theta D^{-}(\frac{\partial C}{\partial z} - qC)\right] - (\alpha\theta + \beta\rho k)C + \gamma\theta\right\}(i,j+1) \quad (6\text{-}14)$$

$$+ \frac{1}{2}\left\{\frac{\partial}{\partial z}\left[\theta D^{+}(\frac{\partial C}{\partial z} - qC)\right] - (\alpha\theta + \beta\rho k)C + \gamma\theta\right\}(i,j)$$

where

$$\{\theta RC\}(i,j) = \theta(i\Delta z, j\Delta t)\quad R(i\Delta z, j\Delta t)\quad C(i\Delta z, j+1)$$

$$D^- = D - q^2\Delta t/(6\theta^2 R),$$

$$D^+ = D + q^2\Delta t/6\theta^2 R),$$

$$\left\{\frac{\partial}{\partial z}\left[\theta D^+\left(\frac{\partial C}{\partial z}\right)\right]\right\}(i,j) =$$

$$\{C(i+1,j)[\theta(i,j)\quad D^+(i,j) + \theta(i+1,j)\quad D^+(i+1,j)]$$

$$- C(i,j)[\theta(i-1,j)\quad D^+(i-1,j) + 2\theta(i,j)\quad D^+(i,j) + \theta(i+1,j)\quad D^+(i+1,j)]$$

$$+ C(i+1,j)[\theta(i,j)\quad D^+(i,j + \theta(i+1,j)\quad D^+(i+1,j)]\}/(2\Delta z^2),$$

$$\left\{\frac{\partial qC}{\partial z}\right\}(i,j) = \{C(i+1,j)\ [q(i,j) + 2q(i+1,j)]$$

$$+ C(i,j)\ [q(i+1,j) - q(i-1,j)] - C(i-1,j)\ [2q(i-1,j) + q(i,j)\ ]\ \}/(6\Delta z),$$

$$\{(\alpha\theta + \beta\rho k)C(i,j)\} = \{C(i+1,j)\ [(\alpha\theta + \beta\rho k)(i,j) + (\alpha\theta + \beta\rho k)(i+1,j)]$$

$$+ C(i,j)\ [(\alpha\theta + \beta\rho k)(i-1,j) + 6(\alpha\theta + \beta\rho k)(i,j) + (\alpha\theta + \beta\rho k)(i+1,j)]$$

$$+ C(i-1,j)\ [(\alpha\theta + \beta\rho k)(i,j) + (\alpha\theta + \beta\rho k)(i-1,j)]\ \}/12,$$

and Δt and Δz are mesh sizes in time and depth, respectively. Equation (6-14) is used for interior mesh points in depth (i = 1, 2, 3, ...) for the soil system. Values of $\theta(i,j)$ and q(i,j) are obtained from the solution to the water flow equation. Special forms of the convection-dispersion equation are used on the boundaries of the soil.

Constant concentration of inflowing solution used in the upper boundary, equation (6.9), the concentration of inflowing solution C_s is known but the concentration at z = 0 in the soil must be found. That is C(0,j) must be determined for each time step, the equation (6.14) for i = 0 can be written as:

$$[\{\theta RC\}(0,j+1) - \{\theta RC\}(0,j)]\Delta z/(2\Delta t) = \{j(0,j+1) - j(0.5,j+1) - \Delta z(\alpha\theta + \beta\rho k)(0,j+1)C(0,j+1)/2 + \Delta z\gamma\theta(0,j+1)/2\}/2 + \{j(0,j) - j(0.5,j) - \Delta z(\alpha\theta + \beta\rho k)(0,j)C(0,j)/2 + \Delta z\gamma\theta(0,j)/2)\}/2 \quad (6.15)$$

where

$$j(0,j) = 1(0,j)C_s,$$

$$j(0.5,j) = [\{\theta D\}(0,j) + \{\theta D\}(1,j)]\,[C(0,j)-C(1,j)]/(2\Delta z) + [2q(0,j)C(0,j)+q(1,j)C(0,j)+q(0,j)C(1,j)+2q(1,j)C(1,j)]/6,$$

and

$$\{\alpha\theta+\beta\rho k\}(0,j)C(0,j) = [3\{\alpha\theta+\beta\rho k\}(0,j)C(0,j)+\{\alpha\theta+\beta\rho k\}(1,j)C(0,j) + \{\alpha\theta+\beta\rho k\}(0,j)C(1,j)+\{\alpha\theta+\beta\rho k\}(1,j)C(1,j)]/6$$

constant concentration at soil depth Z = L = 15 cm (which is lower boundary condition). At Z = L,C(I,j), where IΔt = L is known for all time steps. Therefore, no equation for i = L is required in the set of equations.

Results and Discussion

Field Results

Five centimeter depths of dyed solution and bromide tracer (2190 cm^3 for disc diameter of 23.6 cm) were added at four different tensions, 0, 5, 10 and 15 cm with three replicates for each tension. Volumetric water content and bromide concentration (in ppm) with depth are shown in Table 6.1.

Averages of volumetric water content and bromide concentration have been calculated at each depth for different tensions for ease of comparisons with field predicted data and are in Table 6.2. Water reached depths of 10.0 - 12.5 cm and there are not big differences in water content at different tensions (0, 5, 10 and 15 cm). The water contents are marginally higher at the deepest depth for the zero tension application. This could be true physically if we consider that the water moves faster in bigger pores (at zero tension) and slower for the 15 cm tension.

Comparing bromide concentration at the same depth 10 - 12.5 cm using Table 6.2, we found that the highest concentration for zero tension (5.02 ppm) and the lowest concentration for 15 cm tension (2.87 ppm). The concentration of bromide at the same depth (10 - 12.5 cm) for 5 and 10 cm tension treatments were 3.45 and 3.69 ppm, respectively.

Simulated Model

Programs written by Nofziger et al. (1989) were used to simulate one-dimensional water and chemical movement in the soil. Initial conditions for water used to predict water movement with depth, for a finite soil length of 15 cm was

$$h = -50000 \qquad 0 \, , \, z < 15 \; cm \tag{6.16}$$

This value of h corresponded to $\theta = 0.058$, the average water content in the soil profile to the depth of 15 cm.

Table 6.1. Volumetric water content and bromide concentration (ppm) at the three replicates (R) with four tensions after adding 5 cm depth solution.

		R1		R2		R3	
Tension (cm)	Depth (cm)	θ (cm^3/cm^3)	Br (ppm)	θ (cm^3/cm^3)	Br (ppm)	θ (cm^3/cm^3)	Br (ppm)
zero	0.0	0.283	32.80	0.271	28.86	0.270	32.89
	0.0- 2.5	0.277	34.60	0.249	28.77	0.251	26.16
	2.5- 5.0	0.255	31.10	0.233	25.07	0.248	29.60
	5.0- 7.5	0.232	28.00	0.210	30.33	0.236	25.60
	7.5-10.0	0.208	24.80	0.178	24.18	0.222	24.65
	10.0-12.5	0.084	5.00	0.077	5.01	0.127	5.06
	12.5-15.0	0.058	0.00	0.058	0.00	0.057	0.00
five	0.0	0.261	30.00	0.265	30.41	0.263	30.02
	0.0- 2.5	0.259	26.50	0.255	26.70	0.254	26.06
	2.5- 5.0	0.255	24.90	0.247	25.73	0.251	25.88
	5.0- 7.5	0.220	24.00	0.218	24.31	0.206	24.37
	7.5-10.0	0.119	21.90	0.112	22.81	0.114	23.37
	10.0-12.5	0.091	1.13	0.069	3.88	0.088	5.34
	12.5-15.0	0.058	0.00	0.059	0.06	0.056	0.00
ten	0.0	0.258	30.20	0.253	29.54	0.268	30.08
	0.0- 2.5	0.248	28.00	0.243	26.33	0.256	26.87
	2.5- 5.0	0.231	26.50	0.229	25.96	0.233	25.82
	5.0- 7.5	0.211	25.60	0.214	24.87	0.219	25.10
	7.5-10.0	0.111	24.60	0.134	22.93	0.129	23.50
	10.0-12.5	0.072	2.70	0.092	4.46	0.084	3.89
	12.5-15.0	0.058	0.00	0.058	0.00	0.056	0.00
fifteen	0.0	0.245	32.50	0.255	33.21	0.253	32.18
	0.0- 2.5	0.239	32.20	0.247	28.80	0.248	30.47
	2.5- 5.0	0.233	27.70	0.235	28.26	0.239	31.84
	5.0- 7.5	0.218	30.30	0.220	25.04	0.224	30.99
	7.5-10.0	0.167	23.00	0.176	25.22	0.185	25.13
	10.0-12.5	0.087	4.50	0.066	4.02	0.058	0.00
	12.5-15.0	0.058	0.00	0.058	0.00	0.058	0.00

Table 6.2. Volumetric water content and bromide concentration (ppm) average of three replicates.

Tension (cm)	Depth (cm)	Average θ (cm^3/cm^3)	Average Br (ppm)
	0.0	0.275	31.547
zero	0.0- 2.5	0.259	29.857
	2.5- 5.0	0.245	28.593
	5.0- 7.5	0.226	27.997
	7.5-10.0	0.203	24.560
	10.0-12.5	0.096	5.024
	12.5-15.0	0.058	0.000
	0.0	0.263	30.163
five	0.0- 2.5	0.256	26.420
	2.5- 5.0	0.251	25.533
	5.0- 7.5	0.215	24.237
	7.5-10.0	0.115	22.750
	10.0-12.5	0.083	3.448
	12.5-15.0	0.058	0.000
	0.0	0.260	29.963
ten	0.0- 2.5	0.249	27.090
	2.5- 5.0	0.231	26.093
	5.0- 7.5	0.215	25.200
	7.5-10.0	0.125	23.693
	10.0-12.5	0.083	3.690
	12.5-15.0	0.057	0.000
	0.0	0.251	32.633
fifteen	0.0- 2.5	0.245	30.317
	2.5- 5.0	0.236	29.477
	5.0- 7.5	0.221	28.783
	7.5-10.0	0.176	24.467
	10.0-12.5	0.070	2.870
	12.5-15.0	0.058	0.000

A constant potential used for the upper boundary conditions for water which represent the actual tensions used in the disc permeameters:

$$h(0,t) = h_0 \tag{6.17}$$

with h_o = 0, -5, -10, and -15 cm, a constant potential h = -50000 cm was used in the lower boundary which was the same as for the initial condition:

$$h(15,t) = -50000\ cm \tag{6.18}$$

The initial condition for bromide movement imposed was the same as in equation 6.8 or C(z,t) = C(z.0) for t = 0.

Constant concentration of inflowing solution at the upper boundary was used to simulate movement of bromide when the solution entering the soil has a known and constant concentration

$$-\theta D\frac{\partial c}{\partial z} + q(0,t)C = q(0,t)*350 \qquad q(0,t) \succ 0 \tag{6.19}$$

The lower boundary condition at z = L = 15 cm was constant concentration which was C = 0 equation (6.10).

Briefly, some assumptions which have been made in these simulations:

1. Hydraulic properties do not change with depth, and are equal to average hydraulic properties used from three undisturbed soil cores.

2. The concentration of bromide in the solid phase is zero.

3. First order degradation rate constant for bromide in liquid and solid phase equal to zero.

4. Dispersion coefficient for bromide was 0.36 cm^2/h (Andreini and Steenhuis, 1990).

5. Hydraulic properties do not change by the presence of the bromide and other chemicals in the solution.

The Δz and Δt were constant for all the tensions with Δz = 1 cm Δt = 0.0002 h.

Comparison Between Predicted Models and Actual Field Data

Water Content

The results of model simulation and actual field data with depth is shown in Table 6.3. Water content plotted against depth are shown in Figures 6.1 to 6.4 for different tensions (0, 5, 10, and 15 cm).

The water profiles tended to be deeper in the field than were in the predicted models simulation for all tensions. The greatest difference was for zero tension and the smallest difference was for the 15 cm tension due to eliminating some of the large macropores when we increased the tension to 15 cm in the disc permeameter. Preferential flow was very clearly visible using the dye solution with these tensions.

Bromide Concentration

The results of both simulated model and field data with depth are shown in Table 6.3. Bromide concentration was plotted against depth for both predicted

model and actual field data as shown in Figures 6.5 to 6.8, for 0, 5, 10, and 15 cm tension, respectively. The bromide concentration was higher in field observed data than in predicted models in the deeper depth (starting from 7 cm depth). It is clear from Figures 6.5 to 6.8 that the bromide transport in the field was faster than that predicted using simulated models, which in part could be due to preferential flow. Predicted data and field data were close to each other in the profile where we used 15 cm tension (Figure 6.8) and that is due to eliminating most of the macropores which have big contributions into preferential flow. It was clear visually, that the preferential flow happens in the soil profile using dye solution as shown in Figures 6.9 to 6.12. (These figures were identical copies of color slides done in the field at the time of experiment.) The dye solution advanced more in some parts of the soil profile than others causing some channel and fingering and on the other hand the wetting front was uniform.

It was clear that the preferential flow happened under both saturated and unsaturated flow. It was less obvious as we went to higher tensions, as we found out at 15 cm tension when the predicted model simulation was very close to field data in both water and bromide movement and concentration.

Table 6.3. Difference between predicted model and actual field data after adding 5 cm depth of solution.

		Simulated		Actual	
	Depth (cm)	Moisture (cm^3/cm^3)	Bromide (ppm)	Moisture (cm^3/cm^3)	Bromide (ppm)
Tension 0	0	0.280	343.7	0.275	315.3
	1	0.280	334.1	0.267	306.9
	2	0.279	314.9	0.259	298.6
	3	0.278	297.2	0.252	292.3
	4	0.274	280.3	0.245	285.9
	5	0.268	264.8	0.233	279.5
	6	0.257	251.4	0.227	275.0
	7	0.233	238.3	0.221	273.0
	8	0.188	216.6	0.212	259.0
	9	0.120	164.2	0.203	245.0
	10	0.062	27.2	0.149	147.6
	11	0.058	0.0	0.096	50.1
	12	0.058	0.0	0.077	25.1
	13	0.058	0.0	0.067	12.5
	14	0.058	0.0	0.058	0.0
	15	0.058	0.0	0.057	0.0
Tension 5	0	0.276	322.2	0.263	301.6
	1	0.274	312.9	0.2595	282.9
	2	0.271	299.4	0.256	264.2
	3	0.266	285.8	0.253	259.9
	4	0.258	272.6	0.251	255.5
	5	0.245	260.5	0.231	248.9
	6	0.220	247.4	0.212	242.4
	7	0.177	224.6	0.163	234.9
	8	0.115	168.0	0.139	231.3
	9	0.062	24.1	0.115	227.5
	10	0.058	0.0	0.099	131.0
	11	0.058	0.0	0.083	34.5
	12	0.058	0.0	0.070	17.3
	13	0.058	0.0	0.064	8.7
	14	0.058	0.0	0.058	0.0
	15	0.058	0.0	0.058	0.0

Table 6.3. Difference between predicted model and actual field data after adding 5 cm depth of solution. (Continued)

		Simulated		Actual	
	Depth (cm)	Moisture (cm^3/cm^3)	Bromide (ppm)	Moisture (cm^3/cm^3)	Bromide (ppm)
Tension 10	0	0.271	329.2	0.260	299.2
	1	0.269	321.5	0.254	284.8
	2	0.265	309.8	0.249	270.4
	3	0.260	297.6	0.240	266.0
	4	0.252	285.3	0.231	261.7
	5	0.240	273.1	0.223	259.9
	6	0.220	260.3	0.215	258.3
	7	0.186	240.7	0.170	248.7
	8	0.133	198.9	0.147	243.9
	9	0.075	93.4	0.125	239.1
	10	0.058	0.0	0.103	138.0
	11	0.058	0.0	0.082	36.9
	12	0.058	0.0	0.069	18.4
	13	0.058	0.0	0.063	9.2
	14	0.058	0.0	0.057	0.0
	15	0.058	0.0	0.058	0.0
Tension 15	0	0.266	335.2	0.251	325.6
	1	0.263	329.3	0.248	314.6
	2	0.260	319.6	0.245	303.2
	3	0.256	309.1	0.240	298.9
	4	0.250	297.9	0.236	294.8
	5	0.242	286.2	0.228	291.3
	6	0.230	274.2	0.221	287.8
	7	0.212	261.3	0.198	266.3
	8	0.183	243.3	0.186	255.5
	9	0.138	208.2	0.175	244.7
	10	0.084	119.6	0.122	137.6
	11	0.058	0.0	0.070	30.5
	12	0.058	0.0	0.064	15.3
	13	0.058	0.0	0.061	7.6
	14	0.058	0.0	0.058	0.0
	15	0.058	0.0	0.058	0.0

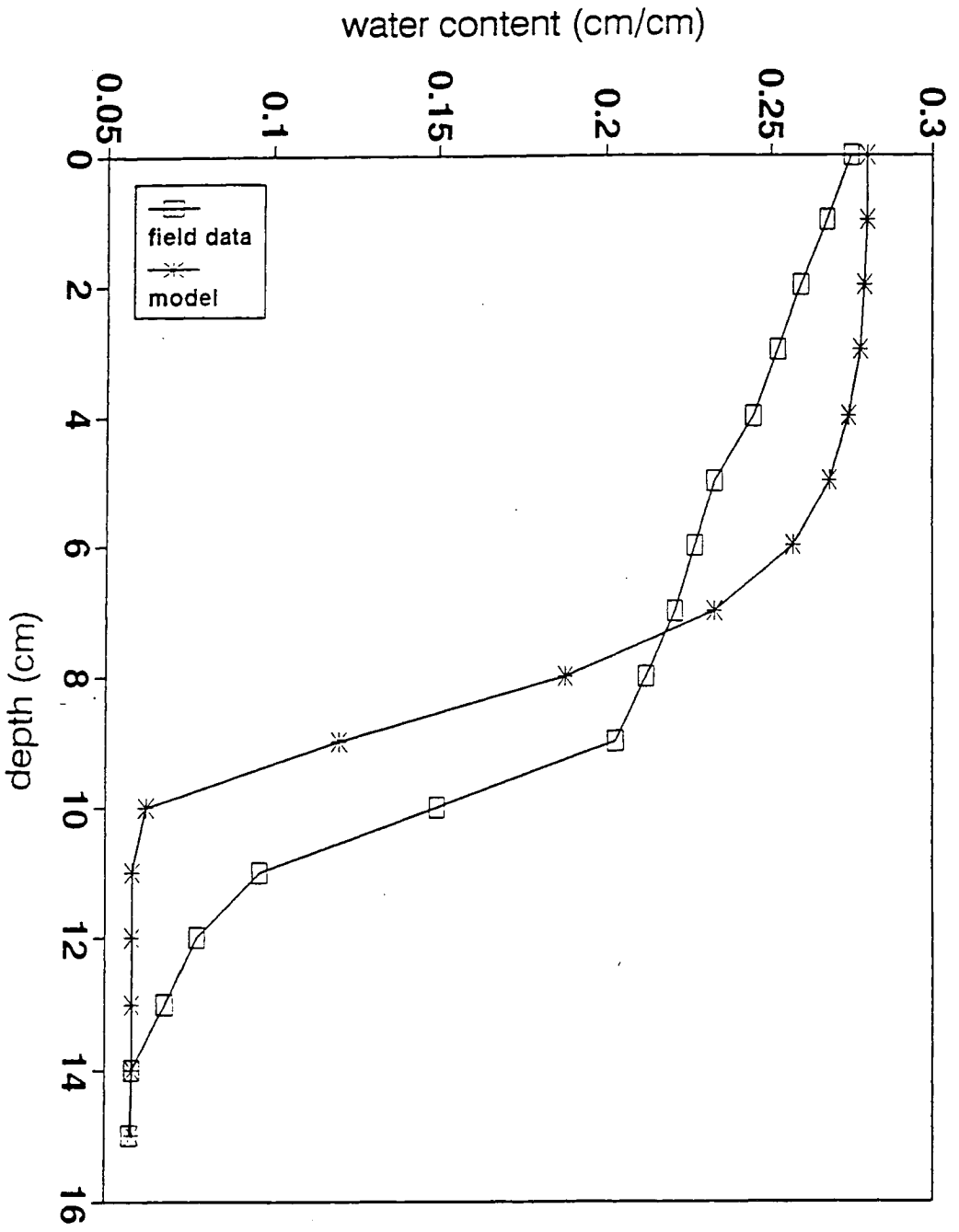

Figure 6.1. Comparison of volumetric water content between field data and model prediction at 0 tension.

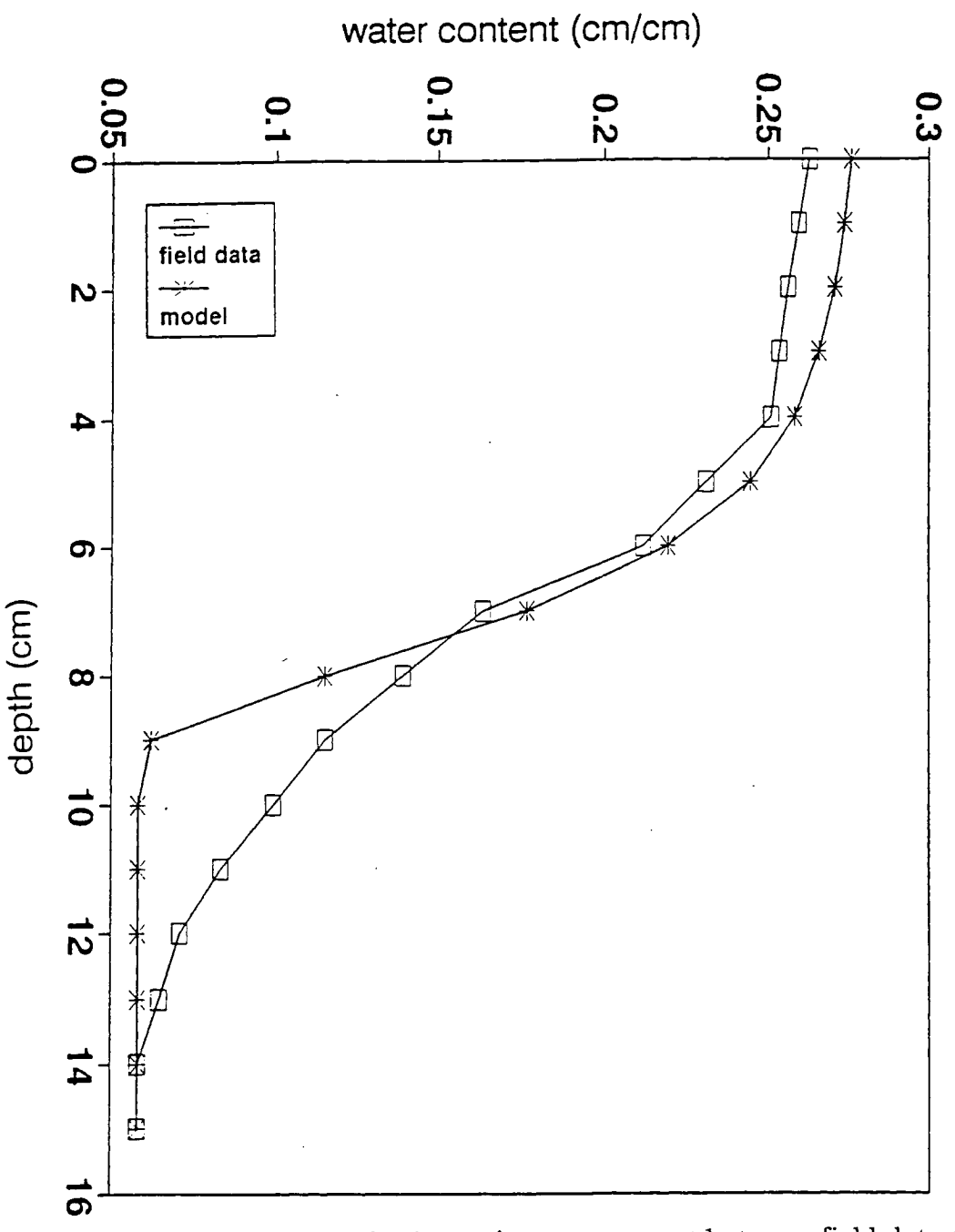

Figure 6.2. Comparison of volumetric water content between field data and model prediction at 5 cm tension.

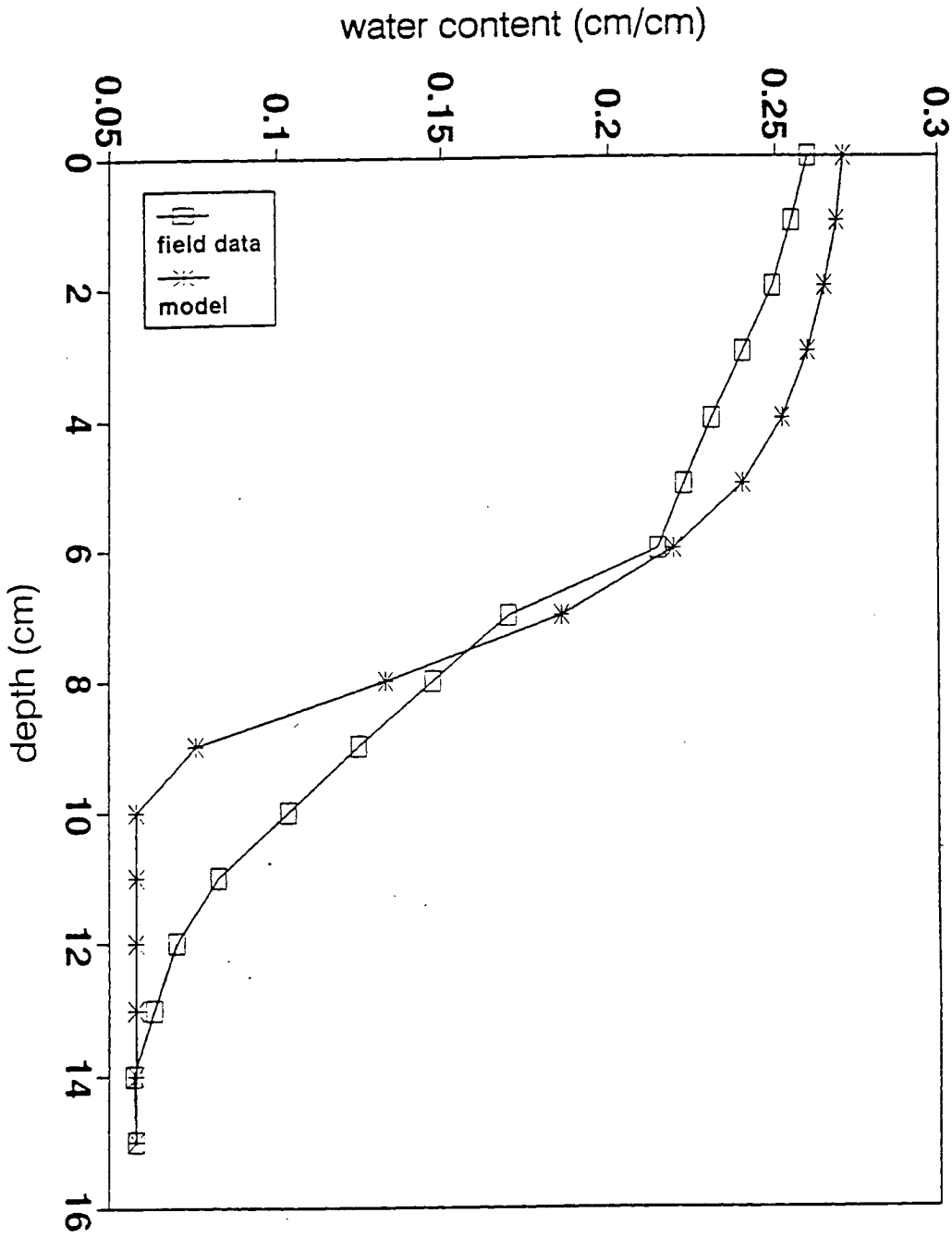

Figure 6.3. Comparison of volumetric water content between field data and model prediction at 10 cm tension.

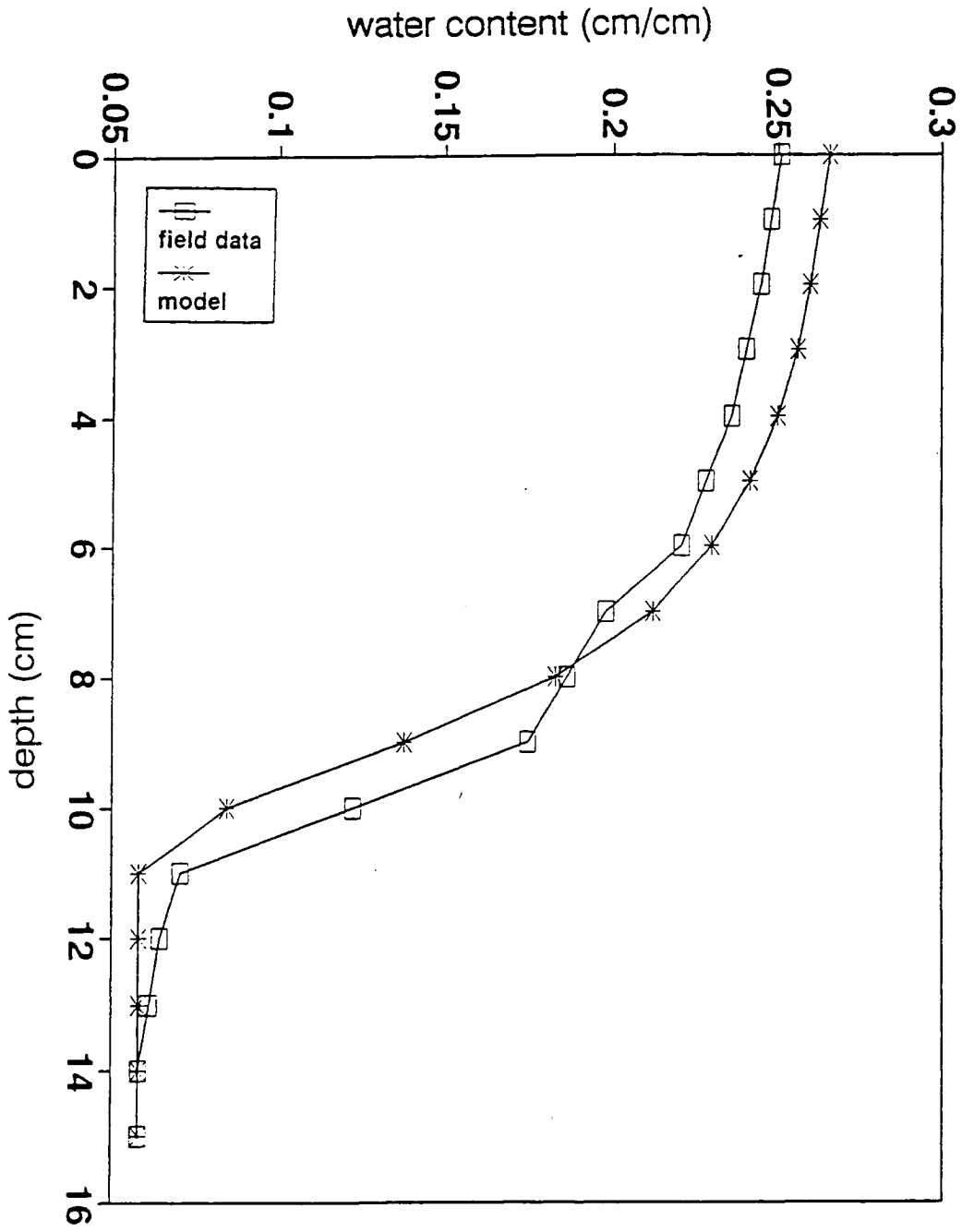

Figure 6.4. Comparison of volumetric water content between field data and model prediction at 15 cm tension.

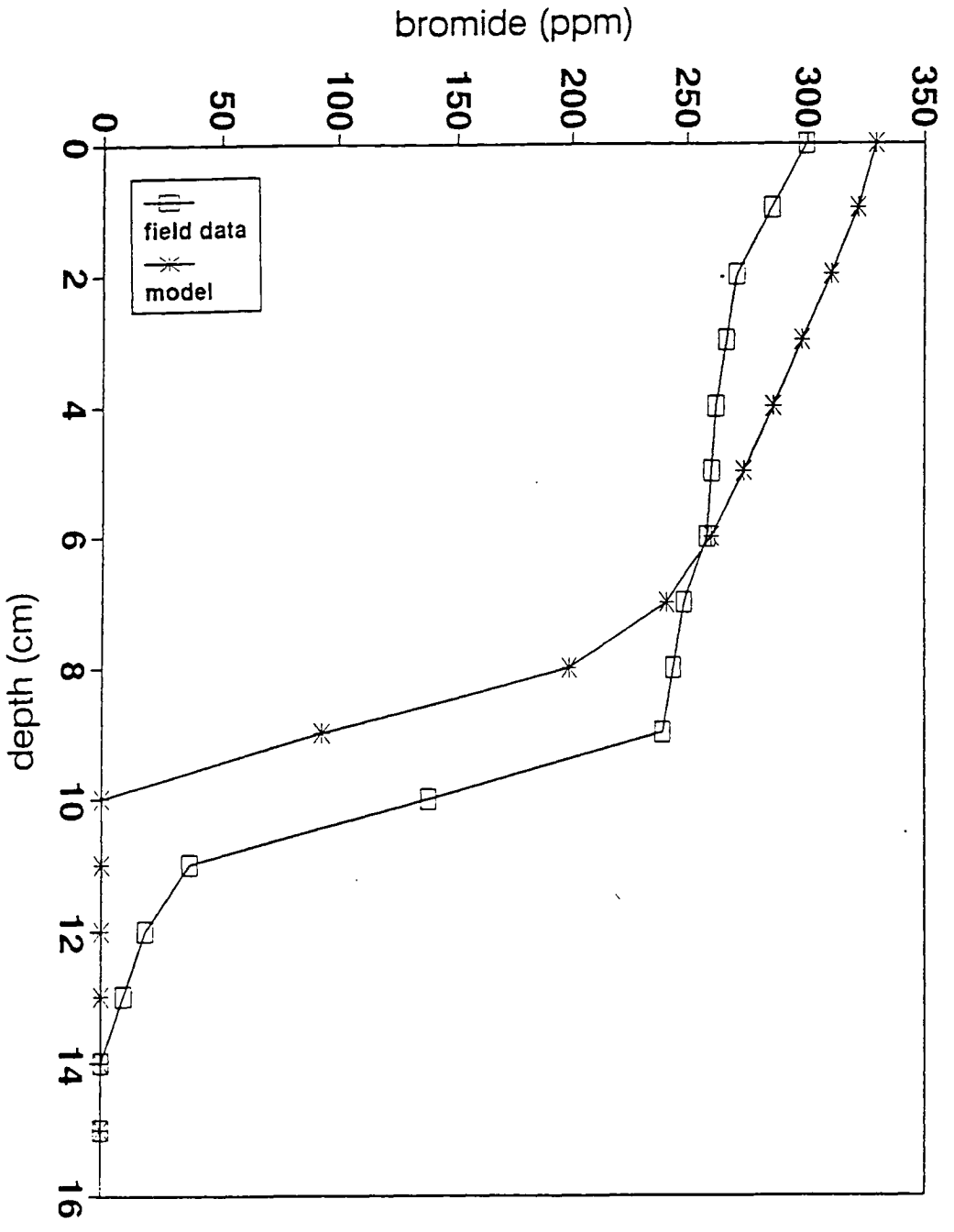

Figure 6.5. Comparison of bromide between field data and model prediction at 0 tension.

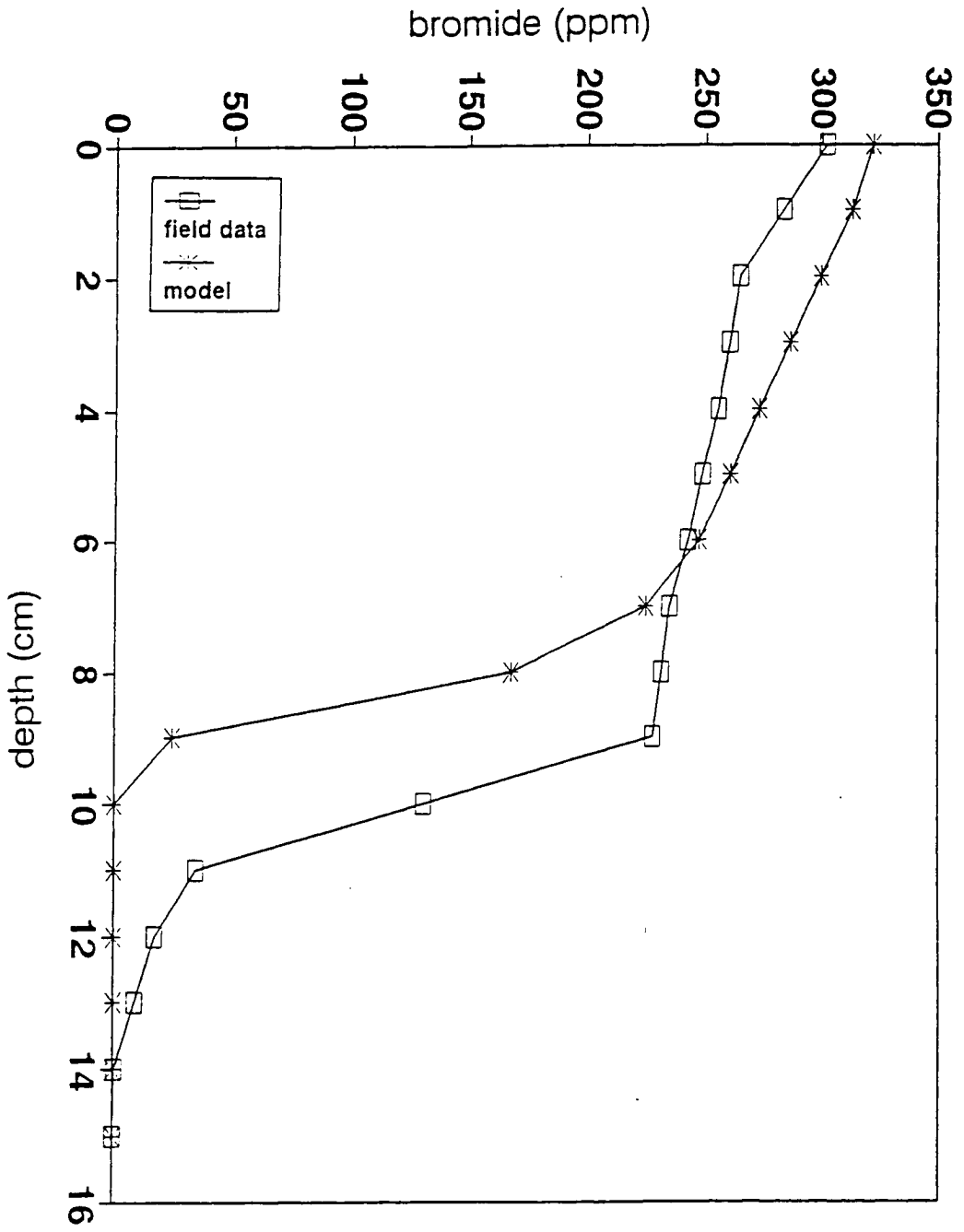

Figure 6.6. Comparison of bromide between field data and model prediction at 5 cm tension.

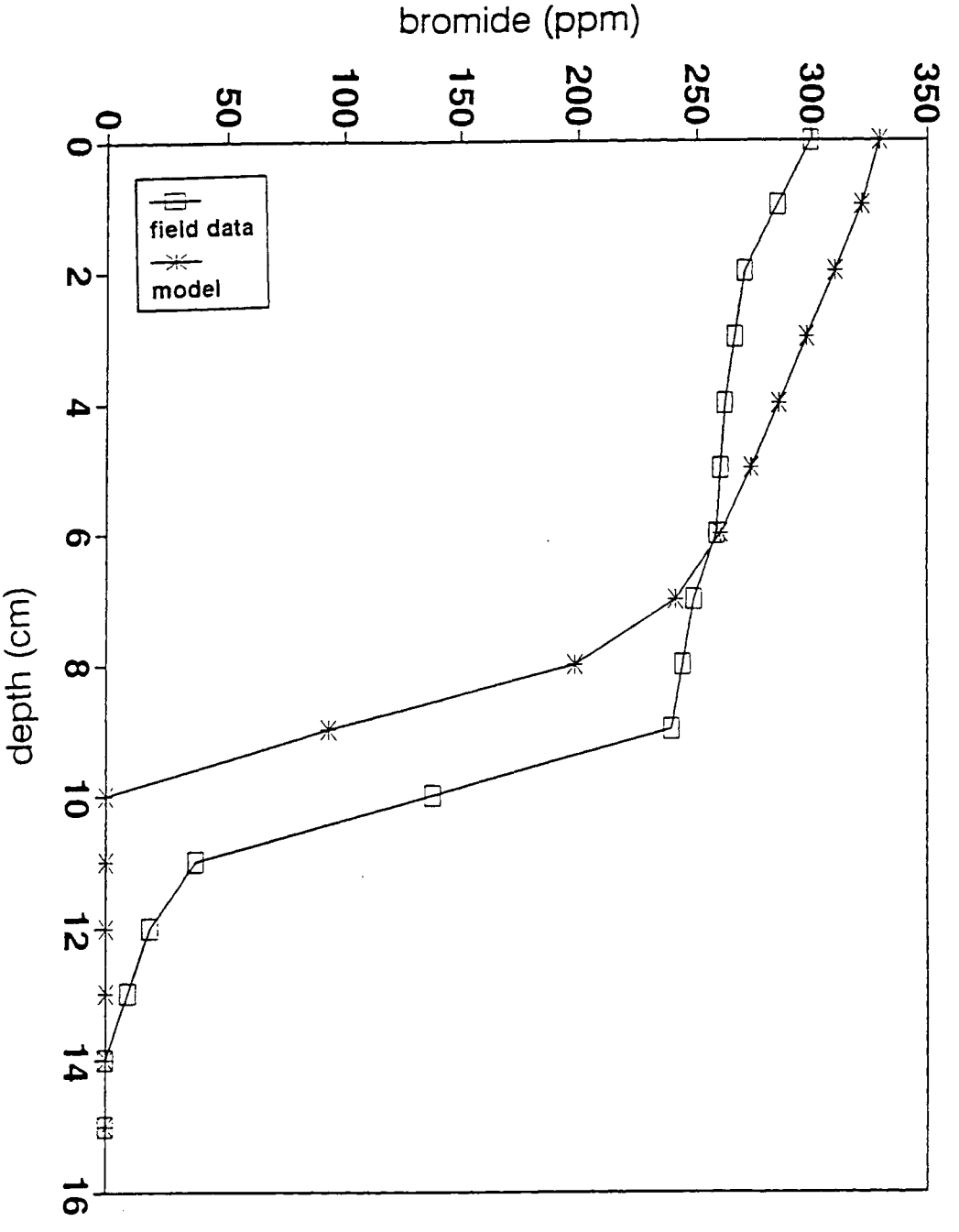

Figure 6.7. Comparison of bromide between field data and model prediction at 10 cm tension.

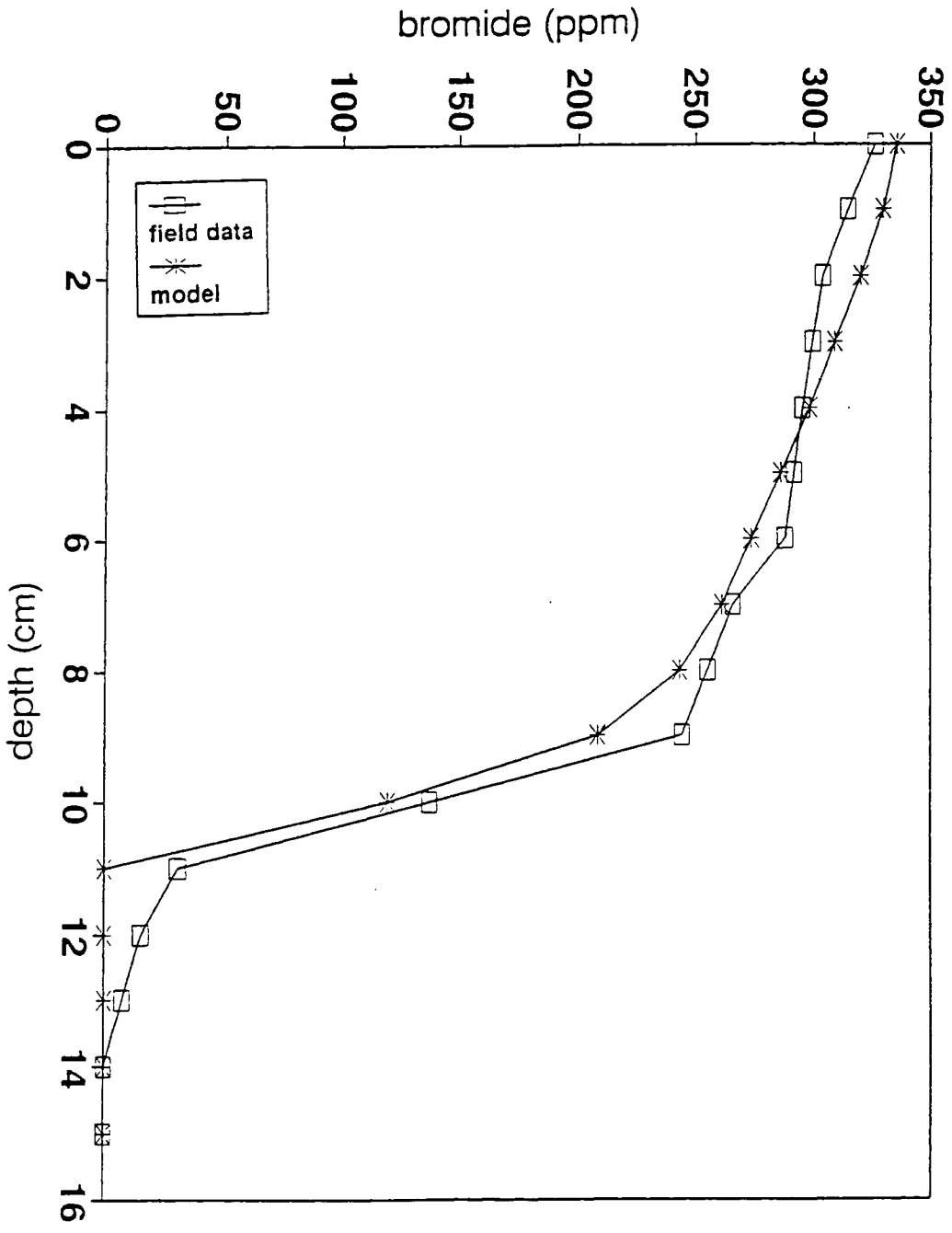

Figure 6.8. Comparison of bromide between field data and model prediction at 15 cm tension.

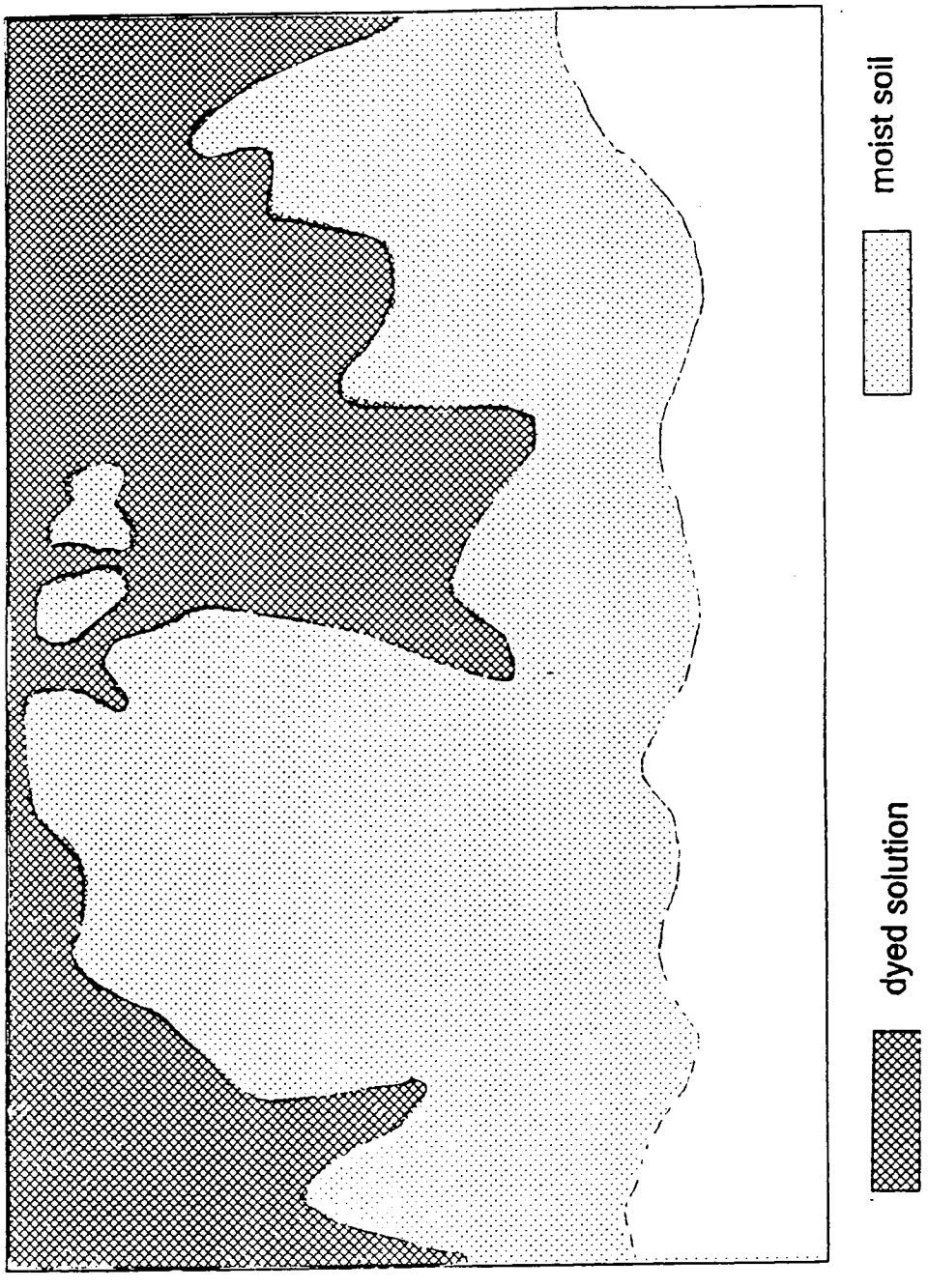

Figure 6.9. Position of dye and water fronts at end of infiltration for zero cm tension.

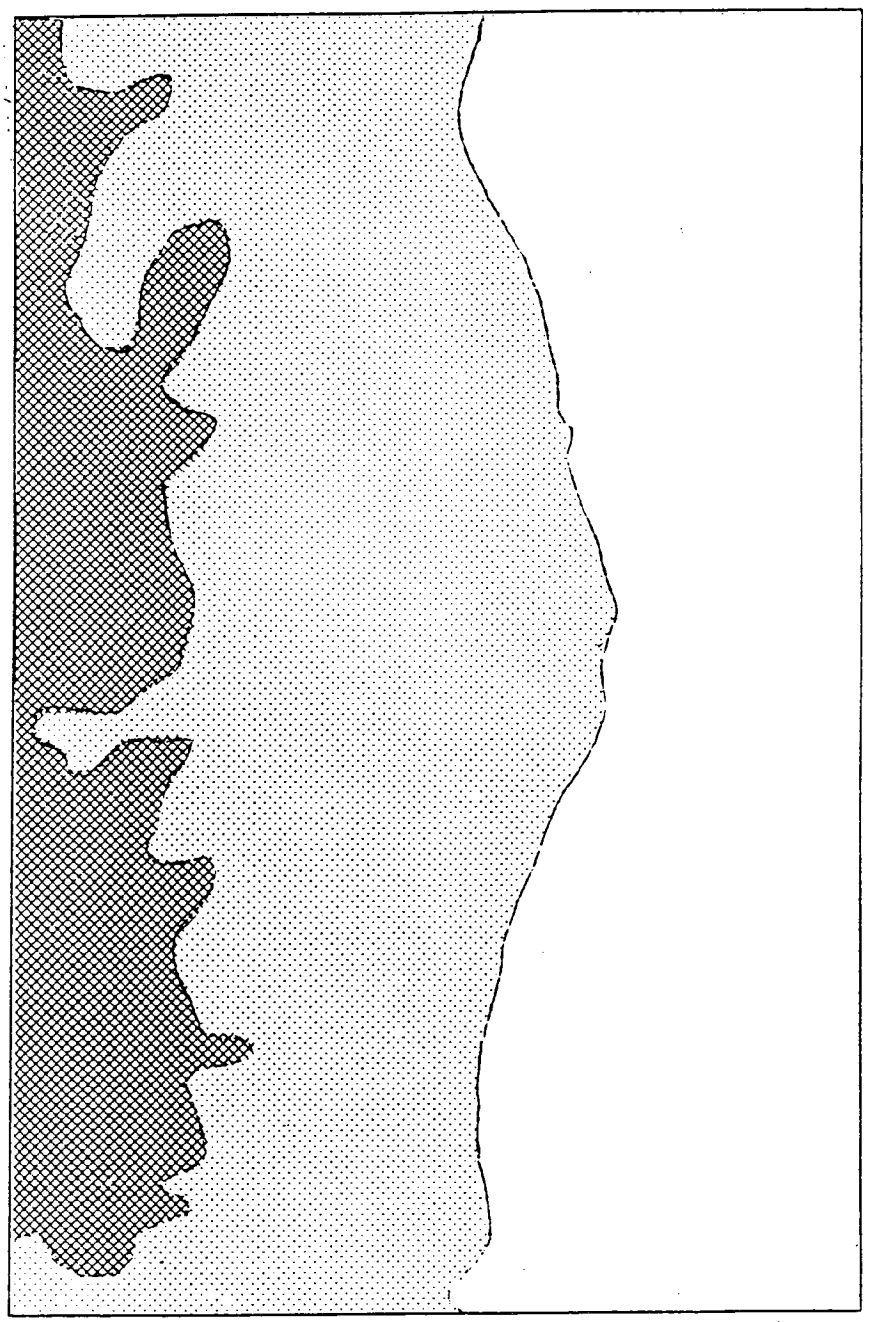

Figure 6.10. Position of dye and water fronts at end of infiltration for five cm tension.

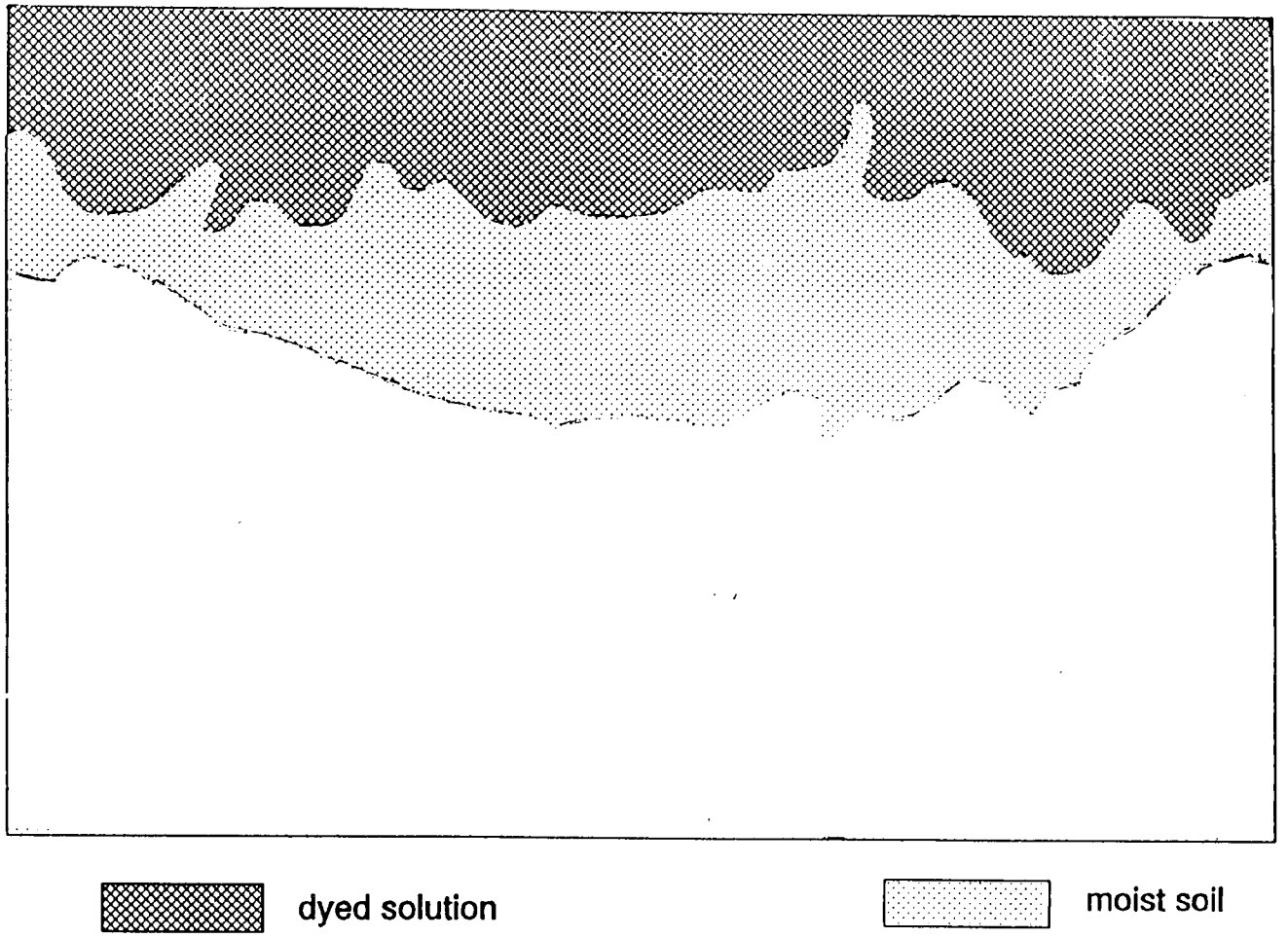

Figure 6.11. Position of dye and water fronts at end of infiltration for ten cm tension.

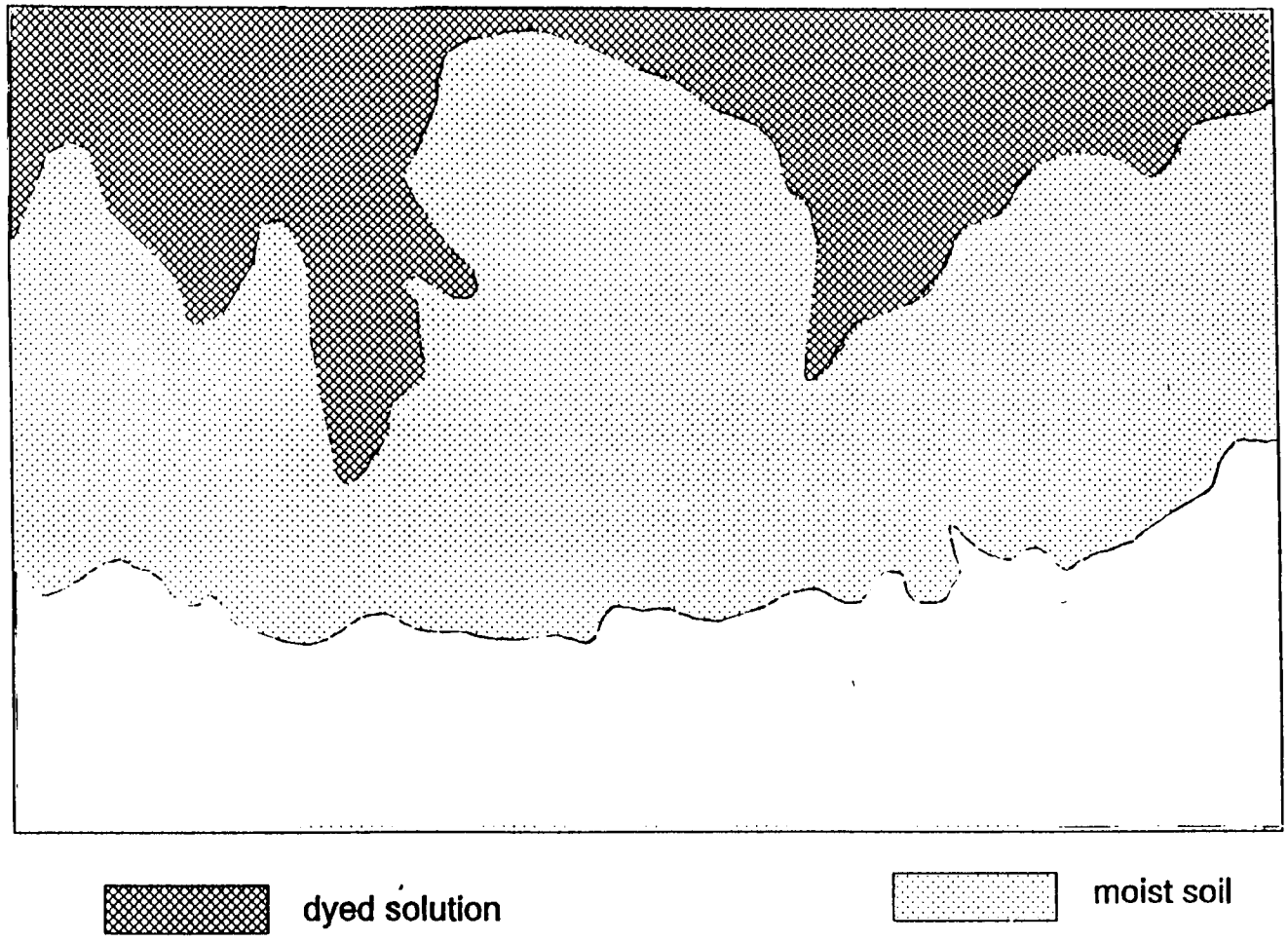

Figure 6.12. Showing the solution and dyed color movement in soil profile for fifteen cm tension.

CHAPTER 7

DETERMINATION OF HYDRAULIC CONDUCTIVITY AND INFILTRATION PARAMETERS

A solution to Richards equation for 1-dimensional vertical infiltration was given by Philip (1957, 1969). His solution gives the cumulative infiltration I in terms as a power series:

$$I(t) = St^{1/2} + (A_2 + K_o)t + A_3t^{3/2} + A_4t^2 + ... \quad (7.1)$$

where S is sorptivity, K_o is hydraulic conductivity at water content θ_o (for the initial condition) and A_2, A_3, A_4 are calculated coefficients. It is generally sufficient to replace Eq. (7.1) by a two or three-term truncated series such as

$$I(t) = St^{1/2} + At + Bt^{3/2} \quad (7.2)$$

For small time when the effects of gravity are negligible, we can write equation (7.1) is simply

$$I \sim St^{1/2} \quad (7.3)$$

Differentiation of equation (7.3) with respect to t leads to the infiltration rate i(t):

$$i(t) = \frac{1}{2}St^{-1/2} \quad (7.4)$$

For large times it is possible to represent equation (7.2) as a two term series

$$I = St^{1/2} + At \quad (7.5)$$

or in differential form

$$i(t) = \frac{1}{2}St^{-1/2} + A \tag{7.6}$$

where A is a the "final" infiltration rate and equal to steady state flow rate. For the disc infiltrometers $\frac{q_\infty}{\pi r^2}$, (cm^3/s) is analogous to S for the one-dimensional case where q_∞ is the steady state flow (cm^3/s) and r is the radius of disc.

An empirical equation for infiltration was introduced by Horton (1940)

$$i = i_c + (i_o - i_c)e^{-kt} \tag{7.7}$$

where i_c is steady state infiltration rate for large time, i_o is initial infiltration rate (for small time), t is the time, and k a characteristic constant related to how quickly i will decrease from i_o to i_c. By substituting the right side of Eq. (7.4) for i_o and the right side of Eq. (7.6) for i_c, we get

$$i = \frac{1}{2}St^{-1/2} + \frac{q_\infty}{\pi r^2}(1 - e^{-kt}) \tag{7.8}$$

where $q_\infty/(\pi r_o)$ has been substituted from s. Integrating Eq. (7.8) with respect to t.

$$I(t) = St^{1/2} + \frac{q_\infty}{\pi r^2}[t + \alpha(1 - e^{-kt})] \tag{7.9}$$

where $\alpha = k^{-1}$. This equation can be used for all times and contains the correct limiting values for small and large times.

For the disc permeameter, other algebraic forms from the one-dimensional case can be borrowed. In each case, I becomes the flow per unit area $q/(\pi r_o^2)$ as used in Chapter 3 already. In (7.2), S and B are simply empirical constants and the

assumption is that for some large t the series no longer applies. Equations (7.8) and (7.9) are more interesting in that they capture both large and small-time behavior. The forms of Equation (7.9) were suggested earlier (A. W. Warrick, personal communication) using both α and k as empirical constants.

Comparison Between Fitted and Calculated Infiltration Parameters

Equation (7.2) and (7.9) were used directly to fit field data. A program called NFIT (The University of Texas Medical Branch at Galveston, 1991) was used to best fit the field data to the parameters of equations (Table 7.1). Figures 7.1 through 7.4 are samples showing results for both equations compared with field data. The input to the program was I(t) as the dependant variable and time (t) as an independent variable along with the chosen model.

Table 7.2 shows the short time parameters (sorptivity) using equation (7.2), (7.9) and measured as determined in Chapter 3. Values of sorptivity calculated using Equation (7.9) match closely to those based on small time slopes only which we can call "conventional." Table 7.3 shows the correlation between calculated sorptivity using Equation (7.2), (7.9) and the conventional method. The correlation between conventional and calculated sorptivity using Equation (7.9) was 0.92. On the other hand, the correlation between conventional and calculated sorptivity using Equation 7.2 was 0.73. Thus, the sorptivity calculated using Equation (7.9) were closer to the Chapter 3 estimates than Equation (7.2).

Table 7.1. Parameters calculated using best fit for Philip equation and modified Horton equation.

Parameters for Philip (7.2)				Parameters for modified Horton (7.9)			
Codes**	S	B	C	S	$q_\infty/\pi r^2$	α	k
B151	0.008	0.001	-0.0000	0.030	0.000	450.59	5.9E+11
B152	0.007	0.001	-0.0005	0.020	0.000	222.85	5.9E+08
B153	0.009	0.001	-0.0000	0.019	0.000	192.88	5.9E+08
B101	0.019	0.001	-0.0000	0.034	0.000	138.74	3.1E+6
B102	0.014	0.002	-0.0001	0.032	0.000	106.22	2.6E+7
B103	0.019	0.002	-0.0001	0.036	0.000	133.99	8.1E+7
B51	0.023	0.004	-0.0007	0.080	0.000	902.14	4.2E+6
B52	0.030	0.003	-0.0005	0.066	0.001	184.34	2.4E+5
B53	0.029	0.003	-0.0004	0.063	0.001	219.73	1.6E+7
B01	0.043	0.003	-0.0004	0.075	0.001	161.00	3.6E+6
B02	0.037	0.005	-0.0001	0.097	0.000	452.13	2.8E+5
B03	0.041	0.004	-0.0008	0.085	0.001	174.40	2.3E+5
S151	0.019	0.001	-0.0000	0.025	0.000	65.85	2.7E+1
S152	0.023	0.001	-0.0000	0.028	0.000	34.67	1.9E+10
S153	0.020	0.001	-0.0000	0.035	0.000	210.95	3.0E+1
S101	0.038	0.002	-0.0000	0.048	0.001	39.49	7.6E+1
S102	0.043	0.001	-0.0000	0.041	0.001	-15.18	8.9E+1
S103	0.044	0.001	-0.0000	0.046	0.001	11.00	1.4E+2
S51	0.066	0.001	-0.0000	0.060	0.001	-13.34	2.9E+4
S52	0.063	0.001	-0.0001	0.054	0.001	-22.93	1.5E+4
S53	0.055	0.002	-0.0001	0.062	0.003	14.95	2.5E+3
S01	0.104	0.001	-0.0005	0.062	0.003	-66.72	3.4E+5
S02	0.114	0.001	-0.0005	0.077	0.003	-70.80	2.8E+7
S03	0.114	0.001	-0.0001	0.076	0.003	-63.48	3.4E+6

* The r^2 between field and fitted data in both equations were above 0.98 for all cases.
**B is the big disc permeameter and S is the small disc permeameter followed by the tension used (0, 5, 10 or 15 cm) and the replicate (1, 2 or 3).

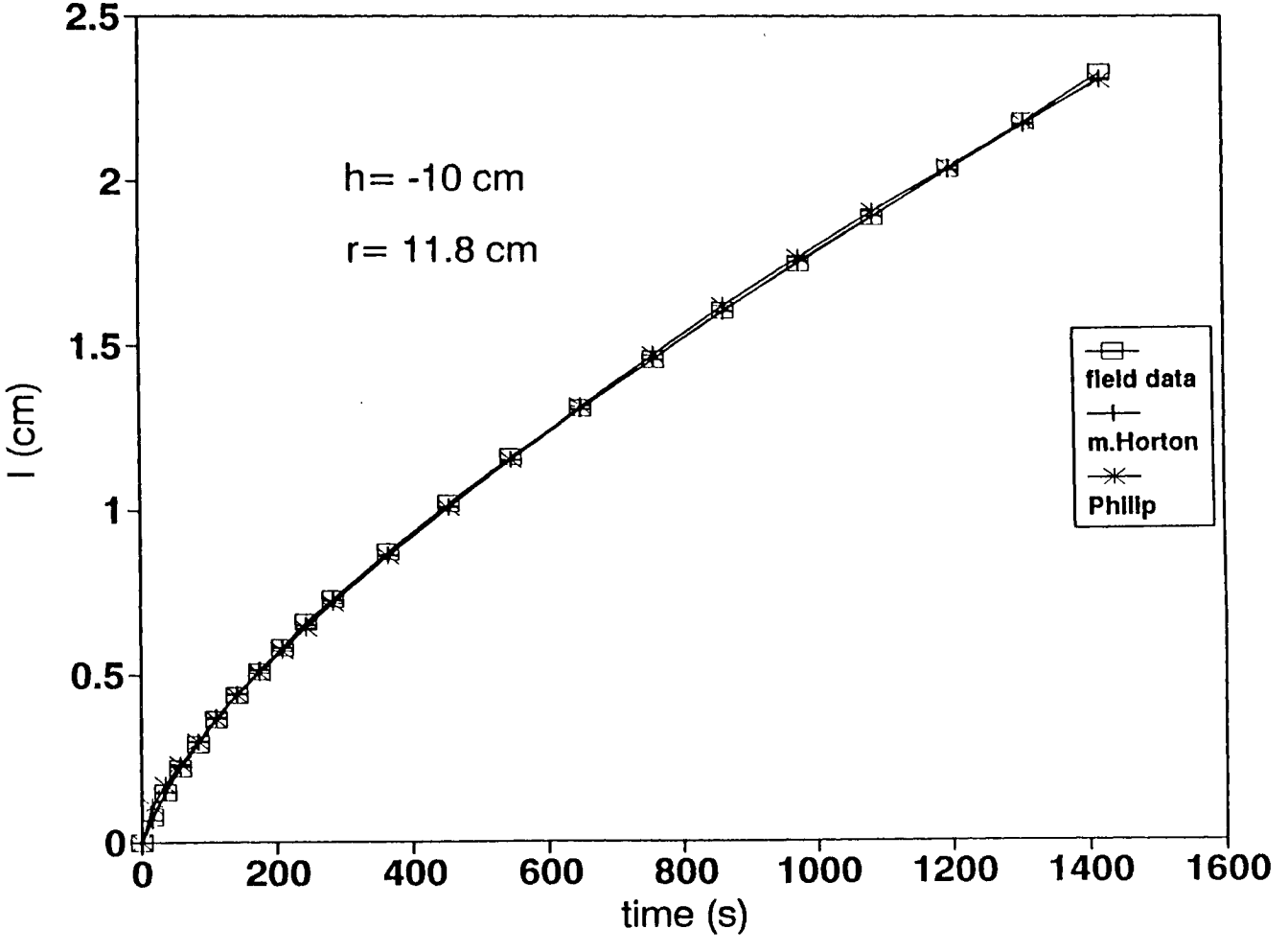

Figure 7.1. Cumulative infiltration for field data fitted using Philip equation and modified Horton equation (Eq. 7.9).

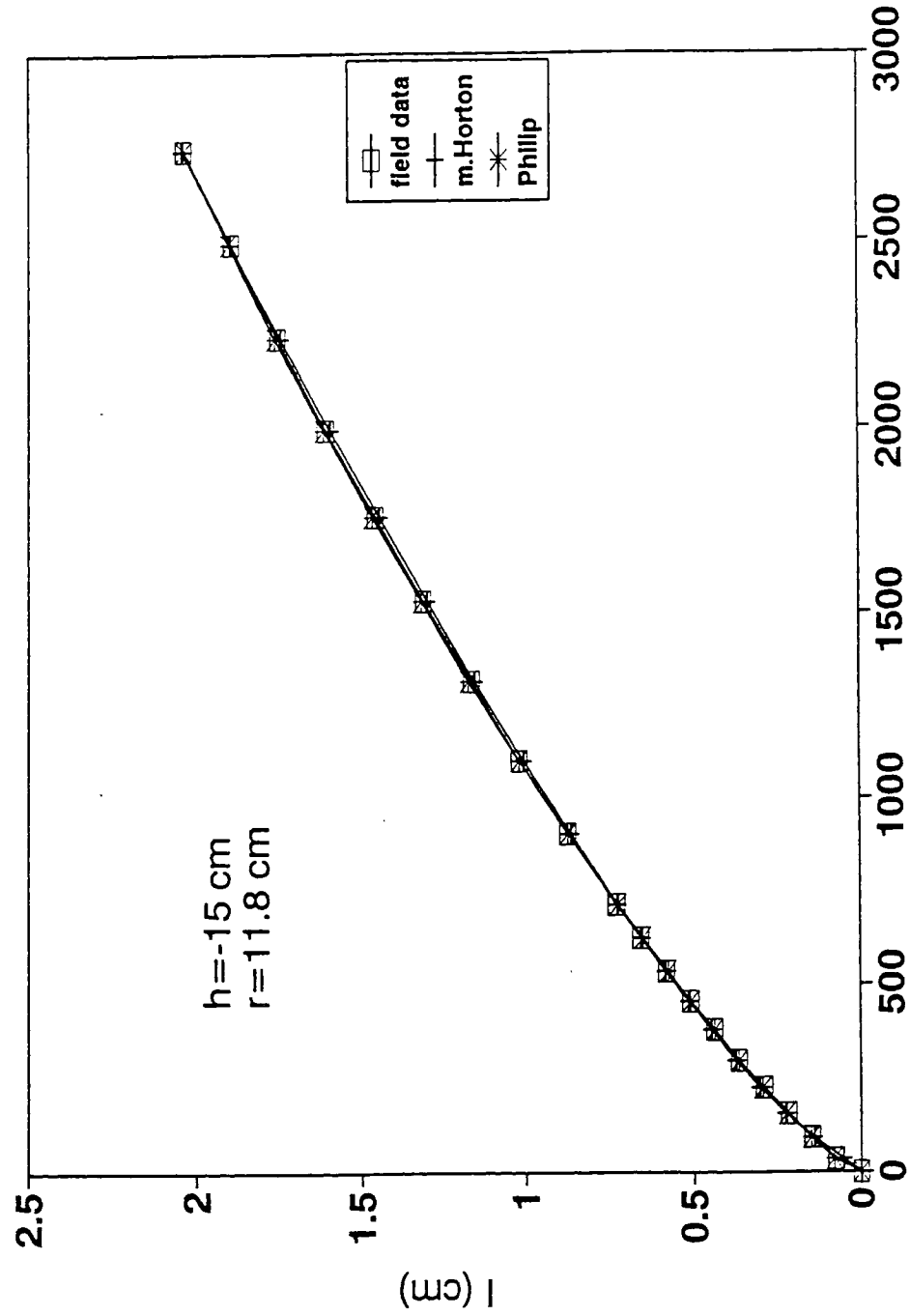

Figure 7.2. Cumulative infiltration for field data fitted using Philip equation and modified Horton equation (Eq. 7.9).

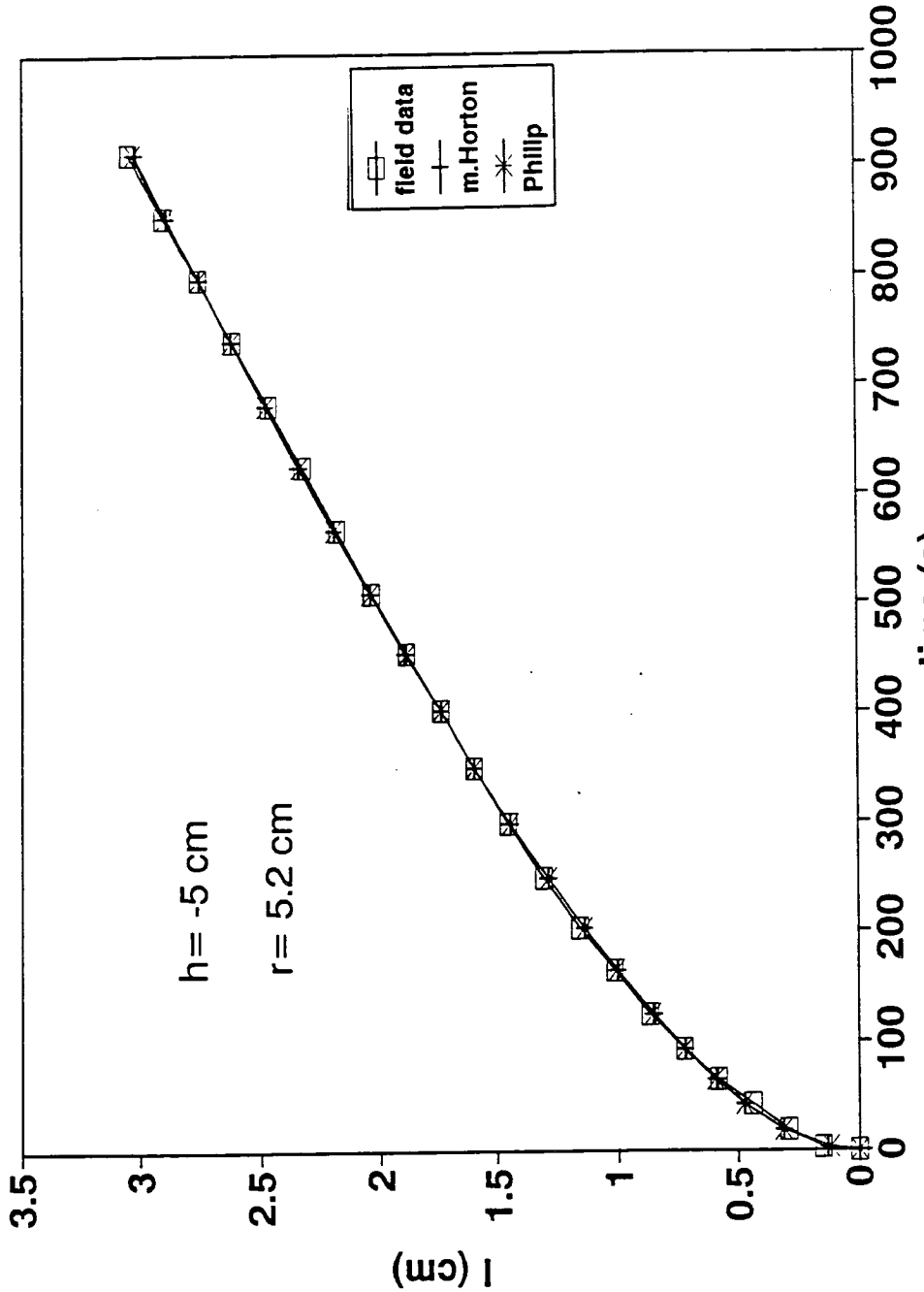

Figure 7.3. Cumulative infiltration for field data fitted using Philip equation and modified Horton equation (Eq. 7.9).

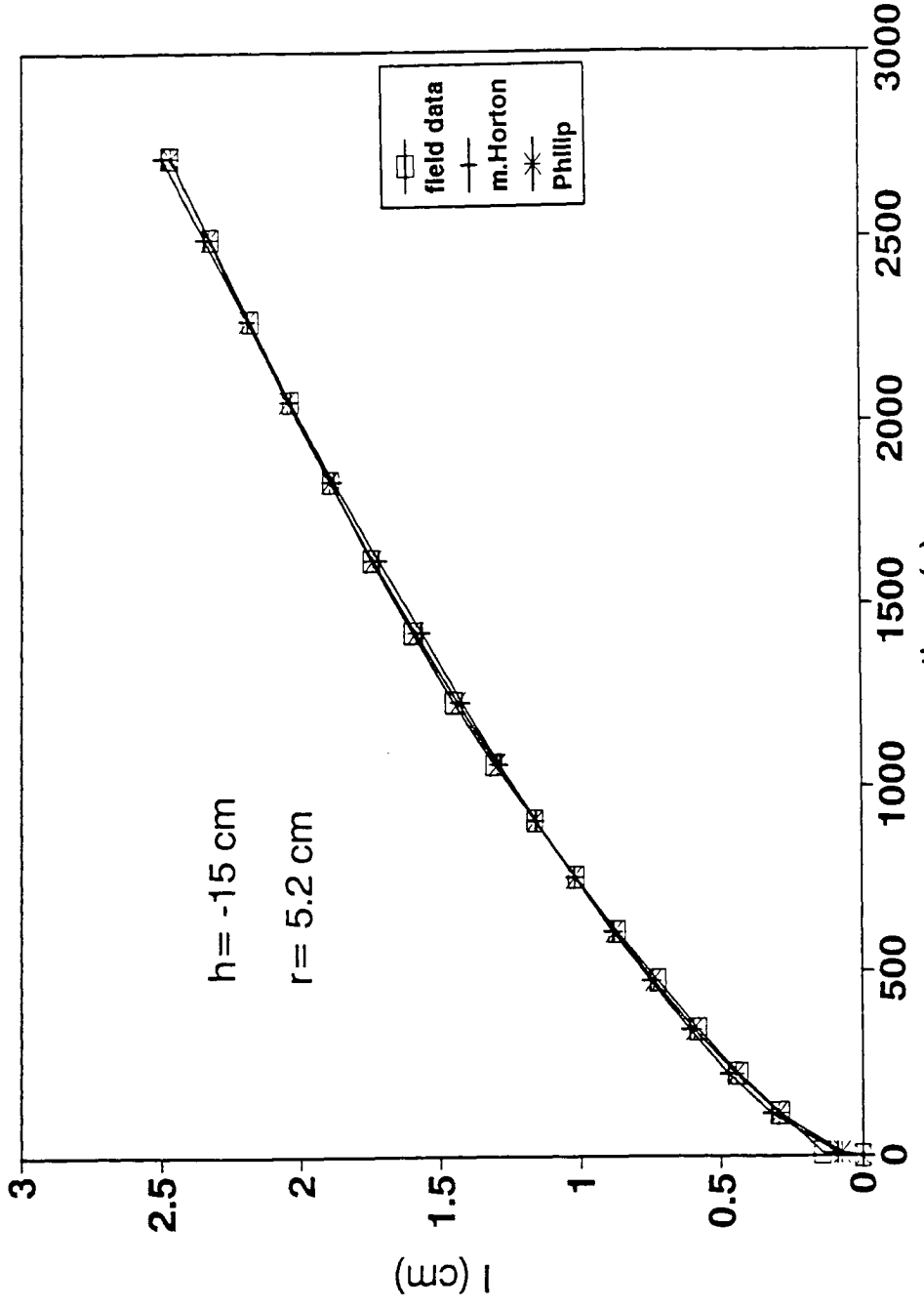

Figure 7.4. Cumulative infiltration for field data fitted using Philip equation and new equation.

Table 7.2. Sorptivity (small time infiltration parameter) calculated by A: Small time slope, B: Philip equation (7.3) and C: Modified Horton (7.9).

Rep	A	B	C
1	0.023	0.008	0.030
2	0.023	0.007	0.020
3	0.023	0.009	0.019
4	0.051	0.019	0.034
5	0.043	0.014	0.032
6	0.047	0.019	0.036
7	0.062	0.023	0.080
8	0.062	0.030	0.066
9	0.064	0.029	0.063
10	0.082	0.042	0.075
11	0.083	0.037	0.097
12	0.083	0.041	0.085
13	0.024	0.019	0.025
14	0.027	0.023	0.028
15	0.026	0.020	0.035
16	0.051	0.038	0.048
17	0.047	0.043	0.041
18	0.051	0.044	0.046
19	0.059	0.066	0.060
20	0.062	0.063	0.054
21	0.061	0.055	0.062
22	0.084	0.104	0.062
23	0.085	0.114	0.077
24	0.086	0.114	0.076

Table 7.3. Correlations r between A: Small time slope, B: Philip equation (7.3) and C: Modified Horton (7.9).

X	Y	(r)	Slope	Y-Intercept	n-2
A	B	0.74	1.04	-0.016	22
A	C	0.92	0.93	0.001	22
B	A	0.74	0.52	0.033	22
B	C	0.56	0.40	0.036	22
C	A	0.92	0.90	0.008	22
C	B	0.57	0.79	-3.411	22

Variable:	Mean	S.D.	Minimum	Maximum	n
A	0.055	0.022	0.023	0.086	24
B	0.040	0.031	0.007	0.004	24
C	0.052	0.022	0.019	0.097	24

The large time slopes (steady state flow) were larger than one calculated using Equation 7.9 (Table 7.4), but still there is good correlation between them, 0.861 (Table 7.5). This may indicate necessary times to approach steady-state flow and may be considerably longer than that indicated in the literature.

Determination of Hydraulic Conductivity Parameters

Another method of determination of hydraulic conductivity is possible, based on the large time results (steady state flow) when more than one measurement exists for the same spot (Lien, 1989; Smettem and Clothier, 1989). Already we have used the double disc method using measurements at the same spot for two different disc radius at the same tension. However, we can generalize using all of the radii and tensions together. The advantage is that the large time results tend to be more stable.

First consider Wooding's (1968) Equation

$$Q_\infty = K_o\left(1 + \frac{4}{\pi r \alpha}\right) \tag{7.10}$$

where $Q_\infty = \frac{q_\infty}{\pi r^2}$, is the steady state flow rate (cm/s), r is the radius of disc permeameter and K_o the hydraulic conductivity evaluated at the supply potential. This assumes the relation between unsaturated hydraulic conductivity (K_o) and saturated hydraulic conductivity (K_s) satisfy the Gardner (1958) equation:

Table 7.4. Steady state flow (large time infiltration parameter) A: measured B: new equation.

Rep	Large time Slope Eq. (7.2)	$q_\infty/\pi r^2$ Eq. (7.9)
1	5.81E-04	3.24E-04
2	5.79E-04	4E-04
3	5.69E-04	3.8E-04
4	0.001316	7.2E-04
5	0.001153	7.9E-04
6	0.001295	7.3E-04
7	0.001556	7.5E-04
8	0.001595	7.3E-04
9	0.001619	6.5E-04
10	0.002392	8.1E-04
11	0.002431	4.7E-04
12	0.002562	8.7E-04
13	6.55E-04	4.36E-04
14	6.75E-04	3.69E-04
15	6.45E-04	2.91E-04
16	0.002060	12.0E-4
17	0.001805	10.8E-4
18	0.002014	11.4E-4
19	0.002542	13.0E-4
20	0.002614	15.0E-4
21	0.002717	31.5E-4
22	0.004295	31.5E-4
23	0.004379	25.7E-4
24	0.004519	29.8E-4

Table 7.5. Correlation between measured steady state flow from slope (A) and modified Horton (C).

X	Y	Corr (r)	Slope	Y Intercept	n-2
A	C	0.863	0.665	-1.947E-04	22

Variable	Mean	S.D.	Minimum	Maximum	n
A	0.002	0.001	5.69E-04	0.005	24
C	0.001	9.192E-04	2.6E-04	0.003	24

$$K_o = K_s \exp(\alpha h_{wet}) \tag{7.11}$$

where h_{wet} is the tension used and α is a constant. Substitution of Eq. 7.11 into Equation 7.10 results in

$$Q_\infty = K_s \exp(\alpha h)\left(1 + \frac{4}{\pi r \alpha}\right) \tag{7.12}$$

Measurement of steady state flow at n tension, yields n equations with two unknowns of K_s and α:

$$Q_\infty^{h_1} = K_s \exp(\alpha h_1)\left(1 + \frac{4}{\pi r \alpha}\right) \tag{7.13}$$

$$Q_\infty^{h_2} = K_s \exp(\alpha h_2)\left(1 + \frac{4}{\pi r \alpha}\right) \tag{7.14}$$

$$\vdots \qquad\qquad \vdots$$

$$Q_\infty^{h_n} = K_s \exp(\alpha h_n)\left(1 + \frac{4}{\pi r \alpha}\right) \tag{7.15}$$

where h_1, h_2 and h_n are the supply potentials.

If n = 2, the value of α is obtained by dividing Eq. 7.14 by Eq. 7.13

$$\alpha = \frac{\ln[Q_\infty^{h_2}/Q_\infty^{h_1}]}{h_2 - h_1} \tag{7.16}$$

Equation 7.16 can be used to solve for α and substituted back into Equation 7.15 to solve for K_s. Also Equation 7.13 can be used to best fit the parameters of K_s and α with n = 4, such as with input from four different tensions. We set the radius (r) to

be constant (5.2 cm for small disc radius and 11.8 cm for large disc radius) during the fitting process. The result of both methods are shown in Table 7.6. The parameters were calculated by solving two equations and by best fitting four equations were closer to the average of the four parameters calculated at different tensions than for the individual tensions (Table 7.7).

Table 7.6. Parameters α and K_s calculated n = 2 and 4 tensions at the same spot.

	n = 2			n = 4	
Codes*	St. Flow	α	K sat.	α	K sat.
B151	.0009	.0410	.00046	.0551	.00067
B101	.0011	.0606	.00072		
B51	.0015	.0569	.00068		
B01	.0020	.0588	.00070		
B152	.0007	.0667	.00077	.0661	.00069
B102	.0010	.0544	.00060		
B52	.0014	.0667	.00073		
B02	.0019	.0606	.00069		
B153	.0009	.0290	.00030	.0480	.00055
B103	.0011	.0508	.00057		
B53	.0014	.0556	.00062		
B03	.0018	.0532	.00060		
S151	.0010	.0385	.00024	.0666	.00051
S101	.0012	.0725	.00055		
S51	.0017	.0733	.00056		
S01	.0024	.0729	.00056		
S152	.0008	.0642	.00042	.0806	.00059
S102	.0011	.0712	.00049		
S52	,0015	.0932	.00067		
S02	.0024	.0822	.00061		
S153	.0010	.0260	.00015	.0586	.00044
S103	.0012	.0685	.00051		
S53	.0016	.0651	.00048		
S03	.0023	.0668	.00049		

* B is the big disc permeameter and S is the small disc permeameter followed by the tension used (0, 5, 10 or 15) and the replicate (1, 2 or 3).

Table 7.7. Comparison between average for n = 2, α and K_s calculated using two equations at the same spot (2 and 4 tensions).

	fitting method			2 Equation method	
Replicate	Radius	α	K sat.	α	K sat.
1	11.8	.0551	.00067	.0543	.00064
2	11.8	.0661	.00069	.0621	.00070
3	11.8	.048	.00055	.0471	.00052
average	11.8	.0564	.00064	.0645	.00062
1	5.2	.0666	.00051	.0643	.00048
2	5.2	.0806	.00059	.0777	.00055
3	5.2	.0586	.00044	.0566	.00041
average	5.2	.0759	.0006	.0732	.00052

CHAPTER 8

SUMMARY AND CONCLUSIONS

Disc permeameters were used to determine unsaturated hydraulic conductivity in the field. Two different methods were used to determine unsaturated hydraulic conductivity in situ. The single disc method introduced by White and Perroux (1987, 1989) is dependent on the measurements of sorptivity, steady state flow rate, initial and final volumetric water content. The double disc method is from Wooding's equation applied to two different disc radii at the same tension and solving for λ_c and unsaturated hydraulic conductivity by measurement of steady state flow. Additionally, a third method was explored (in Chapter 7) using steady state results for combinations of tensions and radii. Unsaturated hydraulic conductivity for disturbed and undisturbed soil cores taken from the same plot were calculated using a soil retention curve and van Genuchten's equation. Results from the different methods have been compared. There were significant differences among the hydraulic conductivity measured using different methods, but there was no significant difference among the means of hydraulic conductivity (using the Student-Newman-Keults Test) for the single disc, the double disc methods, and disturbed soil cores at zero tension. There was a difference between the mean of hydraulic conductivity in undisturbed soil cores and the other methods used. At five cm tension, there were no significant differences in the mean of hydraulic conductivity among the methods used. At 10 and 15 cm tensions, while there were no significant differences in the

mean hydraulic conductivity among the single, double disc methods and undisturbed soil cores; there was a significant difference between results from the disturbed soil cores and other methods used. Thus, we conclude that using disturbed or undisturbed soil cores does not always represent the hydraulic conductivity of soil in the field.

We found that double disc method was fast and an accurate method for calculating unsaturated hydraulic conductivity in the field. The double disc method is much easier to use than the single disc method and can be used to measure unsaturated hydraulic conductivity in moist soil which the single disc method fails to do. Adding a multiple air inlet to the disc permeameter allowed measurement of unsaturated hydraulic conductivity at the same spot for more than one tension and avoids spatial variation using double disc method.

The double disc method was used to compare unsaturated hydraulic conductivity between disturbed and undisturbed soil. There were significant differences between disturbed and undisturbed soil in all the tensions used. We concluded that hydraulic conductivity increased as a result of soil disturbance, or land preparation.

Spatial variation was studied along a 70 m transect. Unsaturated hydraulic conductivity was measured using the double disc method at 70 points, one meter apart. The best fitting variogram models were exponential for the unsaturated hydraulic conductivity in all tensions used except for the zero tension which was random. For steady-state flow measured with the big disc permeameter, the best

fitting variograms were exponential for pores radii of 0.03 - 0.015 and 0.015 - 0.010 cm. For other pore radii, no spatial structure was observed. The best variogram model fitted for steady state flow were Michaelis-Menton models for the five and 15 cm tension, and an exponential model for 10 cm tension.

The disc permeameter was used to add a 5 cm depth of water, bromide and dye solution at 0, 5, 10, and 15 cm tensions with three replicates. Water content and bromide concentration were determined with depth. Averages of the replicated values were compared with a one-dimensional simulation model for water and bromide concentration under the same initial and boundary condition in the field. The results showed that the bromide and water in the field move deeper than the simulated model in all the tensions used. The greatest difference between predicted or simulated model and field data for both bromide and water was in zero tension, and the smallest difference between simulated model and field data was in 15 cm tension for both bromide and water content. We concluded that the preferential flow happens in all tensions we used, and it was bigger in smaller tensions used as a result of eliminating big cracks, root channels, and worm holes from the flow path of preferential flow.

An equation was developed for cumulative infiltration which contain the parameters for small and large time.

$$I(t) = St^{1/2} + \frac{q_s}{\pi r^2}[t + \alpha(1 - e^{-kt})].$$

where $\alpha = k^{-1}$

This equation fitted experimental curves very well, and the parameters calculated matched closely to one measured in the field. It appears superior to a second form used which was analogous to a 3-term Philip equation.

APPENDIX A

Table A-1. The input data for water release curve for the six soil cores used to measure hydraulic parameters (alpha and n).

tension (cm)	first dist. VWC*	second dist. VWC	third dist. VWC	fourth undist VWC	fifth undist VWC	sixth undist VWC
zero	0.409396	0.465957	0.449515	0.410808	0.468691	0.341112
five	0.404922	0.460403	0.443123	0.406534	0.463381	0.333962
ten	0.401585	0.458970	0.439440	0.405156	0.459012	0.332662
fifteen	0.391027	0.448520	0.429251	0.394946	0.448735	0.324679
thirty	0.360039	0.420901	0.401707	0.368082	0.419220	0.299076
sixity	0.287806	0.294051	0.301370	0.276161	0.259242	0.288291
hundred	0.265699	0.242214	0.265558	0.232340	0.236139	0.242041
two h.	0.194005	0.186349	0.195502	0.186594	0.195167	0.186368
three h	0.174278	0.167883	0.167807	0.163962	0.168746	0.175036
thousand	0.130045	0.127227	0.125151	0.129531	0.133539	0.135122
fif.thou.	0.113070	0.109005	0.110942	0.119298	0.114967	0.119291
alpha	0.02381	0.02431	0.02342	0.2488	0.02877	0.01949
N	1.6704	1.8635	1.7787	1.74958	1.7959	1.60326
sat.WC	0.40939	0.4659	0.4495	0.4108	0.4659	0.3411
res.WC	0.09	0.09	0.09	0.09	0.09	0.09
sat.K	3.23	3.88	3.66	5.39	5.63	5.15

VWC is volumetric water content (cm^3/cm^3).

APPENDIX B

Table B-1. Steady state flow for small disc permeameter along the 70 m transect.

	(cm/s)			
POINT	ZERO	FIVE	TEN	FIFTEEN
1	0.004624	0.002306	0.001017	0.000699
2	0.005322	0.002746	0.001043	0.000688
3	0.004302	0.002306	0.001078	0.000848
4	0.005016	0.002887	0.001129	0.000759
5	0.004926	0.002633	0.001121	0.000774
6	0.005916	0.003627	0.001367	0.000851
7	0.005053	0.002613	0.001219	0.000904
8	0.004851	0.002843	0.001309	0.000934
9	0.007127	0.003668	0.001245	0.000691
10	0.00501	0.003328	0.001451	0.001016
11	0.005053	0.003108	0.001379	0.000988
12	0.004705	0.002985	0.001324	0.001073
13	0.004761	0.003037	0.001251	0.000845
14	0.006709	0.003441	0.001396	0.000846
15	0.005187	0.002903	0.0012	0.000786
16	0.005399	0.003344	0.001403	0.000954
17	0.005592	0.003306	0.001456	0.001022
18	0.004107	0.001939	0.000751	0.00045
19	0.003259	0.001612	0.000741	0.000508
20	0.003999	0.001757	0.000738	0.000467
21	0.003098	0.001307	0.000662	0.000457
22	0.003963	0.001792	0.000752	0.00048
23	0.004919	0.003034	0.001246	0.000871
24	0.004296	0.001865	0.000781	0.000447
25	0.004287	0.002378	0.001052	0.000613
26	0.004116	0.002064	0.00094	0.000728
27	0.004153	0.002439	0.001148	0.000862
28	0.005896	0.002548	0.000968	0.000607
29	0.003695	0.001844	0.000831	0.000587
30	0.002933	0.001598	0.000793	0.000573
31	0.004541	0.00257	0.001131	0.000814
32	0.004471	0.002081	0.000833	0.00056
33	0.003947	0.002161	0.001052	0.000774
34	0.004023	0.002211	0.001052	0.000769
35	0.003483	0.002028	0.00093	0.000674
36	0.003962	0.002204	0.001022	0.000745
37	0.004152	0.002005	0.000903	0.000662
38	0.005027	0.002622	0.001036	0.000671
39	0.004698	0.002419	0.000981	0.000649
40	0.004858	0.002179	0.000859	0.000553
41	0.005981	0.002831	0.001067	0.000711
42	0.005649	0.00281	0.001087	0.000738
43	0.004428	0.00254	0.001128	0.000818
44	0.004418	0.002552	0.001147	0.000798
45	0.004557	0.002602	0.001166	0.000797
46	0.004987	0.002475	0.000989	0.000642

Table B-1. Steady state flow for small disc permeameter along the 70 m transect (Continued).

47	0.00567	0.002946	0.001142	0.000744
48	0.005392	0.003064	0.001216	0.000746
49	0.005677	0.002702	0.00109	0.000721
50	0.005297	0.002809	0.001033	0.000634
51	0.004302	0.002509	0.001123	0.000833
52	0.003651	0.00211	0.000959	0.000652
53	0.003171	0.001885	0.000996	0.000748
54	0.004733	0.002968	0.00125	0.000902
55	0.004501	0.002597	0.001178	0.000827
56	0.004088	0.002208	0.00098	0.000658
57	0.004752	0.002803	0.001264	0.000899
58	0.005199	0.002825	0.00135	0.000911
59	0.004525	0.002593	0.001126	0.000784
60	0.00459	0.00248	0.001076	0.000736
61	0.005961	0.003148	0.001256	0.000798
62	0.005229	0.00301	0.001263	0.000849
63	0.004394	0.002551	0.001169	0.000856
64	0.004366	0.002598	0.001405	0.001012
65	0.005724	0.002603	0.000904	0.000603
66	0.004003	0.002412	0.001317	0.001066
67	0.004467	0.002563	0.001286	0.000933
68	0.003915	0.002254	0.001011	0.000692
69	0.004704	0.002904	0.001268	0.000898
70	0.004927	0.002562	0.001331	0.000968

Table B-2. Steady state flow for large disc permeameter along the 70 m transect.

		(cm/s)		
POINTS	ZERO	FIVE	TEN	FIFTEEN
1	0.003022	0.001526	0.000886	0.000564
2	0.003561	0.001865	0.00092	0.000552
3	0.002774	0.001525	0.000965	0.000736
4	0.003325	0.001973	0.00103	0.000633
5	0.003255	0.001778	0.00102	0.00065
6	0.004019	0.002544	0.001338	0.00074
7	0.003353	0.001762	0.001147	0.000801
8	0.003197	0.001939	0.001263	0.000836
9	0.004953	0.002575	0.001181	0.000555
10	0.00332	0.002314	0.001446	0.000931
11	0.003353	0.002144	0.001353	0.000899
12	0.003084	0.002049	0.001283	0.000997
13	0.003128	0.002089	0.001189	0.000733
14	0.004631	0.0024	0.001376	0.000734
15	0.003456	0.001986	0.001122	0.000665
16	0.00362	0.002329	0.001385	0.000859
17	0.003769	0.002296	0.001453	0.000937
18	0.002624	0.001242	0.000542	0.000275
19	0.001969	0.00099	0.00053	0.000343
20	0.00254	0.001102	0.000525	0.000296
21	0.001845	0.000755	0.000427	0.000283
22	0.002512	0.001129	0.000544	0.00031
23	0.00325	0.002087	0.001182	0.000763
24	0.002769	0.001185	0.00058	0.000272
25	0.002762	0.001581	0.000931	0.000464
26	0.00263	0.001339	0.000787	0.000598
27	0.002659	0.001628	0.001055	0.000753
28	0.004004	0.001712	0.000822	0.000457
29	0.002305	0.001169	0.000645	0.000434
30	0.001718	0.000979	0.000596	0.000418
31	0.002958	0.001729	0.001033	0.000697
32	0.002904	0.001352	0.000648	0.000403
33	0.0025	0.001414	0.000932	0.000651
34	0.002559	0.001452	0.000932	0.000645

Table B-2. Steady state flow for large disc permeameter along the 70 m transect (Continued).

35	0.002142	0.001311	0.000774	0.000535
36	0.002511	0.001447	0.000893	0.000617
37	0.002658	0.001294	0.000739	0.000522
38	0.003333	0.001769	0.000911	0.000531
39	0.00308	0.001613	0.00084	0.000506
40	0.003203	0.001428	0.000682	0.000395
41	0.004069	0.00193	0.00095	0.000578
42	0.003813	0.001914	0.000976	0.000609
43	0.002871	0.001706	0.001029	0.000702
44	0.002863	0.001715	0.001055	0.000678
45	0.00297	0.001753	0.001079	0.000677
46	0.003302	0.001656	0.00085	0.000498
47	0.00383	0.002019	0.001047	0.000617
48	0.003615	0.00211	0.001143	0.000619
49	0.003834	0.001831	0.00098	0.00059
50	0.003542	0.001913	0.000906	0.000489
51	0.002774	0.001682	0.001023	0.000719
52	0.002271	0.001374	0.000811	0.000509
53	0.001901	0.001291	0.000858	0.000621
54	0.003106	0.002036	0.001187	0.000799
55	0.002928	0.001749	0.001094	0.000712
56	0.002609	0.00145	0.000839	0.000516
57	0.003121	0.001909	0.001205	0.000795
58	0.003466	0.002182	0.001317	0.00081
59	0.002946	0.001747	0.001027	0.000662
60	0.002996	0.00166	0.000962	0.000607
61	0.004054	0.002174	0.001195	0.000678
62	0.003489	0.002068	0.001204	0.000737
63	0.002844	0.001715	0.001082	0.000746
64	0.002823	0.001982	0.001388	0.000926
65	0.003871	0.001754	0.00074	0.000453
66	0.002543	0.00176	0.001274	0.000989
67	0.002901	0.001878	0.001233	0.000835
68	0.002475	0.001485	0.000878	0.000556
69	0.003084	0.001986	0.00121	0.000795
70	0.003256	0.001877	0.001292	0.000875

Table B-3. Hydraulic conductivity along the 70 m transect.

	(cm/h)			
POINTS	ZERO	FIVE	TEN	FIFTEEN
1	6.335345	3.277073	2.816236	1.645691
2	7.821545	4.211945	2.962418	1.597527
3	5.650164	3.276409	3.153491	2.333345
4	7.170491	4.511973	3.428618	1.921227
5	6.977773	3.972491	3.385336	1.991318
6	9.088482	6.085009	4.735255	2.348264
7	7.248318	3.929455	3.924982	2.593064
8	6.819464	4.417273	4.417936	2.731636
9	11.66549	6.1708	4.068464	1.609745
10	7.157882	5.450164	5.194445	3.111409
11	7.249645	4.980927	4.800082	2.981645
12	6.507209	4.719291	4.503409	3.374536
13	6.628073	4.830582	4.101327	2.319327
14	10.77603	5.688291	4.897773	2.322927
15	7.534409	4.545436	3.817773	2.049191
16	7.986773	5.508045	4.934945	2.822945
17	8.397045	5.402482	5.223	3.135136
18	5.235909	2.495864	1.358209	0.496664
19	3.430155	1.800727	1.307209	0.7677
20	5.0048	2.108718	1.288173	0.578264
21	3.085764	1.151664	0.868855	0.5283
22	4.926973	2.183227	1.366118	0.635236
23	6.9645	4.824609	4.072773	2.438673
24	5.637273	2.338882	1.520918	0.482645
25	5.618409	3.428745	3.009109	1.2501
26	5.2525	2.761764	2.398527	1.780855
27	5.333264	3.558236	3.534927	2.400027
28	9.044782	3.790391	2.546509	1.222064
29	4.3564	2.293855	1.795855	1.129145
30	2.734455	1.771245	1.589155	1.064973
31	6.158836	3.836745	3.440645	2.175545
32	6.010482	2.798545	1.806273	1.004591
33	4.894173	2.968418	3.010909	1.994018
34	5.0558	3.073736	3.012518	1.968491
35	3.905364	2.685264	2.340709	1.530845

Table B-3. Hydraulic conductivity along the 70 m transect (Continued).

36	4.925645	3.060464	2.845691	1.859755
37	5.330609	2.637582	2.193627	1.478182
38	7.193336	3.949645	2.921836	1.516827
39	6.4946	3.518136	2.621755	1.417609
40	6.8334	3.007473	1.954064	0.973855
41	9.225936	4.3931	3.089564	1.701055
42	8.519236	4.348073	3.200182	1.824709
43	5.917773	3.774464	3.423409	2.196573
44	5.8972	3.7993	3.533127	2.101855
45	6.193245	3.905282	3.636927	2.096645
46	7.108873	3.6354	2.666645	1.385264
47	8.564927	4.636818	3.502064	1.857055
48	7.972836	4.8885	3.908455	1.865864
49	8.577536	4.117909	3.215809	1.750118
50	7.769218	4.345418	2.9028	1.346618
51	5.651491	3.707918	3.398264	2.263255
52	4.262364	2.860445	2.498018	1.428218
53	3.242082	2.964409	2.700409	1.872873
54	6.567782	4.683836	4.094509	2.585155
55	6.075036	3.893718	3.700145	2.235218
56	5.1942	3.069091	2.616545	1.457155
57	6.608545	4.334136	4.168855	2.568436
58	7.560573	6.033973	4.645282	2.627209
59	6.126036	3.886418	3.413891	2.037873
60	6.262827	3.646964	3.140564	1.8186
61	9.184509	5.066336	4.128982	2.101855
62	7.625791	4.772282	4.164545	2.336945
63	5.844591	3.798636	3.650755	2.371091
64	5.786291	5.386391	4.946264	3.091282
65	8.678209	3.907273	2.197036	1.206245
66	5.013045	4.4883	4.463727	3.341291
67	6.001191	4.814673	4.289891	2.727327
68	4.825636	3.166445	2.783373	1.613345
69	6.505882	4.547427	4.1922	2.567536
70	6.979764	4.812682	4.541482	2.887827

Table B-4. Different pore size flow rates along the 70 m transect.

POINTS	total	>0.030	>0.015	>0.010
1	10.8792	5.3874	2.304	1.1592
2	12.8178	6.1056	3.4002	1.3266
3	9.9846	4.4937	2.0169	0.8244
4	11.9682	4.8645	3.3957	1.4301
5	11.7171	5.3181	2.7279	1.3302
6	14.4693	5.3118	4.3407	2.1537
7	12.0699	5.7267	2.214	1.2447
8	11.5101	4.5297	2.4327	1.5381
9	17.8308	8.5608	5.0193	2.2545
10	11.9511	3.6225	3.1221	1.854
11	12.0717	4.3551	2.8449	1.6362
12	11.1033	3.7287	2.7549	1.0296
13	11.2608	3.7404	3.2418	1.6416
14	16.6707	8.0307	3.6855	2.3139
15	12.4425	5.2947	3.1095	1.6452
16	13.0329	4.6476	3.3993	1.8936
17	13.5675	5.301	3.0357	1.8567
18	9.4446	4.9725	2.5218	0.9594
19	7.0893	3.5253	1.6569	0.6714
20	9.144	5.1777	2.0754	0.8262
21	6.6402	3.9231	1.1817	0.5157
22	9.0423	4.9788	2.106	0.8415
23	11.6991	4.1868	3.258	1.5093
24	9.9684	5.7015	2.178	1.1106
25	9.9441	4.2543	2.3382	1.6803
26	9.4671	4.6485	1.9854	0.6822
27	9.5715	3.7125	2.061	1.0881
28	14.4126	8.2503	3.2031	1.3131
29	8.298	4.0896	1.8864	0.7596
30	6.183	2.6577	1.3788	0.6426
31	10.6488	4.4262	2.5047	1.2105
32	10.4553	5.5881	2.5362	0.8811
33	8.9991	3.9105	1.7352	1.0098
34	9.2106	3.9843	1.872	1.0341
35	7.7094	2.9907	1.9341	0.8595
36	9.0405	3.8322	1.9953	0.9909
37	9.5679	4.9113	1.9971	0.7821
38	11.9979	5.6286	3.0915	1.3653
39	11.0862	5.2803	2.7828	1.2006
40	11.529	6.39	2.6829	1.0341

Table B-4. Different pore size flow rates along the 70 m transect (Continued).

41	14.6493	7.7004	3.5289	1.341
42	13.7268	6.8364	3.3768	1.323
43	10.3347	4.194	2.4372	1.1772
44	10.3068	4.1337	2.3769	1.3554
45	10.6929	4.3812	2.4273	1.4481
46	11.8872	5.9274	2.8989	1.2672
47	13.7862	6.5196	3.4965	1.5507
48	13.014	5.4189	3.4803	1.8873
49	13.8033	7.2135	3.0627	1.404
50	12.7494	5.8626	3.6252	1.503
51	9.9864	3.9321	2.3724	1.0953
52	8.1756	3.2283	2.0295	1.0854
53	6.8445	2.196	1.5588	0.8559
54	11.1816	3.8538	3.0546	1.3959
55	10.539	4.2417	2.3589	1.377
56	9.3906	4.1706	2.2014	1.1601
57	11.2356	4.3641	2.5353	1.4742
58	12.4767	4.6206	3.1158	1.8252
59	10.6056	4.3182	2.592	1.3122
60	10.7847	4.8105	2.511	1.278
61	14.5944	6.7671	3.5253	1.8612
62	12.5613	5.1174	3.1113	1.6794
63	10.2393	4.0671	2.2761	1.2123
64	10.1628	3.0285	2.1384	1.6614
65	13.9347	7.6203	3.6522	1.0305
66	9.1539	2.817	1.7505	1.026
67	10.4427	3.6837	2.3202	1.4328
68	8.91	3.5631	2.187	1.1601
69	11.1015	3.951	2.7945	1.4949
70	11.7198	4.9635	2.1042	1.5012

APPENDIX C

Table C-1. Small disc permeameter for zero cm tension.

FIRST REPLICATE		SECOND REPLICATE		THIRD REPLICATE	
TIME(S)	DEPTH(CM)	TIME(S)	DEPTH(CM)	TIME(S)	DEPTH(CM)
0	0	0	0	0	0
1.43	0.289941	1.17	0.289941	1.69	0.289941
16.25	0.579882	17.03	0.579882	13.13	0.579882
64.324	0.869822	62.27	0.869822	63.83	0.869822
114.27	1.159763	103.584	1.159763	95.55	1.159763
164.06	1.449704	145.47	1.449704	134.16	1.449704
181.87	1.594675	169.208	1.594675	156.858	1.594675
198.796	1.739645	191.75	1.739645	180.492	1.739645
225.654	1.884615	213.018	1.884615	204.646	1.884615
254.254	2.029586	237.016	2.029586	230.256	2.029586
283.504	2.174556	268.06	2.174556	257.556	2.174556
312.13	2.319527	301.86	2.319527	283.582	2.319527
341.848	2.464497	335.634	2.464497	313.586	2.464497
372.346	2.609467	370.162	2.609467	341.354	2.609467
403.832	2.754438	404.248	2.754438	371.28	2.754438
434.668	2.899408	438.282	2.899408	400.556	2.899408
467.948	3.044379	472.03	3.044379	431.08	3.044379
500.812	3.189349	505.83	3.189349	465.01	3.189349
535.262	3.33432	539.63	3.33432	496.496	3.33432
569.452	3.47929	572.65	3.47929	529.23	3.47929
603.252	3.62426	605.15	3.62426	561.99	3.62426
637.052	3.769231			593.32	3.769231
670.67	3.914201			625.43	3.914201
				658.19	4.059172

Table C-2. Small disc permeameter for -5 cm tension.

FIRST REPLECATE		SECOND REPLICATE		THIRD REPLICATE	
TIME(S)	DEPTH(CM)	TIME(S)	DEPTH(CM)	TIME(S)	DEPTH(CM)
0	0	0	0	0	0
3.03	0.14497	3.36	0.14497	3.93	0.14497
19.65	0.289941	18.36	0.289941	19.68	0.289941
43.65	0.434911	42.51	0.434911	45.18	0.434911
65.19	0.579882	69.54	0.579882	70.41	0.579882
93	0.724852	100.5	0.724852	95.82	0.724852
124.98	0.869822	135.18	0.869822	128.61	0.869822
164.16	1.014793	175.11	1.014793	158.82	1.014793
202.83	1.159763	214.68	1.159763	195.24	1.159763
248.52	1.304734	261.24	1.304734	233.19	1.304734
298.53	1.449704	308.4	1.449704	274.95	1.449704
349.53	1.594675	359.76	1.594675	318.87	1.594675
401.16	1.739645	413.07	1.739645	364.02	1.739645
454.35	1.884615	464.28	1.884615	410.94	1.884615
509.49	2.029586	519.66	2.029586	461.16	2.029586
567.06	2.174556	575.67	2.174556	508.26	2.174556
624.66	2.319527	631.86	2.319527	561.45	2.319527
681.75	2.464497	687.84	2.464497	614.88	2.464497
739.68	2.609467	743.55	2.609467	668.25	2.609467
796.62	2.754438	798.75	2.754438	723.36	2.754438
853.86	2.899408	854.25	2.899408	776.88	2.899408
910.65	3.044379			830.25	3.044379
				883.38	3.189349

Table C-3. Small disc permeameter for -10 cm tension.

FIRST REPLECATE		SECOND REPLICATE		THIRD REPLICATE	
TIME(S)	DEPTH(CM)	TIME(S)	DEPTH(CM)	TIME(S)	DEPTH(CM)
0	0	0	0	0	0
9.75	0.14497	6.36	0.14497	7.65	0.14497
43.14	0.289941	33.9	0.289941	36.69	0.289941
75.45	0.434911	75.51	0.434911	71.55	0.434911
113.07	0.579882	119.07	0.579882	106.68	0.579882
152.1	0.724852	166.71	0.724852	148.83	0.724852
197.1	0.869822	220.11	0.869822	195.69	0.869822
249.12	1.014793	278.01	1.014793	248.34	1.014793
300.6	1.159763	340.11	1.159763	303.9	1.159763
359.13	1.304734	405.18	1.304734	367.95	1.304734
422.85	1.449704	479.07	1.449704	428.88	1.449704
484.71	1.594675	553.38	1.594675	499.32	1.594675
551.13	1.739645	625.65	1.739645	571.65	1.739645
619.77	1.884615	704.94	1.884615	643.8	1.884615
690.36	2.029586	786.45	2.029586	715.95	2.029586
760.74	2.174556	867.45	2.174556	788.55	2.174556
831.03	2.319527	947.85	2.319527	859.74	2.319527
901.65	2.464497	1028.25	2.464497	932.25	2.464497
972.6	2.609467	1108.65	2.609467	1004.25	2.609467
1042.65	2.754438	1188.69	2.754438	1075.65	2.754438
1113.15	2.899408				

Table C-4. Small disc permeameter for -15 cm tension.

FIRST REPLICATE		SECOND REPLICATE		THIRD REPLICATE	
TIME (S)	DEPTH(CM)	TIME(S)	DEPTH(CM)	TIME(S)	DEPTH(CM)
0	0	0	0	0	0
11.28	0.14497	16.2	0.14497	11.4	0.14497
118.24	0.289941	110.2	0.289941	107.4	0.289941
225	0.434911	212.44	0.434911	199.76	0.434911
344.2	0.579882	321.88	0.579882	302.76	0.579882
476	0.724852	447	0.724852	405.2	0.724852
609.04	0.869822	584.92	0.869822	518.16	0.869822
757	1.014793	732.88	1.014793	636.6	1.014793
911.4	1.159763	891.8	1.159763	762.76	1.159763
1065.52	1.304734	1065.4	1.304734	915.24	1.304734
1235.16	1.449704	1262.56	1.449704	1091.04	1.449704
1422.24	1.594675	1476.12	1.594675	1279.52	1.594675
1620.92	1.739645	1691.72	1.739645	1481.52	1.739645
1836.64	1.884615	1906.2	1.884615	1707.4	1.884615
2054.64	2.029586	2120.48	2.029586	1933	2.029586
2276.48	2.174556	2335.4	2.174556	2157	2.174556
2498.04	2.319527	2550.2	2.319527	2382.2	2.319527
2718.2	2.464497			2607	2.464497

Table C-5. Large disc permeameter for zero cm tension.

FIRST REPLICATE		SECOND REPLICATE		THIRD REPLICATE	
TIME(S)	DEPTH(CM)	TIME(S)	DEPTH(CM)	TIME(S)	DEPTH(CM)
0	0	0	0	0	0
15.4	0.18179	13.16	0.18179	12.6	0.18179
35.88	0.363581	30.12	0.363581	30.12	0.363581
69.72	0.545371	63.92	0.545371	62.52	0.545371
111.32	0.727162	95.68	0.727162	95.04	0.727162
152.8	0.908952	127.12	0.908952	128.6	0.908952
203.04	1.090743	158.44	1.090743	165.44	1.090743
222	1.163459	174.28	1.163459	186.08	1.163459
242.2	1.236175	191.2	1.236175	203.76	1.236175
263.84	1.308891	210.28	1.308891	222.92	1.308891
286.84	1.381607	229.32	1.381607	240.4	1.381607
310.56	1.454323	249.68	1.454323	259.56	1.454323
336.32	1.52704	271.68	1.52704	278.64	1.52704
363	1.599756	293.32	1.599756	298.08	1.599756
389.96	1.672472	315.24	1.672472	324.48	1.672472
416.4	1.745188	339.76	1.745188	345.24	1.745188
443.92	1.817904	362.36	1.817904	368.96	1.817904
475.44	1.890621	387.68	1.890621	391.48	1.890621
506.12	1.963337	408.84	1.963337	416.44	1.963337
537.08	2.036053	436.88	2.036053	442.68	2.036053
567.4	2.108769	466.76	2.108769	470.2	2.108769
598	2.181485	495.96	2.181485	498.88	2.181485
627.16	2.254201	525.8	2.254201	527.28	2.254201
658.2	2.326918	555.88	2.326918	555.68	2.326918
689.24	2.399634	586.32	2.399634	583.68	2.399634

Table C-6. Large disc permeameter for -5 cm tension.

FIRST REPLICATE		SECOND REPLICATE		THIRD REPLICATE	
TIME(S)	DEPTH(CM)	TIME(S)	DEPTH(CM)	TIME(S)	DEPTH(CM)
0	0	0	0	0	0
15.4	0.145432	12.32	0.145432	16.84	0.145432
39.88	0.290865	35.56	0.290865	38.56	0.290865
74.48	0.436297	67.36	0.436297	76.4	0.436297
107.8	0.581729	101	0.581729	115.96	0.581729
146.2	0.727162	136.92	0.727162	156.48	0.727162
165.84	0.799878	165.84	0.799878	179.8	0.799878
185.32	0.872594	184.52	0.872594	204.4	0.872594
206.6	0.94531	206.6	0.94531	230.8	0.94531
231.68	1.018026	231.68	1.018026	258.28	1.018026
252.52	1.090743	252.52	1.090743	283.2	1.090743
278.68	1.163459	278.68	1.163459	312.4	1.163459
303.4	1.236175	303.4	1.236175	341.08	1.236175
332.04	1.308891	332.04	1.308891	371.52	1.308891
359.84	1.381607	359.84	1.381607	403.04	1.381607
387.96	1.454323	387.96	1.454323	435.52	1.454323
423.64	1.52704	419.6	1.52704	469.76	1.52704
451.04	1.599756	447.04	1.599756	505.68	1.599756
489.12	1.672472	477.12	1.672472	540.76	1.672472
518.64	1.745188	510.64	1.745188	575.2	1.745188
557.48	1.817904	545.48	1.817904	614.48	1.817904
599.8	1.890621	578.2	1.890621	654	1.890621
647.68	1.963337	613.36	1.963337	696.84	1.963337
694.2	2.036053	653.36	2.036053	742.32	2.036053
742.16	2.108769	695.92	2.108769	787.28	2.108769
789	2.181485	740.16	2.181485	832.24	2.181485
834.76	2.254201	786.24	2.254201	877	2.254201
881.48	2.326918	832.48	2.326918		

Table C-7. Large disc permeameter for -10 cm tension.

FIRST REPLICATE		SECOND REPLICATE		THIRD REPLICATE	
TIME(S)	DEPTH(CM)	TIME(S)	DEPTH(CM)	TIME(S)	DEPTH(CM)
0	0	0	0	0	0
17.32	0.072716	15.08	0.072716	17.08	0.072716
44.04	0.145432	37.24	0.145432	35.68	0.145432
61.32	0.218149	63	0.218149	58	0.218149
89.16	0.290865	89.16	0.290865	83.96	0.290865
123.2	0.363581	128.52	0.363581	111.68	0.363581
155.4	0.436297	162.2	0.436297	143.12	0.436297
189.08	0.509013	196.92	0.509013	176	0.509013
222.16	0.581729	234.56	0.581729	209.28	0.581729
261.24	0.654446	272	0.654446	243.92	0.654446
302.76	0.727162	314	0.727162	283.92	0.727162
391.24	0.872594	401.2	0.872594	365.28	0.872594
485.16	1.018026	489.4	1.018026	454.28	1.018026
588.2	1.163459	583.88	1.163459	547.76	1.163459
693.04	1.308891	682.88	1.308891	651.48	1.308891
803.08	1.454323	783.56	1.454323	758.28	1.454323
914.12	1.599756	898.8	1.599756	863.4	1.599756
1023.68	1.745188	1021.72	1.745188	975.24	1.745188
1134.32	1.890621	1147.76	1.890621	1086.2	1.890621
1246.16	2.036053	1273.04	2.036053	1197.8	2.036053
1355.8	2.181485	1398.84	2.181485	1310.2	2.181485
1466.08	2.326918	1526.24	2.326918	1423	2.326918

Table C-8. Large disc permeameter for -15 cm tension.

FIRST REPLICATE		SECOND REPLICATE		THIRD REPLICATE	
TIME(S)	DEPTH(CM)	TIME(S)	DEPTH(CM)	TIME(S)	DEPTH(CM)
0	0	0	0	0	0
0	0.036358	40.24	0.072716	38.36	0.072716
27.68	0.072716	96.24	0.145432	91.28	0.145432
48.64	0.109074	160.24	0.218149	157.2	0.218149
72.48	0.145432	228.68	0.290865	229.84	0.290865
100.32	0.18179	302.04	0.363581	306.68	0.363581
124.56	0.218149	380.96	0.436297	391.64	0.436297
150.52	0.254507	457.28	0.509013	473.84	0.509013
176.56	0.290865	539.48	0.581729	556.52	0.581729
204.04	0.327223	626.56	0.654446	650.04	0.654446
236.08	0.363581	714.76	0.727162	745.08	0.727162
266.64	0.399939	903.6	0.872594	944.76	0.872594
297.4	0.436297	1103.12	1.018026	1151.2	1.018026
327.6	0.472655	1318.08	1.163459	1375.48	1.163459
358.2	0.509013	1533.88	1.308891	1604.24	1.308891
391.04	0.545371	1758.56	1.454323	1849.16	1.454323
423.96	0.581729	1992.32	1.599756	2104.84	1.599756
455.88	0.618087	2238.36	1.745188	2360.64	1.745188
495.56	0.654446	2493.04	1.890621	2615.68	1.890621
530.04	0.690804	2744	2.036053	2870.6	2.036053
567.8	0.727162				
635.56	0.799878				
714.88	0.872594				
797.56	0.94531				
879.12	1.018026				
966.56	1.090743				
1050.64	1.163459				
1248.84	1.381607				
1492.6	1.52704				
1738.2	1.672472				
1983.4	1.817904				
2230.2	1.963337				
2479	2.108769				
2730.32	2.254201				
2983.8	2.399634				

REFERENCES

Andreini, M.S., and T.S. Steenhuis. 1990. Preferential paths of flow under conventional and conservation tillage. Geoderma 46:85-102.

Beven, K., and P. Germann. 1981. Water flow in soil macropores. II. A combined flow model. Journal of Soil Science 32:15-29.

Beven, K., and P. Germann. 1982. Macropores and water flow in soils. Water Resour. Res. 18:1311-1325.

Bouma, J., and J.H.M. Wosten. 1979. Flow patterns during extended saturated flow in two, undisturbed swelling clay soils with different macro-structure. Soil Sci. Soc. Am. J. 43:16-22.

Bouma, J. C.W. Dekker, and J.H.M. 1978. A case study on infiltration into dry clay soil. II Physical measurements. Geoderma 20:41-51.

Bouma, J., A. Jongerius, O. Boersma, A. Jager, and D. Schoonderbeek. 1977. The function of different types of macropores during saturated flow through four swelling soil horizons. Soil Sci. Soc. Am. J. 41:945-950.

Bowman, R.S., and R.C. Rice. 1986. Transport of conservative tracers in the field under intermittent flood irrigation. Water Resour. Res. 22:1531-1536.

Clothier, B.E., and I. White. 1981. Measurement of sorptivity and soil water diffusivity in the field. Soil Sci. Soc. Am. J. 45:241-245.

Cohen, S. 1988. State and USGS activities in New England. Ground Water Monitoring Review. National Water Well Association.

Dane, J.H. 1980. Comparison of field and laboratory determined hydraulic conductivity values. Soil Sci. Soc. Am. J. 44:228-231.

DaSilva, E.M. 1990. Analysis of furrow irrigation uniformity as affected by furrow spacing. Ph.D. Dissertation, Univ. of Arizona.

Ehlers, W. 1975. Observation on earthworm channels and infiltration on tilled and untilled loess soil. Soil Sci. 119:242-249.

Field, J.A., J.C. Parker, and N.L. Powell. 1984. Comparison of field and laboratory measured and predicted hydraulic properties of a soil with macropores. Soil Sci. 137:385-396.

Gardner, W.R. 1958. Some steady state solutions of the unsaturated moisture flow equation with application to evaporation from a water table. Soil Sci. 85(4).

Germann, P., and K. Beven. 1981. Water flow in soil macropores. I. An experimental approach. Journal of Soil Science 32:1-13.

Gomez, K.A., and A.A. Gomez. 1984. Statistical procedures for agricultural research. Second Edition.

Haverkamp, R., M. Vauchin, J. Touma, P.J. Wierenga, and G. Vachaud. 1977. A comparison of numerical simulation models for one-dimensional infiltration. Soil Sci. Soc. Am. J. 41:295-294.

Horton, R.E. 1940. An approach toward a physical interpretation of infiltration capacity. Soil Sci. Soc. Am. Proc. 5:399-417.

Journel, A.G., and Ch.J. Huijbregts. 1978. Mining geostatistics. Academic Press, New York.

Klute, A., and C. Dirksen. 1986. Method of soil analysis, Part 1: Physical and mineralogical methods, 2nd edition, Am. Soc. of Agron., Madison, WI.

Lien, B.K. 1989. Field measurement of soil sorptivity and hydraulic conductivity. M.S. Thesis, Univ. of Arizona.

Nofziger, D.L., K. Rajender, S.K. Sayuda, and Pei-Yao Su. 1989. One-dimensional water and chemical movement in unsaturated soils. Dept. of Agronomy, Oklahoma State University.

Perroux, K.M., and I. White. 1988. Designs for disc permeameters. Soil Sci. Soc. Am. J. 52:1205-1215.

Philip, J.R. 1957. The theory of infiltration: 1. The infiltration equation and its solution. Soil Sci. 83:345-357.

Philip, J.R. 1969. Theory of infiltration. Adv. Hydrosci. 5:215-290.

Philip, J.R. 1969. Early stages of infiltration in two and three-dimensional systems. Aust. J. Soil Res. 7:213-221.

Philip, J.R. 1986. Linearized unsteady multidimensional infiltration. Water Resour. Res. 22:1717-1727.

Pivetz, B., and T.S. Steenhuis. 1989. Pesticide, nitrate, and tracer loss in agricultural tile lines to ground water under conventional and conservation tillage. ASAE Meeting in St. Joseph, MI, Paper No. 89-2579.

Post, D.F., C. Mack, P.O. Camp. and A.S. Suliman. 1988. Mapping and characterization of the soils on the University of Arizona Maricopa Agricultural Center. Hydrology and Water Res. in Arizona and the Southwest 18:49-59.

Roth, K., H. Fluhler, W.A. Jury, and J.C. Parker. 1990. Field-scale water and solute flux in soils. Birkhauser Verlag, Boston.

Russo, D., and W.A. Jury. 1987. A theoretical study of the estimation of the correlation scale in spatial variable fields. 1. Stationary fields . Water Resour. Res. 23:1257-1268.

Samper-Calvete, F.J. 1986. Statistical methods of analyzing hydrochemical, isotopic, and hydrological data from regional aquifers. Ph.D. Dissertation, Univ. of Arizona, Tucson.

Smettem, K.R.J., and B.E. Clothier. 1989. Measuring unsaturated sorptivity and hydraulic conductivity using multiple disk permeameter. J. Soil Sci. 40:563-568.

Steenhuis, T.S., and J.Y. Parlange. 1988. Simulating preferential flow of water and solutes on hillslopes. In: P.J. Wierenga and D. Bachelet, Validation of Flow and Transport Models for Unsaturated Zone, Int. Conf. Workshop Proc. Ruidoso, NM. May 23-26, pp. 381-391.

Steenhuis, T.S., J.Y. Parlange, and M.S. Andreini. 1990. A numerical model for preferential solute movement in structured soils. Geoderma 46:193-208.

Steenhuis, T.S., J.Y. Parlange, M.B. Parlange, and F. Stagnitti. 1988. A simple model for flow on hillslopes. Agricultural Water Management 14:153-168.

Talsma, T. 1969. In situ measurements of sorptivity. Aust. J. of Soil Res. 7:269-276.

van Genuchten, M.Th. 1978. Mass transport in saturated-unsaturated media: one-dimensional solutions. Princeton University Research Report 78-WR-11. pp. 118-120.

van Genuchten, M.Th. 1980. A closed-form equation for predicting the hydraulic conductivity of unsaturated soils. Soil Sci. Soc. Am. J. 44:892-848.

Warrick, A.W., and P. Broadbridge. 1991. Sorptivity and macroscopic capillary length relationships. (Submitted to Water Resourc. Res.)

Watson, K.W., and R.J. Luxmoore. 1986. Estimating macroporosity in a forest watershed by use of a tension infiltrometer. Soil Sci. Soc. Am. J. 50:578-582.

White, I., and K.M. Perroux. 1987. Use of sorptivity to determine field soil hydraulic properties. Soil Sci. Soc. Am. J. 51:1093-1101.

White, I., and K.M. Perroux. 1989. Estimation of unsaturated hydraulic conductivity from field sorptivity measurements. Soil Sci. Soc. Am. J. 53:324-329.

White, I., and M.J. Sully. 1987. Macroscopic and microscopic capillary length and time scales from field infiltration. Water Resour. Res. 23:1514-1522.

White, I., and M.J. Sully. 1988. Field characteristics of the macroscopic capillary lengths or alpha parameters, In: P.J. Wierenga and D. Bachelet, Validation of Flow and Transport Models for Unsaturated Zone, Int. Conf. Workshop Proc. Ruidoso, NM. May 23-26, pp. 517-524.

Wooding, R.S. 1968. Steady infiltration from a shallow circular pond. Water Resour. Res. 4:1259-1273.

Yitayew, M., and J. Watson. 1986. Field methods for determining unsaturated hydraulic conductivity. ASAE Paper No. 86-2570.